



ΕΘΝΙΚΟ ΚΑΙ ΚΑΠΟΔΙΣΤΡΙΑΚΟ ΠΑΝΕΠΙΣΤΗΜΙΟ ΑΘΗΝΩΝ  
ΣΧΟΛΗ ΘΕΤΙΚΩΝ ΕΠΙΣΤΗΜΩΝ  
ΤΜΗΜΑ ΦΥΣΙΚΗΣ, ΤΜΗΜΑ ΠΛΗΡΟΦΟΡΙΚΗΣ &  
ΤΗΛΕΠΙΚΟΙΝΩΝΙΩΝ

Μεταπτυχιακό Δίπλωμα Ειδίκευσης στην  
Ηλεκτρονική – Ραδιοηλεκτρολογία (Ρ/Η)

ΔΙΠΛΩΜΑΤΙΚΗ ΕΡΓΑΣΙΑ

**Wearable Textile Antennas:  
Study and Evaluation of Embroidery Techniques  
with Conductive Yarns**

Χρυσάνθη Αγγελάκη  
Α.Μ. 2019101

Τριμελής Επιτροπή:  
Επιβλέπων :  
Αντώνης Αλεξανδρίδης,  
Διευθυντής Ερευνών  
Ινστιτούτο Πληροφορικής και Τηλεπικοινωνιών, ΕΚΕΦΕ «Δημόκριτος»

Έκτορας Νισταζάκης  
Καθηγητής  
Τμήμα Φυσικής, ΕΚΠΑ

Ιωάννης Τίγκελης  
Καθηγητής  
Τμήμα Φυσικής, ΕΚΠΑ

ΑΘΗΝΑ 2022

## Πρόλογος

Η παρούσα μεταπτυχιακή διπλωματική εργασία εκπονήθηκε στα πλαίσια του Προγράμματος Μεταπτυχιακών Σπουδών των Τμημάτων Φυσικής και Πληροφορικής & Τηλεπικοινωνιών του Εθνικού και Καποδιστριακού Πανεπιστημίου Αθηνών με τίτλο "Μεταπτυχιακό Δίπλωμα Ειδίκευσης στην Ηλεκτρονική – Ραδιοηλεκτρολογία (P/H)", και σε συνεργασία με το Εργαστήριο Ασύρματων Επικοινωνιών (WiCom) του Ινστιτούτου Πληροφορικής και Τηλεπικοινωνιών του ΕΚΕΦΕ "Δημόκριτος", κατά το ακαδημαϊκό έτος 2021-2022, υπό την επίβλεψη του Δρ. Αντώνη Αλεξανδρίδη (ΕΚΕΦΕ «Δ»).

Θα ήθελα να ευχαριστήσω τον επιβλέποντα της εργασίας μου Δρ. Αντώνη Αλεξανδρίδη, επιστημονικό υπεύθυνο του Εργαστηρίου, για την εμπιστοσύνη και τη βοήθεια καθόλη τη διάρκεια της εκπόνησης της παρούσας εργασίας. Επιπλέον, θα ήθελα να ευχαριστήσω τον κ. Ελευθέριο Αδειλίνη, τεχνικό του Εργαστηρίου, για τη βοήθειά του στην κατασκευή των εργαστηριακών πρωτότυπων κεραιών, καθώς και την Δρ. Σοφία Μπακογιάννη και τον Δρ. Άρη Τσώλη, μεταδιδακτορικούς συνεργάτες του Εργαστηρίου, για τις πολύτιμες συμβουλές και παρατηρήσεις του στην ανάπτυξη των μοντέλων ηλεκτρομαγνητικής προσομοίωσης.



Η εργασία αυτή υποστηρίχτηκε από το Ελληνικό Ίδρυμα Έρευνας και Καινοτομίας (ΕΛ.ΙΔ.Ε.Κ.) στο πλαίσιο της Δράσης «2η Προκήρυξη ερευνητικών έργων ΕΛ.ΙΔ.Ε.Κ. για την ενίσχυση Μεταδιδακτορικών Ερευνητών/τριών», Αριθμός Έργου:205, με τίτλο «Innovative Textile Structures for Mechanical Electromagnetic Reconfigurability of Wearable Antennas» (M-REWEAR).

## Περίληψη

Σκοπός της διπλωματικής εργασίας αυτής είναι η μελέτη και αξιολόγηση τεχνικών κεντήματος με αγωγή νήματα για την κατασκευή υφασμάτων, κεντημένων κεραιών για εφαρμογές φορετών συστημάτων ασύρματων επικοινωνιών.

Η τεράστια ανάπτυξη των ηλεκτρονικών συσκευών τις τελευταίες δεκαετίες έχει οδηγήσει στη δημιουργία μεγάλου εύρους φορητών ασύρματων συσκευών, τις οποίες ο χρήστης μπορεί να έχει μαζί του συνεχώς (π.χ. smartphones, tablets) ή και να τις φοράει (π.χ. smart watch, smart glasses). Ειδικότερα για τις ανάγκες των «φορετών/φορέσιμων» ασύρματων συσκευών στον τομέα των τηλεπικοινωνιών έχουν αναπτυχθεί κεραίες, οι οποίες εφαρμόζονται ενσωματώνονται στην ένδυση του χρήστη. Η έρευνα στον τομέα των φορετών κεραιών είναι εκτεταμένη καθώς οι κεραίες αυτές παρουσιάζουν πληθώρα εφαρμογών καθώς και ερευνητικών προκλήσεων.

Κατά τη διάρκεια της εργασίας σχεδιάστηκαν και προσομοιώθηκαν με το πρόγραμμα ηλεκτρομαγνητικής προσομοίωσης ANSYS HFSS, μοντέλα κεραιών οι οποίες λειτουργούν στην ζώνη συχνοτήτων των 2.4 GHz. Επίσης δημιουργήθηκαν σχέδια κεντήματος στο PE-Design Plus 2, ένα από τα λογισμικά σχεδιασμού κεντημάτων για τις κεντητικές μηχανές της Brother. Τα κεντήματα κατασκευάστηκαν με αγωγή νήματα της Shieldex στην κεντητική μηχανή Brother PR670E, που διαθέτει το εργαστήριο Ασύρματων Επικοινωνιών του Ινστιτούτου Πληροφορικής και Τηλεπικοινωνιών του ΕΚΕΦΕ «Δημόκριτος».

Στην αρχή της εργασίας γίνεται αναφορά στις μεθόδους κατασκευής υφασμάτων, φορετών κεραιών, με έμφαση στις κεντημένες κεραίες. Στη συνέχεια γίνεται αναφορά σε διάφορες μεθόδους χαρακτηρισμού των ηλεκτρομαγνητικών ιδιοτήτων υφασμάτων. Ακολουθεί η μέτρηση με δύο διαφορετικές μεθόδους των διηλεκτρικών ιδιοτήτων μιας τσόχας, η οποία χρησιμοποιήθηκε ως διηλεκτρικό υπόστρωμα υφασμάτων κεραιών. Έπειτα, γίνεται καταγραφή των παραμέτρων κεντήματος με κεντητική μηχανή και δίνονται λεπτομέρειες για την κατασκευή κεντημάτων με αγωγή κλωστές.

Στο επόμενο τμήμα της εργασίας γίνεται σχεδίαση και κατασκευή κεντημένων γραμμών μικροταινίας σε σκληρό υπόστρωμα, με σκοπό να μελετηθεί η επίδραση διαφορετικών παραμέτρων κεντήματος στις επιδόσεις τους (απώλειες διάδοσης). Τέλος, σχεδιάστηκαν και κατασκευάστηκαν υφασμάτινες, κεντημένες κεραίες μικροταινιακού καλύμματος. Τα μοντέλα των κεντημένων κεραιών προσαρμόστηκαν κατάλληλα, ώστε να λειτουργούν στην επιθυμητή συχνότητα. Οι κεραίες μετρήθηκαν στον ανηχικό θάλαμο του Ινστιτούτου Πληροφορικής και Τηλεπικοινωνιών του ΕΚΕΦΕ «Δημόκριτος».

### *Λέξεις-κλειδιά:*

Φορετές, υφασμάτινες κεραίες, μέθοδοι κεντήματος

## Summary

The aim of this thesis is the study and evaluation of e-textile embroidery techniques with conductive threads for the fabrication of fully textile, embroidered antennas for wireless wearable systems' applications.

The large growth of electronics in the past decades has led to the development of a wide range of wireless devices that the user may carry around (e.g., smartphones, tablets) or wear (e.g., smart watch, smart glasses). For the needs of wireless, wearable devices, antennas that can be integrated into the clothes of the user have been developed. The research in the field of wearable antennas is extensive due to the wide variety of wearable antennas applications and research challenges.

Throughout the course of this thesis, antenna models which operated at 2.4 GHz were designed and simulated in ANSYS HFSS. Also, embroidery designs were created in PE-Design Plus 2, one of Brother's personal embroidery design software systems for computerized embroidery machines. The embroideries were created with conductive yarns by Shieldex, using a Brother PR670E embroidery machine, which was provided by the Wireless Communications lab of the Institute of Informatics & Telecommunications at NCSR "Demokritos".

At the beginning of the thesis, different fabrication methods of textile, wearable antennas are discussed, with a focus on embroidered antennas. Afterwards, several methods of measuring the dielectric properties of fabrics are introduced. Two different dielectric measurement methods of a felt sample, which was used as a dielectric substrate for textile antennas, are described. The parameters of embroideries created with an embroidery machine, as well as details about embroidering using conductive threads are outlined in the next chapter.

In the remaining of this thesis, the design and fabrication of embroidered microstrip lines on rigid substrate is described, with the aim of evaluating their effect of different embroidery parameters on their performance (transmission loss). Lastly, textile, embroidered microstrip patch antennas were designed and fabricated. The embroidered antenna models were then modified to resonate in the desired frequency. The textile antennas were measured in the anechoic chamber of the Institute of Informatics and Telecommunications, NCSR 'Demokritos'.

### *Keywords:*

Wearable, textile antennas, e-textile embroidery

## Table of Contents

Wearable Textile Antennas: Study and Evaluation of Embroidery Techniques with Conductive Yarns.....	1
Πρόλογος .....	i
Περίληψη .....	ii
Summary .....	iii
Table of Contents.....	iv
Table of Figures.....	vi
Chapter 1 Wearable Textile Antennas: Fabrication Techniques .....	1-1
Abstract.....	1-1
1.1 Introduction .....	1-1
1.2 E-textiles.....	1-2
1.3 E-textile Embroidery Process .....	1-4
References .....	1-6
Chapter 2 Measurement of the Dielectric Properties of Fabrics .....	2-1
Abstract.....	2-1
2.1 Dielectric Properties of Materials .....	2-1
2.2 Methods of Dielectric Measurement.....	2-4
2.2.1 Non-Resonant Methods.....	2-4
2.2.2 Resonant Methods.....	2-7
2.3 Electrical Characterization of Felt Fabric .....	2-10
2.3.1 T-resonator Method.....	2-10
2.3.2 Split-Post Dielectric Resonator Method.....	2-14
2.4 Conclusions .....	2-16
References .....	2-17
Chapter 3 Embroidery Machine: Operating Parameters and Process Using Conductive Threads.....	3-1
Abstract.....	3-1
3.1 Parameters of Machine Embroidery.....	3-1
3.1.1 Stitch Patterns.....	3-1
3.1.2 Stitch Density .....	3-3
3.1.3 Under Sewing.....	3-3
3.2 Machine Embroidery Process Details .....	3-4
3.3 E-textile Embroidery Details .....	3-5
3.3.1 Conductive Threads .....	3-5
3.3.2 Conductive Thread Position .....	3-9
3.3.3 Stitch Pattern and Direction.....	3-10
3.3.4 Stitch Density .....	3-12

3.3.5	Under Sewing .....	3-16
3.3.6	Base Fabric .....	3-17
	References .....	3-18
Chapter 4	Embroidered Microstrip Transmission Lines.....	4-1
	Abstract.....	4-1
4.1	Design, Fabrication and Measurement of Copper Microstrip Line.....	4-1
4.2	Embroidered Microstrip Transmission Lines .....	4-5
4.2.1	Embroidery Designs .....	4-5
4.2.2	Embroidery Process and Microstrip Line Assembly.....	4-7
4.3	Results/Discussion .....	4-11
4.3.1	Effect of Stitch Density on the Performance of Embroidered Microstrip Lines .....	4-12
4.3.2	Effect of Under Sewing on the Performance of Embroidered Microstrip Lines .....	4-15
4.4	Conclusions .....	4-17
	References .....	4-18
Chapter 5	Embroidered Microstrip Patch Antennas.....	5-1
	Abstract.....	5-1
5.1	Copper Microstrip Patch Antenna .....	5-1
5.1.1	Antenna Modeling .....	5-3
5.1.2	Fabrication and Measurement.....	5-5
5.2	Embroidered Microstrip Patch Antennas .....	5-8
5.2.1	Embroidery Designs .....	5-8
5.2.2	Embroidery Process and Patch Antenna Assembly .....	5-8
5.2.3	Measurement and Results .....	5-10
5.3	Optimized Embroidered Microstrip Patch Antenna .....	5-11
5.3.1	Simulation Model Modification .....	5-12
5.3.2	Antenna Design Model Adjustment.....	5-13
5.3.3	Measurement.....	5-14
5.4	Conclusions .....	5-18
	References .....	5-20
Chapter 6	Summary and Future Work.....	6-1
	References .....	6-3

## Table of Figures

Figure 1-1. Knitted (left) and woven (right) fabrics with conductive fibers [4].	1-2
Figure 1-2. (Right) Nickel-plated fabric without weft fibers. (Left) Metal coating cross-section [4].	1-3
Figure 1-3. Printed dipole antenna on polyester fabric [5].	1-3
Figure 1-4. Embroidered meshed microstrip patch antenna on denim base fabric [6].	1-4
Figure 1-5. Embroidery process of an e-textile antenna: (a) EM software antenna model, (b) digitized format in embroidery design software, (c) embroidery using computerized embroidery machine and (d) finished embroidery of e-textile antenna on base fabric [1].	1-5
Figure 2-1. Parallel plate capacitor with AC voltage source [1].	2-2
Figure 2-2. Permittivity ( $\epsilon'$ and $\epsilon''$ ) as a function of frequency for theoretical dielectric [4].	2-3
Figure 2-3. Vector diagram of complex permittivity.	2-3
Figure 2-4. Reflection method using an open-circuited coaxial line [2].	2-5
Figure 2-5. Reflection method of electrical characterization equivalent circuit, (a) Transmission line with matched impedance, and (b) transmission line with mismatched impedance [2].	2-5
Figure 2-6. Measurement fixture for the transmission-line method [2].	2-6
Figure 2-7. Transmission/reflection method schematic diagram [2].	2-6
Figure 2-8. Signals in a matched transmission line with a stub [2].	2-7
Figure 2-9. Basic T-resonator structure and stub length [4].	2-8
Figure 2-10. Split post dielectric resonator structure [4].	2-9
Figure 2-11. HFSS simulation model of the T-resonator.	2-12
Figure 2-12. Fabricated model of the T-resonator.	2-12
Figure 2-13. T-resonator measured (black trace) and simulated (red trace) $S_{21}(dB)$ parameter.	2-13
Figure 2-14. Measured (black trace) and simulated (red trace) $S_{21}(dB)$ curves coincide.	2-13
Figure 2-15. Reviewed permittivity T-resonator $S_{21}(dB)$ parameter simulation (red trace) and measurement (blue trace).	2-14
Figure 2-16. Microwave Frequency Q-Meter connected to the SPDR and to the computer [3].	2-15
Figure 3-1. Example of a satin and running stitch line with a density of 2 lines/mm.	3-2
Figure 3-2. 2 lines/mm-density rectangles (without outline).	3-2
Figure 3-3. Satin stitch pattern with two different densities.	3-3
Figure 3-4. Under sewing example [2].	3-3
Figure 3-5. Common types of underlay [2].	3-4
Figure 3-6. Process of lock stitch formation using an embroidery machine [6].	3-4
Figure 3-7. Cross section of base fabric with lock stitch [4].	3-5
Figure 3-8. (a) Monofilament conductive thread, sewn on white fabric, (b) hybrid multifilament conductive thread with two conductive filaments wrapped around a conventional yarn, and (c) multifilament polymer-based conductive thread [4].	3-6
Figure 3-9. Cross section of the twined filaments of a conductive thread [4].	3-7
Figure 3-10. Close up of the Shieldex 117/17 2-ply conductive thread [3].	3-8
Figure 3-11. Twisting directions used for the Shieldex 117/17 2-ply thread [3].	3-8
Figure 3-12. Single yarn of Shieldex 117/17 [3].	3-8
Figure 3-13. Visualization of top and bobbin thread tensions [23].	3-9
Figure 3-14. Embroidered dipole type RFID tag antennas with different embroidery patterns, along with copper reference antenna on base fabric [20].	3-11
Figure 3-15. Vertical, horizontal, and diagonal stitch directions for embroidered rectangular patch antennas [4].	3-12

Figure 3-16. Embroidered tag antennas with different densities 9 [5].	3-13
Figure 3-17. Read range of embroidered tag antennas with different stitch densities 9 [5].	3-13
Figure 3-18. Embroidered antennas with: A – full horizontal stitching, B – full vertical stitching, C – partial vertical stitching, C – partial horizontal stitching, E – contour stitching [22].	3-14
Figure 3-19. Non-uniform mesh patch antenna design [4].	3-15
Figure 3-20. Embroidered non-uniform, meshed microstrip patch antenna [4].	3-15
Figure 3-21. Embroidered mesh patch antenna on denim [1].	3-16
Figure 4-1. HFSS model of copper microstrip line on FR4 substrate.	4-2
Figure 4-2. Prototype of reference copper microstrip line.	4-2
Figure 4-3. Microstrip line measurement set-up.	4-3
Figure 4-4. Simulated and measured $S_{21}(dB)$ parameter of reference copper transmission line.	4-3
Figure 4-5. Copper tape over denim reference microstrip line prototype.	4-4
Figure 4-6. Measured insertion loss of reference microstrip lines; with and without denim.	4-5
Figure 4-7. Outline example on a section of a 2 mm-wide transmission line embroidery design.	4-6
Figure 4-8. Same density lines with three different under sewing options.	4-7
Figure 4-9. Conductive and conventional thread positions on embroidery machine.	4-8
Figure 4-10. Embroidered lines on frame after the completion of the embroidery process.	4-9
Figure 4-11. Embroidered lines on base fabric with markings for cutting.	4-10
Figure 4-12. Measurement arrangement for embroidered microstrip lines.	4-10
Figure 4-13. Measured insertion loss of all the embroidered transmission lines, reference copper line and copper line over denim base fabric.	4-11
Figure 4-14. No under sewing: Insertion loss of different density embroidered microstrip lines.	4-13
Figure 4-15. Conductive under sewing: Insertion loss of different density embroidered microstrip lines.	4-14
The embroidered microstrips of the group with non-conductive under sewing (Figure 4-16) had similar behavior to the microstrips of the group with no under sewing. More specifically, the microstrips with the two highest densities (i.e., 40_1, 25_1) display almost identical losses over the studied frequency spectrum. Moreover, these microstrip designs had approximately the same losses as the 40_3 and 25_3 microstrips, which can also be observed in Figure 4-13. However, the 2.5 lines/mm-density microstrip lines have almost half the number of stitches than the 4 lines/mm microstrips. The microstrip line with the lowest density exhibited approximately 1.7 dB higher losses than the denser lines of the non-conductive under sewing group.	
Figure 4-17. Non-conductive under sewing: Insertion loss of different density embroidered microstrip lines	4-15
Figure 4-18. Insertion loss of 4 lines/mm-density embroidered microstrip lines.	4-16
Figure 4-19. Insertion loss of 2.5 lines/mm-density embroidered microstrip lines.	4-16
Figure 4-20. Insertion loss of 1.3 lines/mm-density embroidered microstrip lines.	4-17
Figure 5-1. Physical and electrical length of a rectangular microstrip patch [1].	5-2
Figure 5-2. Quarter wavelength transformer schematic [2].	5-2
Figure 5-3. HFSS model of copper microstrip patch antenna on textile (felt) substrate.	5-3
Figure 5-4. Simulated $S_{11}(dB)$ graph of copper microstrip patch antenna on felt substrate with (blue trace) and without (red trace) denim base fabric.	5-4
Figure 5-5. Copper microstrip patch antenna with denim base fabric over felt substrate.	5-5
Figure 5-6. Fabricated reference copper patch antenna on textile substrate (Right: top, Left: back).	5-5
Figure 5-7. Measured and simulated $S_{11}(dB)$ of reference copper patch antenna on textile substrate.	5-6

Figure 5-8. E-plane ( $\varphi = 90^\circ$ ): Simulated and measured gain radiation patterns of copper patch antenna.....	5-7
Figure 5-9. H-plane ( $\varphi=0^\circ$ ): Simulated and measured gain radiation patterns of copper patch antenna. ....	5-7
Figure 5-10. 2.5 lines/mm-density patch antenna design on PE design.....	5-8
Figure 5-11. 2.5 lines/mm-density embroidered microstrip patch antenna front and back.....	5-9
Figure 5-12. 4 lines/mm-density embroidered microstrip patch antenna front and back. ....	5-9
Figure 5-13. $S_{11}(dB)$ of embroidered microstrip patch antennas with two different stitch densities. ....	5-11
Figure 5-14. Simulated $S_{11}(dB)$ parameter of the modified HFSS patch antenna model and measured $S_{11}(dB)$ of the 4 lines/mm-density embroidered patch antenna. ....	5-12
Figure 5-15. Measured $S_{11}(dB)$ parameter of embroidered microstrip patch antenna with modified dimensions (orange trace), initial embroidered patch antenna (red trace) and reference copper patch antenna (black trace). ....	5-13
Figure 5-16. Final embroidered patch antenna prototype with 4 lines/mm density and modified patch and microstrip dimensions. ....	5-14
Figure 5-17. $S_{11}(dB)$ parameter of embroidered microstrip patch antennas with modified dimensions (orange trace), and also corrected microstrip dimensions (light purple dashed traces). The purple trace is the average of the two dashed purple traces. ....	5-15
Figure 5-18. Measurement set-up inside the anechoic chamber.....	5-16
Figure 5-19. E-plane ( $\varphi = 90^\circ$ ): gain radiation patterns of copper and embroidered patch antennas. ....	5-17
Figure 5-20. H-plane ( $\varphi = 0^\circ$ ): gain radiation patterns of copper and embroidered patch antennas.	5-18

# Chapter 1 Wearable Textile Antennas: Fabrication Techniques

## Abstract

Smart garments are clothing components which provide wireless sensing, localization, and communication functionality, while they exhibit the flexibility and comfort of conventional clothes. Wearable textile antennas are an essential component of smart clothes. They must be unobtrusive and easily integrated on the clothes, while satisfying the high demands of wearables, such as always-on operation.

Several fabrication methods of wearable antennas will be introduced in this chapter, while e-textile embroidery techniques will be the main focus. Since the objective of this thesis is the fabrication of embroidered textile antennas, the basic steps of embroidering an antenna with conductive yarn, using a computerized embroidery machine will also be introduced.

## 1.1 Introduction

Wireless wearable devices, or simply wearables, have attracted significant technological attention in the last decade. Wearables are wireless electronic devices, which are integrated into clothing or accessories (e.g., glasses, jewelry, shoes, belts etc.) that can be worn on the human body, as well as invasive devices such as microchips and smart tattoos. The most common fields of wearable applications include remote healthcare, wellness, sports, navigation, entertainment and fashion as well as defense and security.

Some of the most important aspects of wearables are portability, hands-free access, always-on operation and low power consumption. Moreover, wearables must be lightweight and easy to carry, seamless and unobtrusive to the wearer. Since wearable devices are meant to operate near the human body, the safety of the user should also be ensured.

Wearable textile antennas are the main interest of this thesis. They constitute a key component of wearable communications by implementing the wireless connectivity of the worn, on-body electronic devices. Wearable textile antennas consist of conventional fabrics as well as conductive fabrics (e-textiles) and threads/yarns (e-threads), for their non-conductive and conductive parts accordingly. Both their mechanical and EM properties should be considered carefully to design high efficiency, fully textile, wearable antennas.

The conductive parts of wearable antennas may be fabricated from woven or knitted conductive fabrics, prints using conductive inks or embroideries with conductive threads on conventional fabrics and more. While conductive fabrics are usually characterized by their sheet resistance, measurement techniques based on transmission lines and waveguide cavities are necessary to acquire accurate information on the electrical properties of highly conductive fabrics [2]. According to [2], e-textiles must be as homogeneous as possible since discontinuities in the conductive surface may block the current routes and thus increase the resistance of the fabric. It is therefore essential to take into account the structure of conductive fabrics in terms of density, uniformity, as well as alignment of the conductive components (i.e., conductive threads, fibers or surface covers), before integrating them in RF applications. The most common types of e-textiles will be briefly described in the next section.

As far as the non-conductive parts of textile antennas are concerned, fabrics like felt or fleece are commonly used. In order to properly integrate conventional fabrics into wearable antennas, it is essential to accurately measure their dielectric properties. Several methods of EM characterization that are suitable for textiles will be mentioned in Chapter 2.

## 1.2 E-textiles

Metal plated woven or knitted fabrics are commonly used for wearable applications. Traditional fabrics can also be turned to e-textiles through a metallization process. Screen- or inkjet-printing using conductive inks, as well as e-textile embroidery (i.e., embroidery using conductive threads on traditional fabrics) on conventional clothes are also popular methods for creating conductive patterns with high accuracy. More details on each method will be presented in the next paragraphs.

### *Conductive woven and knitted fabrics*

Highly conductive woven fabrics with conductive fibers are widely available and have been successfully used in textile electronics [3]. Current paths are provided by the metal plated fibers, which may be in the warp, weft or both directions. When both warp and weft fibers are conductive, the resistance of the fabric is minimized since the current can flow towards all directions through the conductive fibers and their interconnection points. However, woven conductive fabrics exhibit limited flexibility and excessive fraying at the edges. Moreover, their highly conductive surface is usually stiff and may feel uncomfortable when integrated into clothes. Conductive knitted fabrics are also commercially available. Knitted fabrics are naturally very flexible and can get easily deformed. In the case of conductive knits, the resistivity of the fabric may greatly vary due to excessive bending [4]. Thus, woven conductive fabrics are usually preferred compared to knits.

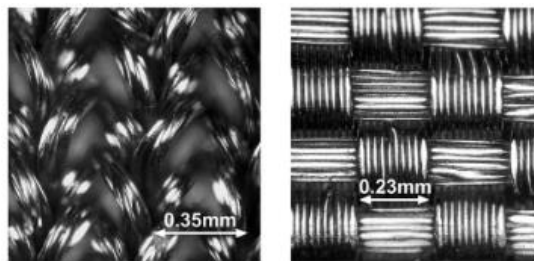


Figure 1-1. Knitted (left) and woven (right) fabrics with conductive fibers [4].

### *Metal plated fabrics*

There are several methods of metalizing fabrics, such as vacuum deposition, ion plating, electroplating, chemical and electro-less nickel plating [3]. Since the conductive plating is applied on fabrics that have already been woven, the metal coating covers only the outer area of the fabric. As a result, the parts where the fibers of the fabric cross each other are non-conductive, as seen in Figure 1-2, where the weft (vertical) fibers have been removed and the non-plated sections are exposed. The non-conductive regions of the fabric contribute to the relatively high sheet resistance of the metalized fabrics.

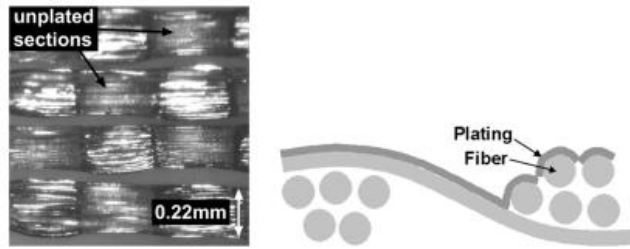


Figure 1-2. (Right) Nickel-plated fabric without weft fibers. (Left) Metal coating cross-section [4].

### *Printing with conductive ink*

Screen printing with conductive ink is another method to deposit a conductive layer on fabrics that is widely used. Inkjet printing is also an attractive alternative, since it results in highly accurate designs with minimal material consumption, while fabrication time is also reduced. However, since only a thin layer of conductive ink can be printed at once, multiple layers may need to be printed to provide sufficient current routes. In addition, when the base fabric gets elongated, breaks may appear on the conductive surface, leading to increased resistance [5].



Figure 1-3. Printed dipole antenna on polyester fabric [5].

### *E-textile embroidery*

E-textile embroidery refers to creating embroidery patterns with conductive threads (e-threads) on traditional fabrics. The e-threads are usually suitable for conventional embroidery machines, thus mass production of textile RF components is possible with this method [6]. E-textile embroidery is a very promising method of creating wearable electronics, due to the robust and durable nature of conductive threads, high accuracy [1], fast fabrication as well as due to the easy integration of the embroideries into conventional clothes.

The aim of this thesis is to create fully textile embroidered antennas, as well as evaluate different embroidery parameters based on the performance of embroidered RF components. The e-textile embroidery process will be briefly described next, while more details on e-textile embroidery will be presented in Paragraph 3.3.



Figure 1-4. Embroidered meshed microstrip patch antenna on denim base fabric [6].

### 1.3 E-textile Embroidery Process

A computerized embroidery machine is an essential tool to create high precision embroideries using conductive threads. The embroidery process of creating a wearable antenna using a computerized embroidery machine, has been broken down into a series of four basic steps (Figure 1-5 (a) to (d)) in [1].

The first step is the creation of the antenna design on an EM simulator software, while considering the limitations introduced by the precision of the embroidery machine. The second step is digitization, which refers to creating an embroidery design of the modeled antenna, into a format that is readable by the embroidery machine. The model of the antenna can be converted into a Drawing Interchange File (DXF) by the EM software and then converted into a Windows Metafile Format (WMF), which can be imported into an embroidery design software in the format of a vector file [1]. However, simple antenna designs like the dipole antenna in Figure 1-5, can also be easily created in the embroidery design software, according to the dimensions of the modeled antenna.

After the digitization process, the embroidery design can be imported to the embroidery machine and the embroidery process can be initiated [1]. While in this example no frame is needed for the base fabric, bigger embroidery machines require the base fabric to be inserted in a frame in order to get embroidered. The main difference of e-textile embroidery, compared to conventional embroidery is the use of conductive threads. More details on setting up the embroidery machine and the embroidery process will be discussed in Chapter 3.

The last step of the creation of an embroidered antenna is testing and validation. A conventional (e.g., copper sheet) antenna can be used as reference. If significant variations are observed between the reference antenna and the e-textile antenna, it is advised to optimize the embroidery design to minimize the differences between the two models. The embroidery parameters may also be altered with the aim of increasing the surface conductivity of the embroidery and consequently enhance its performance [1].

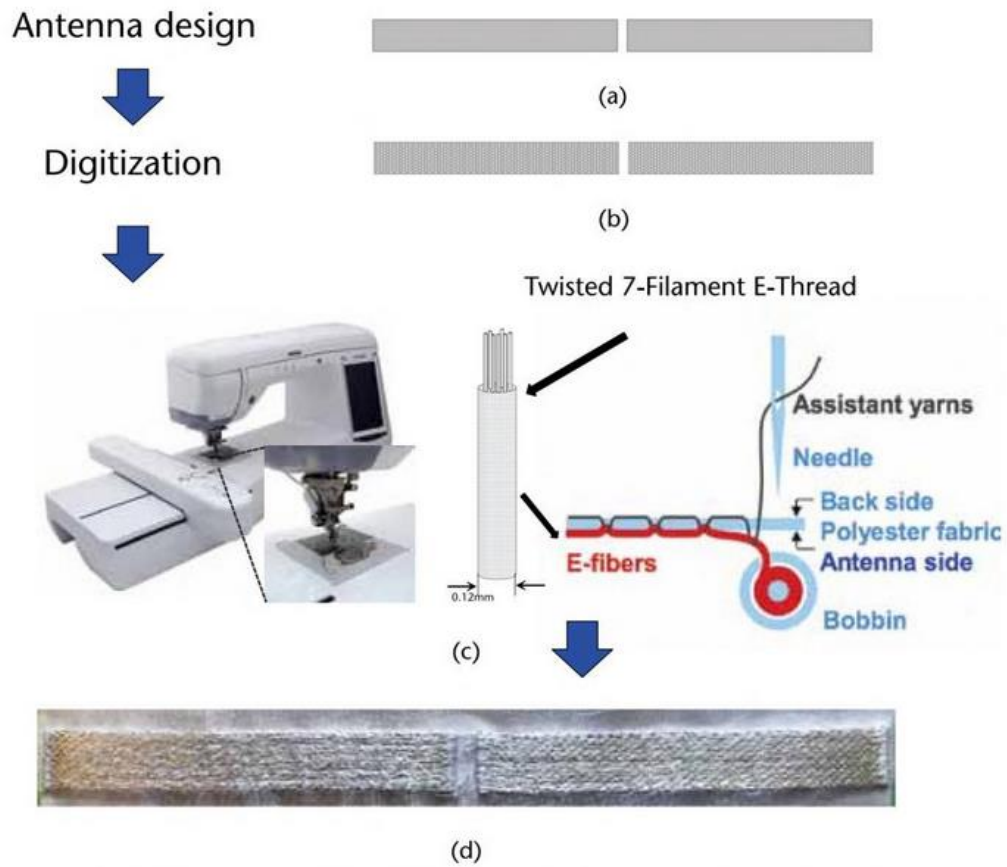


Figure 1-5. Embroidery process of an e-textile antenna: (a) EM software antenna model, (b) digitized format in embroidery design software, (c) embroidery using computerized embroidery machine and (d) finished embroidery of e-textile antenna on base fabric [1].

## References

- [1] A. Kiourti and J. Volakis, *Wearable Antennas and Electronics*, 2022.
- [2] R. Salvado, C. Loss, R. Gonçalves, and P. Pinho, "Textile Materials for the Design of Wearable Antennas: A Survey," *Sensors*, vol. 12, pp. 15841-15857, 2012.
- [3] *TEXTILE METALIZATION*. Available:  
<https://www.swicofil.com/consult/innovations/conductivity/textile-metalization>
- [4] I. Locher, M. Klemm, T. Kirstein and G. Troster, "Design and Characterization of Purely Textile Patch Antennas," in *IEEE Transactions on Advanced Packaging*, vol. 29, no. 4, pp. 777-788, Nov. 2006, doi: 10.1109/TADVP.2006.884780.
- [5] A. Chauraya, W. G. Whittow, J. C. Vardaxoglou, Y. Li, R. Torah, K. Yang, *et al.*, "Inkjet printed dipole antennas on textiles for wearable communications," *IET Microwaves, Antennas & Propagation*, vol. 7, pp. 760-767, 2013.
- [6] S. Zhang, "Design advances of embroidered fabric antennas," PhD, Loughborough University, 2014.

# Chapter 2 Measurement of the Dielectric Properties of Fabrics

## Abstract

Dielectric materials are commonly used for applications in the microwave frequency range, along with conductors. Precise knowledge of the materials' dielectric properties is crucial for accurate modeling of microwave circuits. There are several methods to electrically characterize materials and acquire information on their behavior in presence of an external electromagnetic field.

Conventional fabrics, such as felt, fleece and denim, are commonly used in WBAN (Wireless Body Area Network) applications as substrates for textile microwave circuits (e.g., microstrip transmission lines, patch antennas). Since the dielectric properties of common fabrics are not provided by the suppliers, dielectric measurement is necessary before incorporating them in textile applications. The complex permittivity of fabric substrates is the main interest of this chapter, given that fabrics are generally non-magnetic materials.

In this chapter, the dielectric properties of materials will be briefly discussed first, with permittivity being the main interest. Two general categories of methods for electrically characterizing substrate samples, namely non-resonant and resonant methods will be presented. The T-resonator and split-post dielectric resonator (SPDR) methods are two resonant methods, which will be described thoroughly. Lastly, using these two methods, the dielectric properties of a 3.2 mm-thick felt fabric will be measured.

## 2.1 Dielectric Properties of Materials

Dielectric materials are defined as materials that have the ability to store energy when exposed to an external electric field [1]. The dielectric properties of materials describe the storage and dissipation of electric and magnetic fields inside them. More specifically, the electric polarizability of a dielectric is expressed by permittivity ( $\epsilon$ ) [5]. Electrical resistivity ( $\rho$ ) is a measure of how strongly a material resists electric current [6]. Permeability ( $\mu$ ) expresses the magnetization that a material acquires when exposed to an external magnetic field [7]. Therefore, the electrical characterization of materials, meaning the measurement of their dielectric properties, is essential to determine the feasibility of incorporating them in various applications [4].

While some materials, like ferrites, have magnetic properties, the permeability of many dielectric materials, including conventional fabrics, is close to that of free space ( $\mu \cong \mu_0$ ) [8]. Consequently, in the remaining of this chapter the magnetic properties of materials will not be considered and complex permittivity of dielectric materials will be discussed.

When a DC voltage source ( $V$ ) is placed across a parallel plate capacitor, inserting a dielectric material between its plates will increase the charge storage, according to the next equation.

$$C' = \epsilon \frac{E}{Qd} = \epsilon C \quad (1)$$

Where,

- $C'$ : the capacity of the capacitor after inserting the dielectric material,
- $\epsilon$ : the permittivity of the dielectric,
- $E$ : the amplitude of the electric field,
- $Q$ : the charge on the plates,
- $d$ : the distance between the plates of the capacitor, and

$C$ : the initial capacity of the capacitor.

The change in the storage capacity is determined by the dielectric constant of the material. If an AC sinusoidal voltage source was used instead, the resulting current ( $I$ ) would be made up from a charging current ( $I_c$ ) and a loss current ( $I_l$ ). Both these currents are dependent on the permittivity of the dielectric. The losses introduced by the dielectric material can be expressed as a capacitor ( $C$ ) parallel to a conductance ( $G$ ) [1], as pictured in Figure 2-1.

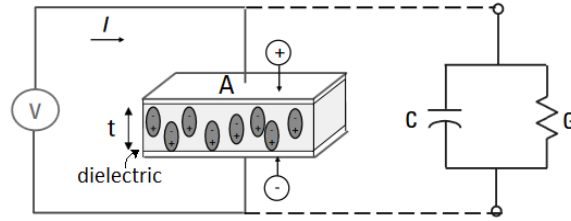


Figure 2-1. Parallel plate capacitor with AC voltage source [1].

Permittivity is defined as the amount of energy needed in order to generate one unit of electric flux inside a specific medium. The standard S.I. unit for permittivity is Farad per meter ( $F/m$ ). According to electromagnetic theory, the definition of electric flux density ( $D_f$ ) is:

$$D_f = \epsilon E \quad (2)$$

Where,

$\epsilon$  : permittivity of the medium and  
 $E$  : the applied electric field.

The ratio of a medium's absolute permittivity ( $\epsilon$ ) to the vacuum permittivity ( $\epsilon_0 = \frac{1}{16} \cdot 10^{-9} \frac{F}{m}$ ), namely relative permittivity ( $\epsilon_r$ ) is most commonly used instead of permittivity [5]. Therefore, relative permittivity is a dimensionless quantity. From this point on, relative permittivity is going to be referred to as permittivity or dielectric constant.

As seen in the following equation, permittivity is generally a complex number.

$$\epsilon_r = \epsilon_r' - i \epsilon_r'' \quad (3)$$

The real part of permittivity ( $\epsilon_r'$ ) represents the lossless permittivity. It expresses the amount of power stored in the medium when an external electric field is applied. As far as the imaginary part of permittivity ( $\epsilon_r''$ ) is concerned, it expresses the amount of energy loss from the material due to the presence of the external electric field. As seen in the following equation, the imaginary part of permittivity is associated to the dielectric "conductivity" of the material, as well as the frequency of operation, according to the next equation.

$$\epsilon_r'' = \frac{\sigma}{\epsilon_0 \omega} \quad (4)$$

Where,

$\sigma$  : (dielectric) conductivity of the material and  
 $\omega$  : angular frequency of operation.

The conductivity of the dielectric expresses the dissipative effects of the material, such as conductivity originating from moving charge carriers inside the medium or dispersion of the real part of permittivity. A perfect dielectric material is considered to have zero electrical conductivity

(insulator) [9]. However, it should be noted that not all insulators have the ability to store an electric field through the polarization of the medium and therefore they are not dielectrics [1].

The permittivity of a material is not constant, and it is in fact dependent on multiple factors. Most importantly, permittivity changes with frequency. The typical behavior of a dielectric's permittivity (real and imaginary part) with frequency is shown in the Figure 2-2. The permittivity of a material is related to a variety of physical phenomena such as ionic conduction, dipolar relaxation, atomic polarization and electronic polarization. As seen in Figure 2-2, the impact of each phenomenon on the complex permittivity is pronounced on the respective frequency range that it occurs. For example, dipolar relaxation is the main reason for the variation of permittivity in the microwave frequency range [4]. Other factors that affect the permittivity of a material are temperature, humidity, pressure, orientation and molecular structure of the material.

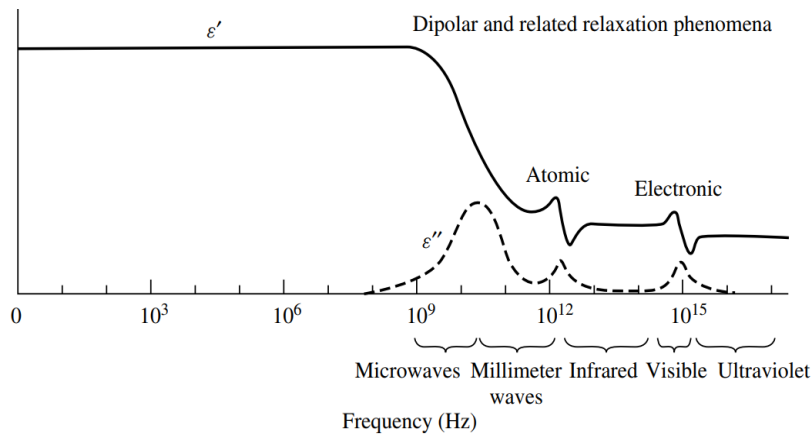


Figure 2-2. Permittivity ( $\epsilon'$  and  $\epsilon''$ ) as a function of frequency for theoretical dielectric [4].

Last but not least, the vector diagram of complex permittivity (Figure 2-3) is also commonly used. If  $\delta$  is the angle between the net force (of the real and imaginary part), and the real component, the total losses of a dielectric can be expressed by the tangent of this angle. The loss tangent ( $\tan \delta$ ) is also known as loss factor or dissipation factor. It is defined as the ratio of the imaginary part of permittivity to the real part [1], as seen in the next equation.

$$\tan \delta = \frac{\epsilon_r''}{\epsilon_r'} = \frac{1}{Q} \tag{5}$$

Where,  
 $Q$  : Quality factor.

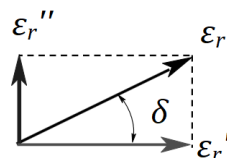


Figure 2-3. Vector diagram of complex permittivity.

Therefore, the loss tangent quantifies a dielectric's inherent dissipation of electromagnetic energy, and it inherits the frequency dependency of permittivity.

## 2.2 Methods of Dielectric Measurement

The dielectric measurement of materials is an essential tool for applications in microwave frequencies, as it provides insight on their behavior at very high frequencies. Generally, the methods of electrical characterization of materials in this frequency range fall into two categories; the non-resonant methods and the resonant methods. The methods of the first category are often used to acquire accurate knowledge of the electromagnetic properties of a material over a certain frequency range. On the other hand, resonant methods are most commonly used to measure the electromagnetic properties of the sample at a single frequency or several discrete frequencies. When non-resonant and resonant methods are used in combination, accurate information on the dielectric properties of a material over a wide range of frequencies can be derived [4].

There are a great number of both non-resonant and resonant methods for the electrical characterization of materials. The assessment and final choice of the preferred method for a specific application is usually based on the frequency of operation, the nature of the measured material, the dielectric properties of interest and the desirable resolution of measurement.

In this chapter, the objective is to measure the dielectric characteristics of a felt fabric, which will be used as a substrate for textile microwave circuits. Various methods of electrical characterization will be briefly described, focusing on methods that are suitable for the measurement of the felt sample.

### 2.2.1 Non-Resonant Methods

When an electromagnetic wave travels from one medium to another (e.g., from free space to sample) its velocity and impedance change, while part of its energy gets reflected. The reflected and transmitted waves can provide insight into the dielectric properties of the sample. In non-resonant methods, a transmission line or waveguide is usually used to direct electromagnetic energy towards the sample under test. The permittivity and permeability of the sample can then be deduced by measuring the reflected and transmitted power [2].

Non-resonant methods are generally divided into two categories; the reflection methods and transmission/reflection methods. In reflection methods, the sample's permittivity or permeability can be determined from the reflection coefficient. However, it is usually not possible to measure both properties at once. In transmission/reflection methods, the sample is also inserted in a transmission line or waveguide. However, both the reflected energy from the sample and the transmitted energy through it are taken into account in order to measure its dielectric properties. Moreover, it is possible for the sample's permittivity and permeability to be acquired in one measurement [2].

In the following paragraphs, more details on reflection and transmission/reflection methods of dielectric measurement will be presented.

#### *Reflection methods*

Various types of transmission lines can be used to direct electromagnetic energy towards the sample in reflection methods. When coaxial lines are employed, the sample under test gets attached at the open end of the line, in order to measure its dielectric properties. However, when measuring planar materials like fabrics, employing a method that uses the sample as the substrate or part of the substrate of a planar transmission line should also be considered, as it might be more convenient.

Figure 2-4 depicts the most commonly used configuration in reflection methods; an open-circuited coaxial line with the sample attached to its open end. In this measurement set-up, the reflected power is determined from the impedances inside the transmission line and sample. Thus, by measuring the reflection coefficient, the electromagnetic properties of the sample can be obtained [2].

Planar transmission lines can also be used in reflection methods, with the sample under test being used directly as the substrate of the line. The basic structure of a planar transmission line consists of conductive parts (including grounding conductors and conductive strips) and dielectric parts (substrates). The electromagnetic characteristics of these conductors and dielectrics determine the performance of the transmission line. Hence, provided that the electromagnetic properties of the rest of components are known, the dielectric properties of the sample can be derived. These methods are also known as transmission-line methods.

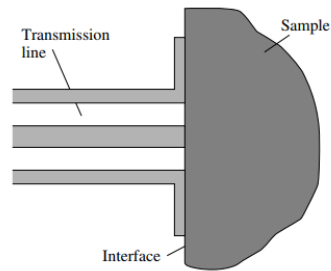


Figure 2-4. Reflection method using an open-circuited coaxial line [2].

Figure 2-5 illustrates the principle of operation of the transmission-line method, where the sample under test is used as the substrate of a planar transmission line.

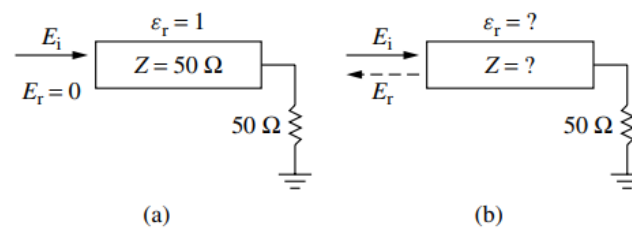


Figure 2-5. Reflection method of electrical characterization equivalent circuit, (a) Transmission line with matched impedance, and (b) transmission line with mismatched impedance [2].

Specifically, when a transmission line with a substrate of permittivity that is equal to 1 is designed to match a  $50\ \Omega$  termination line, no reflection occurs at the input port (Figure 2-5 (a)). However, if the transmission line with the same dimensions is built on a material of unknown permittivity, the characteristic impedance of the line changes, resulting in a mismatched condition. In this case, part of the input wave will be reflected back at the input port (Figure 2-5 (b)). Provided that the electrical length of the microstrip line is relatively long, the characteristic impedance of the transmission line can be experimentally determined through measuring the reflections due to the mismatch. Finally, the permittivity of the substrate can be calculated from the impedance and the width of the line [2].

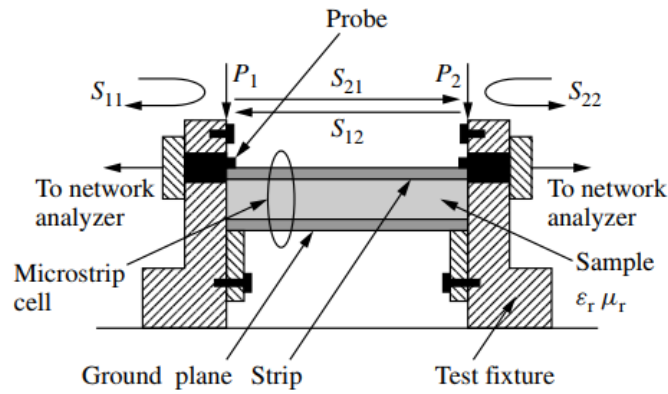


Figure 2-6. Measurement fixture for the transmission-line method [2].

Figure 2-6 illustrates the measurement fixture used in the transmission-line method for dielectric measurement of the substrate sample. A microstrip line is most commonly employed for this method. The microstrip line is designed based on an approximate, expected value of the complex permittivity of the substrate. The dimensions of the line can then be selected accordingly, in order to achieve a characteristic impedance of roughly  $50 \Omega$ . The permittivity of the substrate is deduced from the change in the  $S_{11}$  parameter of the simulated model and the measured structure [2].

### Transmission/Reflection Method

If a sample is placed in a segment of a transmission line or waveguide, part of the incident wave will be reflected due to the discontinuity, while the rest will be transmitted through the sample towards the other end of the transmission line. The reflected wave may then be partially reflected again, resulting in a wave travelling along the direction of the incident wave (Figure 2-7). By measuring the impedance and scattering parameters of the structure, the dielectric properties of the sample can be derived [2].

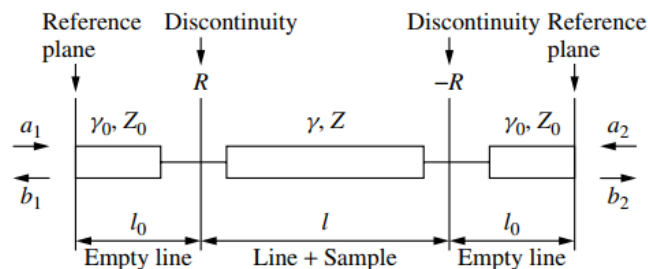


Figure 2-7. Transmission/reflection method schematic diagram [2].

In the aforementioned measurement structures for the transmission/reflection methods, the sample under test is required to completely fill the cross section of the waveguide or transmission line without the presence of any air gaps. . Thus, the accurate measurement of samples' dielectric characteristics using such methods can be challenging. In addition, since the wave must propagate through the sample, measurement sensitivity limitations are introduced for thin materials like fabrics [2]. Thus, employing a planar transmission line can be more practical when measuring the dielectric properties of substrate fabrics, like felt or fleece.

## 2.2.2 Resonant Methods

Resonant methods for the electrical characterization of samples are generally more accurate and have higher sensitivity than non-resonant methods. They are commonly used for the dielectric measurement of low-loss dielectrics [2].

Since these methods employ resonant structures, the dielectric properties of the sample under test can be measured only in a single frequency or in discrete frequencies. The working principle of resonant methods is based on the fact that the resonant frequency and Quality factor (or Q-factor) of a dielectric resonator of fixed dimensions is determined by its permittivity and permeability. The sample's dielectric properties can be derived either directly from the frequency and the Q-factor of the resonator (resonator methods) or from the change in their values when the resonator is unloaded and loaded with the sample (resonant-perturbation methods) [2].

Shielded dielectric resonators (i.e., dielectric resonators inside a metal cavity) or planar resonator structures, where the sample plays the role of the substrate, are commonly used in resonant methods of dielectric measurement. Some typical examples are the ring-resonator method, the cross-resonator method, the T-resonator method and the split-post resonator method [2]. The structures and methods of measurement of the last two methods will be described in the following paragraphs.

### *T-resonator method*

The T-resonator (or open stub resonator) method is a resonant method that provides accurate information on the dielectric properties of the sample for a specific frequency. The measured sample is used as a substrate for the resonator. The dielectric constant of the sample is derived from the resonant frequency, while the loss tangent is calculated from the total Q-factor.

The basic structure of the T-resonator consists of a segment of a transmission line with an open circuit stub in the middle of it. The insertion loss diagram ( $S_{21}(dB)$  to frequency) of a uniform transmission line with roughly matched terminations would drop monotonically over frequency, mainly due to dielectric and conduction losses (frequency dependent attenuation). However, in the case of the T-resonator structure, part of the current will travel towards the stub. After getting reflected at the open end, the current will travel back towards the output, along with the initial wave (Figure 2-8). If the two signals are out of phase and cancel out each other, a large absorption dip will appear at a certain frequency, in the insertion loss diagram [10].

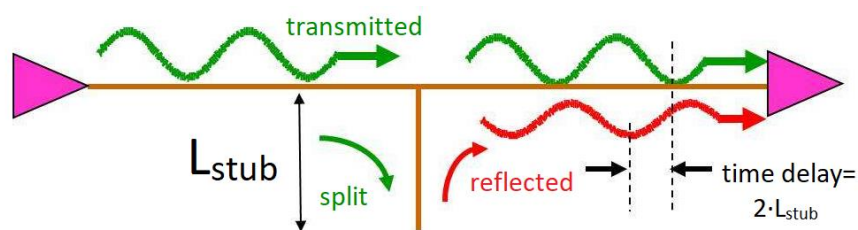


Figure 2-8. Signals in a matched transmission line with a stub [2].

The length of the open stub determines the phase difference between the incident and reflected waves, and consequently the signal at the receiving end of the resonator. To be more exact, the reflected signal has traveled an extra distance that is equal to two times the length of the stub ( $2L_{stub}$ ), as displayed in Figure 2-8. If the length of the round trip through the stub is close to half a wavelength (of the frequency that is of interest), the reflected and incident waves will be  $180^\circ$  out of phase. Thus, the two signals will cancel out completely and result in a minimum output signal at the corresponding frequency [2]. Therefore, for the structure to resonate is a certain frequency, the length of the stub must be approximately equal to:

$$2 \cdot L_{stub} = \frac{\lambda_{eff}}{2} \Leftrightarrow L_{stub} = \frac{\lambda_{eff}}{4} \quad (6)$$

Where,

$\lambda_{eff}$  : wavelength inside the dielectric.

The equation above is satisfied for stub lengths equal to an odd integer ( $2n + 1$ ,  $n = 0,1,2 \dots$ ) multiples of the quarter wavelength, as depicted in the next figure.

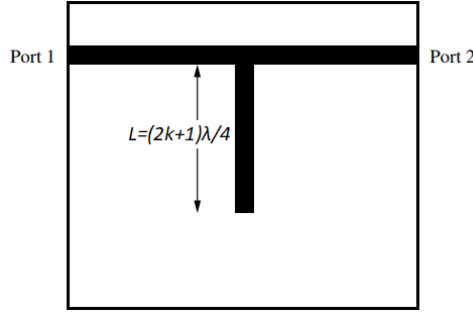


Figure 2-9. Basic T-resonator structure and stub length [4].

Nonetheless, in reality the stub will appear longer than its physical length ( $L$ ), because of the fringing effects at the open end. The extra length ( $L_c$ ) is dependent on the dimensions of the structure and the permittivity of the substrate. The relation between the electrical length of the stub ( $L_{el}$ ) and the effective permittivity ( $\epsilon_{r,eff}$ ) of the T-resonator structure will thus be [11]:

$$L_{el} = \frac{\alpha \lambda_{eff}}{4} \quad (7)$$

$$L + L_c = \frac{\alpha}{4\sqrt{\epsilon_{r,eff}}} \lambda = \frac{\alpha}{4\sqrt{\epsilon_{r,eff}}} \frac{c}{f_n}, n = 0,1,2 \dots \quad (8)$$

The effective permittivity of the structure at the operating frequency is given by:

$$\epsilon_{r,eff} = \left( \frac{\alpha c}{4f_n(L + L_c)} \right)^2, n = 0,1,2 \dots \quad (9)$$

Where,

$\lambda$  : free space wavelength,

$\alpha$  :  $2k+1$  ( $k=1, 2, 3\dots$ ),

$c$  : speed of light in free space, and

$f_n$  : frequency of operation.

The extra length  $L_c$  expresses the open-end effect (expressed by  $l_{eo}$ ), which causes the stub to seem electrically longer, as well as the T-junction effect (expressed by  $d_2$ ), which reduces the electrical length of the stub [11]. The total length of the stub can be calculated as follows:

$$L_c = \frac{w}{2} + l_{eo} - d_2 \quad (10)$$

Where,

$w$ : the width of the stub.

The loss tangent of the sample is given by the Quality factor ( $Q$ ) of the structure. The Quality factor takes into account the conduction, dielectric and radiation losses [11], according to the following equation:

$$\frac{1}{Q} = \frac{1}{Q_c} + \frac{1}{Q_d} + \frac{1}{Q_r} \quad (11)$$

Where,

- $Q_c$ : Quality factor for the conduction losses,
- $Q_d$ : Quality factor for the dielectric losses, and
- $Q_r$ : Quality factor for the radiation losses.

The loss tangent can be expressed through the Q-factor, as a function of the dielectric losses, the dielectric constant, and the effective dielectric constant:

$$\tan \delta = \frac{\varepsilon_{r,eff}(\varepsilon_r - 1)}{Q_d \varepsilon_r (\varepsilon_{r,eff} - 1)} \quad (12)$$

### Split-post dielectric resonator

The split-post dielectric resonator (SPDR) method is a resonant-perturbation method for electrically characterizing fabrics in a specific frequency. The dielectric properties of the sample can be derived from the changes in the Q-factor and resonant frequency, when the resonator is loaded and unloaded. The split-post dielectric resonator structure, loaded with a sample of height  $h$ , can be seen in Figure 2-10.

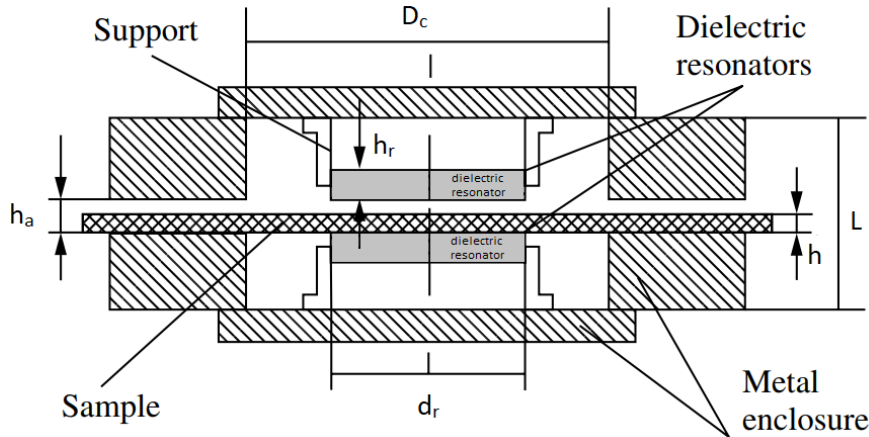


Figure 2-10. Split post dielectric resonator structure [4].

The structure of the resonator consists of two dielectric disks inside a metal cavity. The dielectric disks are fairly thin ( $h_r$ ) and the height of the metal enclosure is small ( $h_a$ ). The presence of an air gap inside the cavity does not affect the measurement, since the electromagnetic fields generated in the air gap are strongly evanescent. This also applies to the area of the measured substrate, which exceeds the borders of the dielectric discs inside the cavity. The electromagnetic fields inside the cavity are thus attenuated and may be neglected in these areas. As a result, the numerical analysis is simplified, and unwanted radiation is limited [12].

Apart from thicker fabrics like felt, the split-post resonator can also be used to accurately measure the dielectric properties of fabrics which are relatively thin, such as denim. For example,

an SPDR which operates at 2.5 GHz can accurately measure fabrics that are thinner than 4 mm. Besides, this method is also suitable for characterizing low-loss, non-dispersive materials [3].

While the accuracy of the SPDR method is very high, and the electrical characterization of various fabrics is feasible using the same structure, there are also some limitations. Firstly, the samples under measurement are required to have a relatively low profile ( $h \leq h_a$ ) in order to fit inside the air gap. Also, a large enough surface of the sample must be available to cover the horizontal cross section of the metal enclosure ( $D_c \times D_L$ , where  $D_L$  is the length of the cavity). Last but not least, the operating frequency of the resonator is determined from the dimensions of the resonator, which are fixed for each structure and cannot be altered [8].

## 2.3 Electrical Characterization of Felt Fabric

The measurement of the dielectric properties of fabrics that can be used as substrates for planar circuits in wearable applications is the main interest of this chapter. Felt is a non-woven, thick, non-stretchable fabric that could easily be integrated into clothing or other accessories, like belts. It typically has a low dielectric constant and is generally lossless; thus exhibiting great potential to be used as a substrate material.

In the next paragraphs, the electrical characterization of a 3.2 mm-thick, blue felt fabric will be described. Two different resonant methods were implemented for the dielectric measurement of the felt sample; the T-resonator method and split-post dielectric resonator method. As already mentioned, resonant methods can provide results on a discrete frequency. However, since felt is a non-dispersive material, it is expected that the results will apply to a wide frequency range around the frequency of measurement.

### 2.3.1 T-resonator Method

At first, an approximate value for both the dielectric constant and the loss tangent must be presumed for the fabric under test, according to the values found in the bibliography. A model of the T-resonator, based on the expected value of the permittivity and the thickness (height) of the fabric is then designed on the preferred frequency.

The next step of the procedure is the fabrication and measurement of the modeled T-resonator. The resonant frequency can be determined by the minimum value of the insertion loss ( $S_{21}$  parameter), expressed in dB.

$$\begin{aligned} \text{Insertion loss (dB)} = S_{21}(\text{dB}) &= 10 \log_{10} \frac{P_R}{P_T} = 10 \log_{10} \frac{|V_2|^2}{|V_1|^2} = 20 \log_{10} \frac{|V_2|}{|V_1|} \Rightarrow \\ S_{21}(\text{dB}) &= -20 \log_{10} |S_{21}| \text{ dB} \end{aligned} \quad (13)$$

Subsequently, the  $S_{21}$  parameter of the modeled T-resonator must be derived from simulation. In order to bring the simulated  $S_{21}(\text{dB})$  curve to coincide with the measured curve, in terms of resonant frequency, the value of the dielectric constant must be altered. After adjusting the resonant frequency, the substrate's (felt) loss tangent must be modified for the two curves to coincide as far as the  $S_{21}(\text{dB})$  amplitude is concerned. Consequently, the dielectric characteristics of the sample (felt) are the values of permittivity and loss tangent, which bring the simulated graph to coincide with the measured graph.

#### *T-resonator fabrication*

The expected values of the dielectric constant and loss tangent for the felt sample under test, according to the bibliography and previously measured felt fabric samples, are presented below.

$$\begin{aligned}\varepsilon_{r,ap} &= 1.23 \\ \tan \delta_{ap} &= 0.02\end{aligned}$$

Based on these characteristics, a 3D model of the T-resonator structure was designed in ANSYS HFSS (Figure 2-11). The width of the microstrip line and stub was determined based on the thickness and speculated (bibliography) value of the dielectric constant of the felt fabric, at 12.44 mm. As seen in Figure 2-11, the corners of the microstrip line's open ends were cut off, in order to avoid unintentional connection with the outer conductor (i.e., the ground plane of the SMA connector), as well as to optimize the current flow.

According to the equations in [13] the stub's length correction factor was calculated:

$$\begin{aligned}l_{eo} &= 2.063 \text{ mm} \\ d_2 &= 3.379 \text{ mm} \\ A &= \frac{w}{2} + l_{eo} - d_2 = 4.9 \text{ mm}\end{aligned}\tag{14}$$

and the corrected stub length was calculated as follows:

$$L_{cor} = \frac{\lambda_{eff}}{4} - A = 22.81 \text{ mm}\tag{15}$$

According to these values, a simulation was carried out on HFSS. Since the resonance occurred at a higher frequency near 2.75 GHz, the correction factor was adjusted to achieve a resonance near 2.5 GHz, based at the simulation results. Eventually, the correction factor was set to  $A' = 2.6 \text{ mm}$  and the resonance appeared at 2.52 GHz. According to this approximation, the length of the open stub was set to 25.11 mm.

A 0.08 mm-thick copper sheet was used for the conductive parts of the structure. In order to ensure the accuracy in the dimensions of the microstrip and stub, an LPKF PCB-plotter was used to cut the copper sheet. After attaching the conductive parts on the felt substrate, two (female) SMA connectors were soldered to the open ends of the feed line respectively. The fabricated prototype of the T-resonator on the blue felt sample under test can be seen in Figure 2-12.

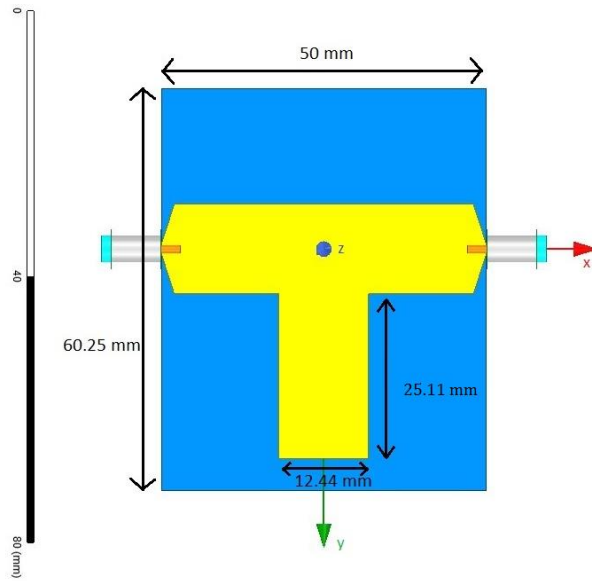


Figure 2-11. HFSS simulation model of the T-resonator.

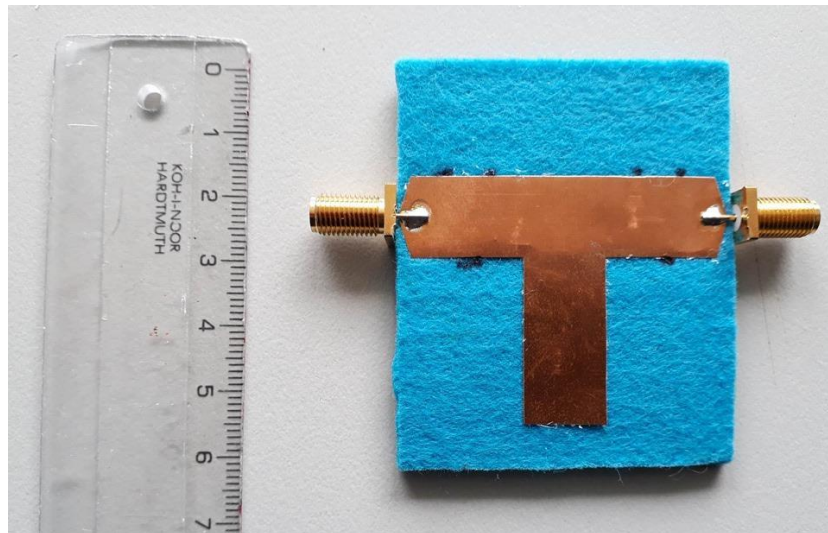


Figure 2-12. Fabricated model of the T-resonator.

### Measurement and results

At first, the Vector Network Analyzer (VNA) was calibrated and then the T-resonator was connected to its input and output ports accordingly. The insertion loss of the structure was measured, and the resonant frequency was observed at 2.539 GHz, where the  $S_{21}$  amplitude reached a minimum of -40.6 dB (Figure 2-13).

Afterwards, a simulation of the modeled structure was carried out in HFSS. The insertion loss diagram of both the simulation and the measurement are displayed in Figure 2-13. The resonant frequency of the modeled structure occurred at 2.52 GHz. The minimum amplitude of the  $S_{21}$  parameter at resonance is -30.88 dB. The shift of the resonant frequency between the simulation and the measurement indicates that the actual value of the dielectric constant is lower than the estimated value. As far as the loss tangent is concerned, the simulated  $S_{21}$  amplitude at

resonance exceeded the measured value by approximately 10 dB, which indicates that the losses of the material are lower than assumed in simulation.

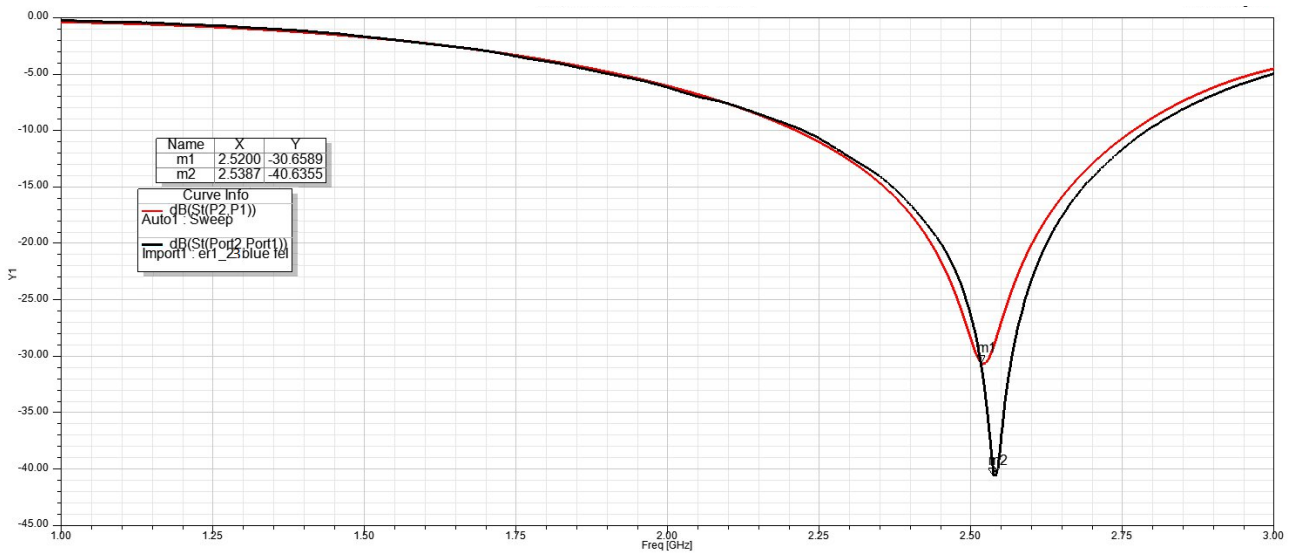


Figure 2-13. T-resonator measured (black trace) and simulated (red trace)  $S_{21}(dB)$  parameter.

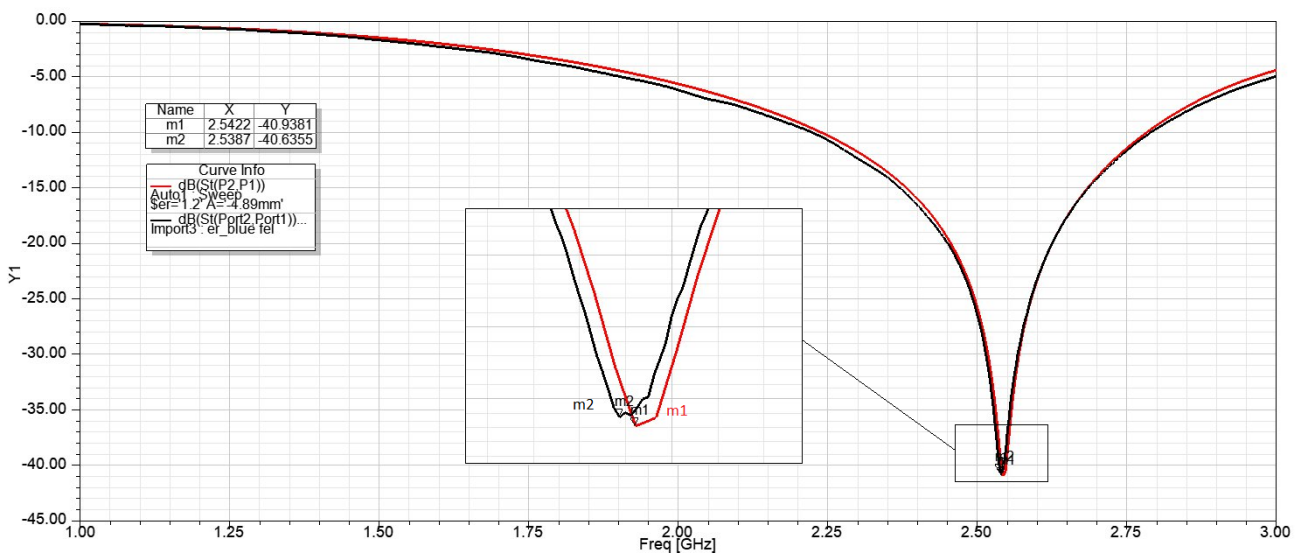


Figure 2-14. Measured (black trace) and simulated (red trace)  $S_{21}(dB)$  curves coincide.

Based on divergence of the measured and simulated results, an improved estimation of the complex permittivity of the substrate was made. In order to make the two curves coincide in terms of resonant frequency, the dielectric constant had to be set to  $\epsilon_r = 1.2$ . The value of the loss tangent was then adjusted to match the measured -40 dB absorption dip in the resonance frequency. Specifically, its value had to be decreased from  $\tan\delta_{ap} = 0.02$  to  $\tan\delta = 0.001$ . As seen in Figure 2-14, when a new simulation was carried out with these values for the permittivity and loss tangent, the two curves coincided.

It is important to note that these values were measured at approximately 2.54 GHz, instead of 2.5 GHz, which was the frequency of interest. However, it may be assumed that the dielectric constant and loss tangent will not change noticeably in the 2.5 - 2.54 GHz frequency

range, considering that felt is generally non-dispersive. In order to verify this hypothesis, a follow-up measurement was performed.

A new T-resonator was modeled at 2.5 GHz, assuming that the dielectric characteristics would not change from the measured results at 2.54 GHz. So, the expected values of the substrate's permittivity and loss tangent at 2.5 GHz are:

$$\epsilon_r=1.2, \tan \delta=0.001$$

In order to exhibit a  $50 \Omega$  impedance, the width of the new microstrip line and stub was calculated at 13.8 mm. According to the process described in section 0, the correction factor was set to  $A'' = 2.4 \text{ mm}$  which resulted to a 25.31 mm-stub, in order for the structure to resonate near 2.5 GHz.

A second T-resonator with the revised values for the permittivity and loss tangent was fabricated and measured, as well as simulated. The measured results of the T-resonator's  $S_{21}(dB)$  parameter, over the 1 – 3 GHz range can be seen in the following figure, along with the simulated results. The reviewed T-resonator structure displayed a  $-43.323 \text{ dB}$  resonance dip at 2.501 GHz. This also agreed with the simulated results, where the resonance was observed at 2.498 GHz with an amplitude of  $-39.303 \text{ dB}$ . In other words, the simulated and measured curves coincide, and therefore the measured dielectric characteristics of the felt substrate are accurate. The results also verify that the dielectric properties of the felt fabric are approximately the same in a small region near 2.54 GHz, where the initial measurement was realized.

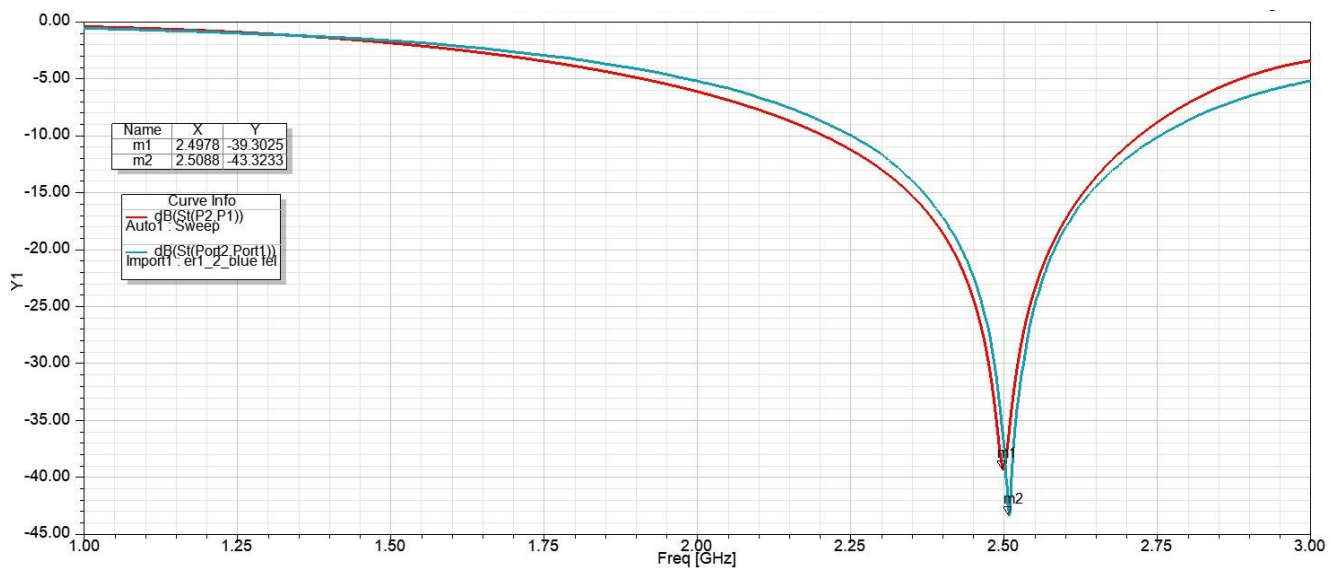


Figure 2-15. Reviewed permittivity T-resonator  $S_{21}(dB)$  parameter simulation (red trace) and measurement (blue trace).

### 2.3.2 Split-Post Dielectric Resonator Method

In order to determine the permittivity and dielectric loss of a substrate sample using split-post dielectric resonator method, two measurements are required. At first, a reference measurement must be conducted, with the cavity of the resonator being empty (unloaded). Afterwards, the sample will be placed in the air gap region of the cavity, and the measurement is repeated with the resonator being loaded.

By comparing the  $S_{21}(dB)$  curves of the two measurements (unloaded and loaded) the dielectric characteristics of the sample can be extracted. The sample's permittivity is determined by the frequency shift between the measurements of the empty and loaded states of the

resonator [3]. The value of the loss tangent can be extracted from the Q-factor, which is obtained by measuring the  $-3 \text{ dB}$  bandwidth of the  $S_{21}$  curve [14], according to the following formula:

$$\tan \delta = \frac{1}{Q} = \frac{BW_{-3dB}}{f_r} \quad (16)$$

Where,

$f_r$ : resonant frequency.

Last but not least, the sample's thickness must be taken into consideration for the accurate calculation of its dielectric properties, using the split-post dielectric resonator method.

### Measurement and results

While the frequency of interest is  $2.5 \text{ GHz}$ , limitations on the frequency of measurement were introduced by the dimensions of the SPDR's cavity. More specifically, the maximum thickness of the samples that could be measured by the split-post resonator that operated at  $2.45 - 2.5 \text{ GHz}$  is  $3 \text{ mm}$ . Since the felt substrate's thickness exceeded that value, an SPDR which operated at  $1.1 \text{ GHz}$  was used instead, as it was able to measure substrates as thick as  $6 \text{ mm}$ .

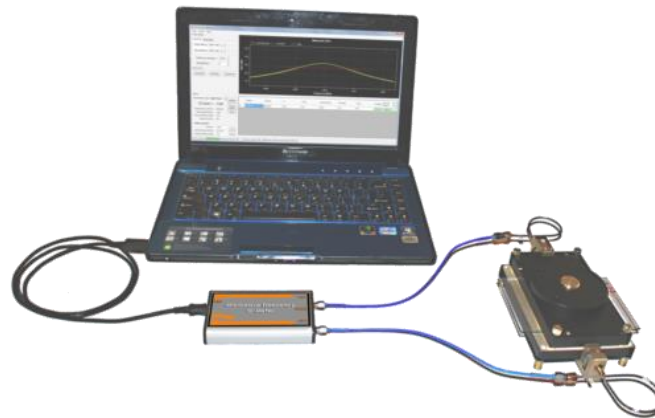


Figure 2-16. Microwave Frequency Q-Meter connected to the SPDR and to the computer [3].

A Q-meter was used for the measurements, which was connected to the resonator and a computer (Figure 2-16). A VNA could be used alternatively to provide higher accuracy of measurement. However, using a Q-meter ensures simplicity and lowers the overall cost of the measurement.

An unloaded measurement was carried out first. Afterwards, the felt sample was inserted in the air cavity of the resonator. By observing the changes of  $S_{21}(\text{dB})$  graph before and after inserting the sample, the permittivity and loss tangent of the sample can be extracted. More specifically, the change in the frequency of resonance provides insight to the permittivity of the sample. On the other hand, the value of the loss tangent can be determined from the change in the Q-factor, which is calculated from the ratio of the  $-3 \text{ dB}$ -bandwidth to the resonant frequency, as described in Paragraph 2.2.2.

The results for the permittivity and loss tangent of the  $3.2 \text{ mm}$ -thick blue felt, measured at  $1.1 \text{ GHz}$  can be seen below:

$$\varepsilon_r = 1.22, \tan \delta = 1.7 \cdot 10^{-3}$$

## 2.4 Conclusions

The results of the two electrical characterization methods for the 3.2 mm thick blue felt can be seen in the table below. The results are in agreement, despite the difference in the frequency of each measurement.

Method	Frequency	$\epsilon_r$	$\tan\delta$
T-resonator	2.5 GHz	1.2	$1 \cdot 10^{-3}$
SPDR	1.1 GHz	1.22	$1.7 \cdot 10^{-3}$

Table 2-1

Even though the SPDR method was much simpler and faster than the T-resonator method, the measurement could not be conducted on the desired frequency. On the other hand, the T-resonator method is more complicated, less accurate and requires the complete fabrication of the structure. Also, additional simulations must be carried out. However, the T-resonator structure can be designed to operate at the desired frequency.

Moreover, the T-resonator method does not require special equipment, as the whole structure can be fabricated from scratch, using simple materials/components. However, a VNA must be used for measuring the  $S_{21}(dB)$  parameter of the structure, while in the case of the SPDR a simple Q-meter can be used instead.

Lastly, contrary to the SPDR method, the T-resonator method is not suitable for electrically characterizing thinner fabrics, like cotton jersey or denim.

Both methods of electrical characterization realized in this chapter are convenient for the dielectric measurement of thick fabric samples, like felt, in discrete frequencies. Either the T-resonator method or SPDR method can be chosen for the electrical characterization of fabrics, based on the desirable frequency and accuracy of measurement. The thickness of the fabric sample as well as the available equipment also play a decisive role on the method of choice.

## References

- [1] A. Technologies, "Basics of Measuring the Dielectric Properties of Materials," Application Note2006.
- [2] L. F. Chen, C. K. Ong, C. P. Neo, V. V. Varadan, and V. K. Varadan, Microwave Electronics: Measurement and Materials Characterization, 2004.
- [3] P. A., "Body-Centric Wireless Communications: Wearable Antennas, Channel Modelling, and Near-Field Antenna Measurements," PhD, Loughborough University, National Center for Scientific Research "Demokritos", 2016.
- [4] G. Brodie, M. V. Jacob, and P. Farrell, "Techniques for Measuring Dielectric Properties," in Microwave and Radio-Frequency Technologies in Agriculture, 2015.
- [5] Permittivity. Available: <https://en.wikipedia.org/wiki/Permittivity>
- [6] Electrical resistivity and conductivity. Available: [https://en.wikipedia.org/wiki/Electrical\\_resistivity\\_and\\_conductivity](https://en.wikipedia.org/wiki/Electrical_resistivity_and_conductivity)
- [7] Permeability (electromagnetism). Available: [https://en.wikipedia.org/wiki/Permeability\\_\(electromagnetism\)](https://en.wikipedia.org/wiki/Permeability_(electromagnetism))
- [8] K. Technologies, "Split Post Dielectric Resonators for Dielectric Measurements," Application Note2017.
- [9] Dielectric loss. Available: [https://en.wikipedia.org/wiki/Dielectric\\_loss](https://en.wikipedia.org/wiki/Dielectric_loss)
- [10] S. Zhang, "Design advances of embroidered fabric antennas," PhD, Loughborough University, 2014.
- [11] K. P. Latti, M. Kettunen, J.-P. Strom, and P. Silventoinen, "A Review of Microstrip T-Resonator Method in Determining the Dielectric Properties of Printed Circuit Board Materials," IEEE Transactions on Instrumentation and Measurement, vol. 56, pp. 1845-1850, 2007.
- [12] J. Krupka, "Measurements of the complex permittivity of microwave circuit board substrates using split dielectric resonator and reentrant cavity techniques," vol. 1996, pp. 21-24, 1996.
- [13] M. Kirschning, "Accurate model for open end effect of microstrip lines," vol. 17, 1981.
- [14] electronicsnotes. Quality Factor / Q Factor; formulas and equations. Available: [https://www.electronics-notes.com/articles/basic\\_concepts/q-quality-factor/basics-tutorial-formula.php](https://www.electronics-notes.com/articles/basic_concepts/q-quality-factor/basics-tutorial-formula.php)

# Chapter 3 Embroidery Machine: Operating Parameters and Process Using Conductive Threads

## Abstract

The most significant parameters of the machine embroidery process will be introduced in this chapter. After briefly explaining the machine embroidery process, the distinctive characteristics of embroidery using conductive threads (e-textile embroidery) will be thoroughly discussed. While taking into account the cost and feasibility of fabrication, suggestions for optimal performance of several RF components, such as microstrip lines and patch antennas, will be presented.

## 3.1 Parameters of Machine Embroidery

The stitch pattern, direction of the stitches and stitch density are some of the most significant parameters of an embroidery design. Modern computerized embroidery machines offer a fast and convenient way of defining these parameters when generating embroidery designs. Accurate digitized embroidery designs can also be created on a computer using embroidery design software and then get imported on the machine for fabrication.

The embroidery machine used in this thesis is Brother PR670E, while all the embroidery designs were created in PE-Design Plus 2 software (referred to as PE-Design for the rest of the thesis), which is one of Brother's personal embroidery design software packages.

### 3.1.1 Stitch Patterns

Embroidery stitch patterns determine the path followed by the thread when creating a line or shape. The direction of the stitches is also specified by the stitch pattern [4]. The most commonly used stitch patterns are running stitch and satin stitch. Running stitch is created by passing the needle in and out of the fabric (i.e., needle punches) at a regular distance [7] (Figure 3-1). Running stitch is considered the building block of all other stitch designs, since they can be created by altering the length, spacing, and direction of the running stitch. Satin stitch is a simple zigzag pattern that is mainly used for covering large areas of the base fabric. The stitches are perpendicular to the stitching direction of the design, as seen in Figure 3-1.

Naturally, a line created using running stitch is as wide as the thread used for embroidering it. On the other hand, the width of a line created using satin stitch is equal to the stitch length, which is adjusted by the user (in the example of Figure 3-1 the width was set to 2 mm). The resulting line is much bolder than the running stitch line; hence this design is commonly used for filling shapes and creating dense designs. However, it is obvious that using a satin stitch to create a line requires a far larger number of stitches as well as thread length. As far as the running stitch is concerned, the stitch length (i.e., the distance between two consequent needle punches) can be manually selected.

Fill patterns are embroidery patterns used when embroidering a whole region, instead of a line. The fill stitch pattern (also known as contour pattern or tatami fill stitch) resembles a running stitch. The satin fill stitch looks like an enlarged satin stitch, whose width is usually equal the width of the object. However, when the object is very wide (like in the example of Figure 3-2), additional needle punches (black dots in Figure 3-2) of set length are made along the length of one line (split stitch). This way, the finished embroidery is sturdier, and threads are prevented from snagging. Last but not least, when using an embroidery design software, the direction of the stitches can be manually adjusted. In this example, the direction was set to 90°, which created vertical stitches.

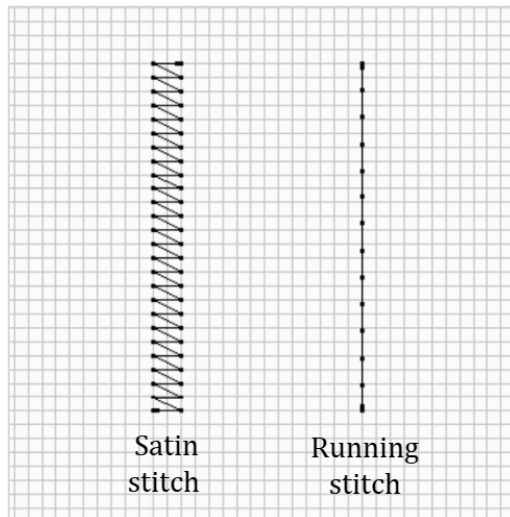


Figure 3-1. Example of a satin and running stitch line with a density of  $2 \text{ lines/mm}$ .

For the same density, the fill stitch pattern generally requires more stitches compared to satin stitch. In the example of the two rectangles of Figure 3-2, the number of stitches created when using the fill stitch pattern are almost three times the stitches needed for the satin stitch pattern. This is mainly due to the large stitch length of the split stitches. However, while in this case the number of the stitches for the satin stitch pattern is only a fraction of the stitches needed for the fill stitch; this is not always the case. The geometry and dimensions of the embroidery design, as well as the selected direction of stitches will determine the final number of stitches. Stitch length is an important factor in embroidery designs, since apart from the visual result; it may affect the durability of the embroidery. Lastly, a larger number of stitches lead to a greater amount of thread usage, which may significantly raise the cost. A way to decrease the stitch count of a fill stitch design could be choosing a larger stitch length. However, the fill stitch length is automatically set by the embroidery design software that was used in this thesis. Moreover, a larger stitch length could result in a messier and less defined embroidery.

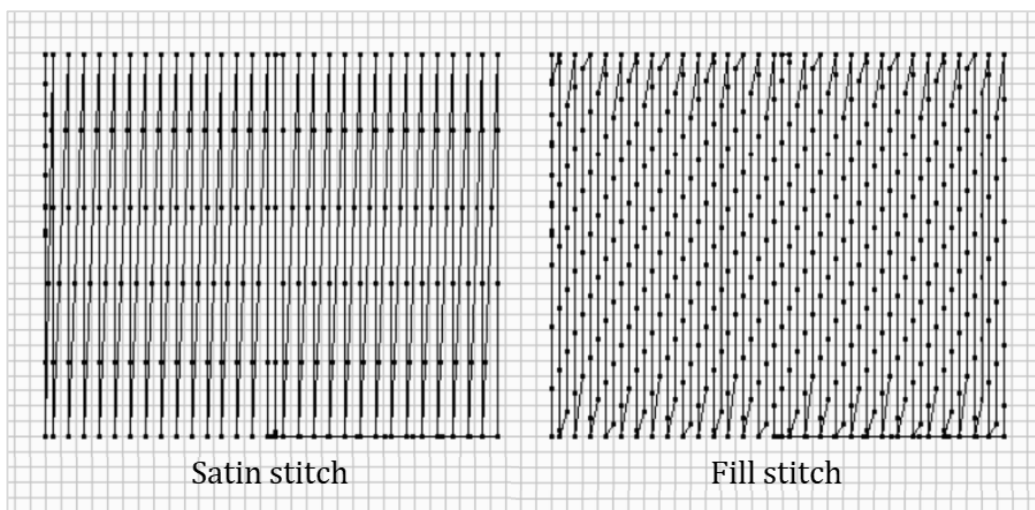


Figure 3-2.  $2 \text{ lines/mm}$ -density rectangles (without outline).

### 3.1.2 Stitch Density

Stitch density refers to the number of parallel threads over 1 mm and is measured in *lines/mm*. An example of two rectangles with different stitch densities can be seen in Figure 3-3. The stitch pattern used for the two rectangles is vertical satin fill stitch. Stitch spacing is an alternative parameter that refers to how densely stitched an embroidery design is. The stitch spacing value is the reciprocal of the stitch density. It is usually measured in *mm* and refers to the distance between two adjacent, parallel stitches.

It is obvious that higher density designs require more thread and provide a fuller, more solid shape. In less dense designs, a larger space separates adjacent stitches and the base fabric may be exposed.

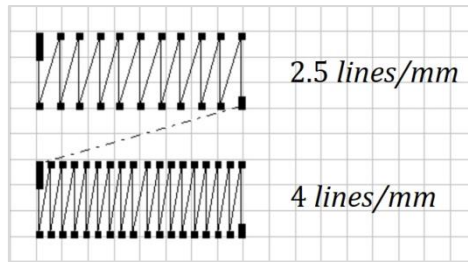


Figure 3-3. Satin stitch pattern with two different densities.

### 3.1.3 Under Sewing

Under sewing (widely known as underlay) refers to an embroidery pattern underneath the primary design and its main purpose is to minimize the amount of pull in the design (Figure 3-4), thus preventing the base fabric from puckering. It usually consists of a set of stitches perpendicular to the stitches of the primary design and gets embroidered first.

Underlay stitches elevate the stitches of the design and prevent them from sinking into the fabric. Therefore, under sewing serves as a foundation for the design. Using under sewing consequently leads to an improved design definition, at the expense of an increased stitch count, which corresponds to greater thread usage and fabrication duration [2, 8].

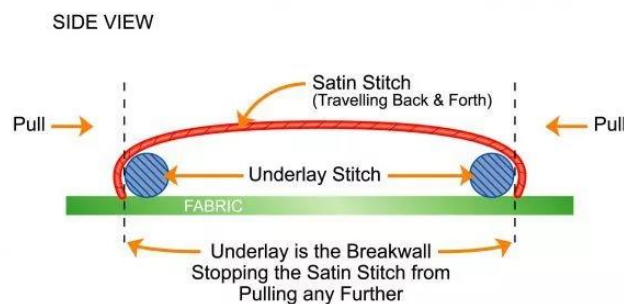


Figure 3-4. Under sewing example [2].

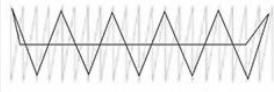
Underlay	Type
	Zigzag underlay
	Tatami underlay
	Edge Run underlay
	Center Run underlay

Figure 3-5. Common types of underlay [2].

There are a few under sewing types like zigzag, edge run, center run etc. (Figure 3-5). The optimal type of under sewing mainly depends on the shape of the primary design and the base fabric [2]. Most embroidery design software systems provide automatic under sewing. PE-Design also has an option for automatic under sewing, which is a combination of edge and center underlay. The underlay stitches are automatically embedded to the design and get embroidered first, for the design to get stitched on top of. The automatic under sewing gets created with the same thread used for design, and it's not possible to alter its characteristics.

### 3.2 Machine Embroidery Process Details

In the embroidery process followed by most personal embroidery machines (like the one used in this thesis); lockstitch is used to attach the embroidery thread onto the base fabric. This technique is also commonly used in sewing machines. Lockstitch requires a second, bottom thread (bobbin thread) besides the main thread (embroidery thread, which is also called top thread). The top thread runs through a tension system, take-up lever and finally the eye of the needle. On the other hand, the bobbin thread is wrapped on a bobbin which is placed inside a case at the bottom of the embroidery machine, underneath the frame that holds the base fabric, just below the needle [6] (Figure 3-6).

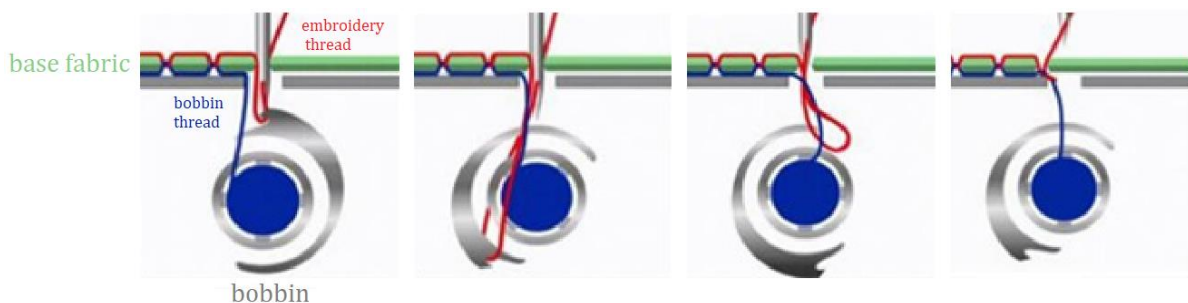


Figure 3-6. Process of lock stitch formation using an embroidery machine [6].

While embroidering, the needle moves up and down and pierces the base fabric, while the bobbin rotates counterclockwise, as displayed in Figure 3-6. After the needle penetrates the fabric and starts heading up, the top thread forms a small loop. At this point, the rotating bobbin grabs the loop and makes

it get wrapped around the unwound bobbin thread [4]. This way, the embroidery thread gets "locked" together with the bobbin thread in the hole of the base fabric created by the needle [9] (Figure 3-7).

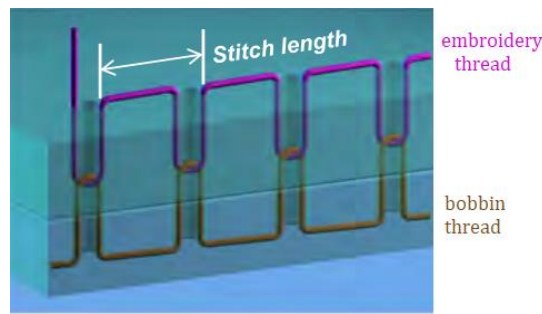


Figure 3-7. Cross section of base fabric with lock stitch [4].

As seen in the above figure, the length of the thread used to embroider a line is greater than the length of the line, since part of the top thread sinks into the fabric. The shape of the embroidery thread, including the visible part and the sunken part was modeled in [4]. According to this study, when embroidering a 10 cm long straight line, with a 2 mm stitch length, onto a 0.5 mm thick cotton base fabric, the extra length of thread is 52% of the designed length.

The interlacing between the top thread and the bobbin thread is supposed to be formed in the middle of the base fabric, as illustrated in Figure 3-7. However, this is not always the case. While it is optimal for the bobbin thread to not be visible from the top of the embroidery, sometimes due to the thread tensions, it is possible that the threads entwine at the top of the fabric and the bobbin thread gets exposed. On the other hand, if the top thread gets pulled down, the entwining could go through the fabric, to the bottom of the embroidery [10]. In both cases, the tensions of the top and bobbin threads must be adjusted.

### 3.3 E-textile Embroidery Details

E-textile embroidery commonly uses conventional computerized embroidery machines and conductive, as well as non-conductive threads to embroider textile circuits, antennas, or other electromagnetic components in an automated way [11]. In this section, several e-textile embroidery variables will be outlined, such as the types of conductive threads, conductive thread position on the embroidery machine, stitch patterns, direction, and density etc.

#### 3.3.1 Conductive Threads

Conductive threads (e-threads) are probably the most important parameter when it comes to e-textile embroidery. Conductive threads must be similar to wires, as far as the ability to carry current is concerned, while they should be flexible enough to be integrated into clothing. Moreover, the conductive threads should be suited to machine embroidery, meaning that they must not break or fray under significant tension [12].

A great variety of conductive threads are commercially available. Shieldex 117/17 2-ply (the name coding will be explained later in this section) was used in this thesis. While its conductivity is relatively low, it exhibits high flexibility and fraying is limited, compared to threads that have thicker conductive cladding and are therefore more conductive [3]. Thus, it is a worthy candidate for e-textile embroidery.

### Conductive Threads Parameters

The most common conductive threads available for machine embroidery fall into two main categories, based on the composition of their filaments; monofilament and multifilament conductive threads. While monofilament threads resemble a simple thin metal wire (Figure 3-8 (a)), multifilament threads usually include both conductive and non-conductive components (Figure 3-8 (b) and (c)). The stiff monofilament threads are seldom embedded in wearable structures since they are hard to embroider using an embroidery machine and they break easily. On the contrary, multifilament conductive threads, and especially polymer-based e-threads are more convenient for machine embroidery since they bear a closer resemblance to conventional embroidery threads [4].

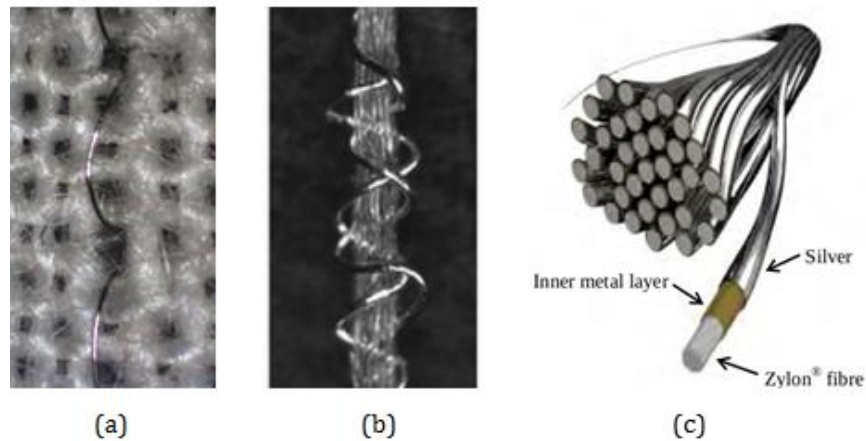


Figure 3-8. (a) Monofilament conductive thread, sewn on white fabric, (b) hybrid multifilament conductive thread with two conductive filaments wrapped around a conventional yarn, and (c) multifilament polymer-based conductive thread [4].

Generally, there are two types of multifilament threads. The first type, which is sometimes called hybrid or dual filament, consists of a non-conductive (conventional) thread with a single or multiple conductive wires coiled around it (Figure 3-8 (b)). The second type of multifilament threads is composed of a specific number of identical filaments, which are twisted together to form a strand. Each filament has a polymer core which is chemically coated with a metallic layer (Figure 3-10). The final thread results from twisting these flexible, yet conductive filaments together (Figure 3-8 (c)). This type of thread is the most commonly used for conductive embroidery as it combines electrical conductivity with mechanical strength and flexibility that resemble conventional threads the most [4].

A variety of metals can be used for the conductive layer of the filaments, like silver, copper, nickel etc. The type of metal, as well as the thickness of the metal layer will determine the conductivity of the multifilament thread, which will consequently play a significant role in the effective conductivity of the end embroidery pattern [6].

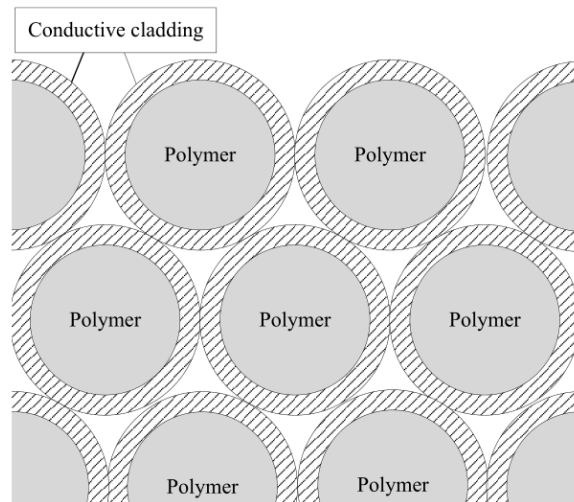


Figure 3-9. Cross section of the twined filaments of a conductive thread [4].

Electrical conductivity ( $\sigma$ ) is a measure of how well a material conducts an electric and is measured in  $S/m$ . Conductivity is the inverse to resistivity ( $\rho$ ), which describes how difficult it is to make electrical current flow through a material. Resistivity is measured in  $\Omega \cdot m$  (S.I.) and for a uniform piece of resistive material, it can be calculated as follows [13]:

$$\rho = R \frac{A}{l} \quad (17)$$

Where,

$R$ : electrical resistance of a uniform sample of the material,

$l$  : length of the sample, and

$A$ : cross-sectional area of the sample.

In the case of multi-filament conductive threads, their equivalent resistivity can be computed by measuring the DC resistance ( $R$ ) of a certain length ( $l$ ) of thread sample, and the cross-sectional area of the thread's conductive coating ( $A$ ). The equivalent conductivity can then be calculated. The value of the equivalent conductivity of the thread will always be less than the conductivity of the cladding, since only the outermost layer of the thread is metalized [4].

While threads with a thicker conductive layer tend to exhibit much higher conductivity, they lack in terms of embroiderability, since they resemble wires and thereby are thicker and stiffer. On the other hand, conductive threads with thinner coatings may bear a close resemblance to conventional threads, but their resistivity can be rather high [10]. While the trade-off between the conductivity and embroidery compatibility of the conductive threads is inevitable, the overall cost of the conductive threads must also be taken into account for any conductive embroidery application.

Except for the metal used for coating of the filaments, the multifilament threads are also characterized by the number of filaments which are twisted together. According to [4], embroidered microstrip lines that were created using threads with a larger number of filaments, exhibited reduced resistance and insertion loss. Based on this study, multifilament threads with more filaments had a favorable DC and RF performance.

Another commonly used parameter to characterize conductive yarns is linear density, measured in dtex. It is defined as the mass (in grams) of 10 km of yarn [14]. Linear density is widely used to describe conventional threads.

## Shieldex 117/17 Specifications

The conductive thread used in this thesis is Shieldex 117/17 dtex 2-ply (Figure 3-10). As the name suggests it is composed of two identical strands, entwined with 550 turns per meter, clockwise (S-twist). Each strand contains 17 identical filaments (Figure 3-12), twisted together with 620 turns per meter, counterclockwise (Z-twist), as seen in Figure 3-11. The yarn count of 117 dtex refers to one strand only, before the metallization process [15].

The core of each filament is Polyamide 6.6, a polymer which is popular for its mechanical strength and rigidity [16]. The conductive layer is made of 99% pure silver. According to the manufacturer's specifications the linear resistance of the thread doesn't exceed  $1500 \Omega/m$ .



Figure 3-10. Close up of the Shieldex 117/17 2-ply conductive thread [3].



Figure 3-12. Single yarn of Shieldex 117/17 [3].

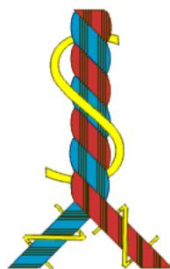


Figure 3-11. Twisting directions used for the Shieldex 117/17 2-ply thread [3].

### 3.3.2 Conductive Thread Position

In the case of conductive machine embroidery, the stiffness of the metal coating of the yarns can make the process challenging. The conductive threads easily get damaged, which could lead to demoted electrical performance. Also, potential breakage of the thread would delay the embroidery process, as well as increase the wastage of the conductive yarn. According to the embroidery process described in Paragraph 3.2, two separate threads participate in the embroidery process. The top thread goes through the needle after running through a complicated tension system and take-up lever. The bottom thread is simply placed on the rotating bobbin driver, at the bottom part of the embroidery region. Commonly both conductive and conventional threads are used in e-textile embroidery. The optimal conductive thread position will be discussed in this section.

The complicated tension system that the top thread goes through before going into the needle can damage the conductive thread, while the lock-stitch process can also be challenging (Figure 3-13). The thread gets bent when the needle pierces through the base fabric. Then, in order to form the lock stitch, the hook of the bobbin driver catches the top thread and draws it around the bobbin [10], as described in Paragraph 3.2. The speed of this process is generally high, but it can be adjusted by the user based on the embroidery machine's features. It becomes apparent that the top thread can get strained or even break through this process. On the other hand, the thread used for the bottom requires less mechanical strength and flexibility. Also, contrary to the top thread, the bobbin thread doesn't have to go through the eye of the needle, so friction is minimal.



Figure 3-13. Visualization of top and bobbin thread tensions [23].

Placing the thread in the bobbin (bottom) position, could prevent the thread from going through much strain and getting damaged. A conventional thread can be placed on the top position, like a cotton or polyester thread. It should be noted that in this case, the conductive embroidery will be created at the bottom of the base fabric. Different conductive thread placements for an embroidered dipole antenna were studied in [17]. According to this study, placing the conductive thread on the bobbin resulted in more robust embroideries, while impedance matching was also improved. However, placing the conductive thread on the bottom position requires threading the spool, which is difficult to do manually and is not always provided by the embroidery machine, so a separate machine should be used. Also, as opposed to the top position thread, the bobbin spool cannot hold a great amount of thread, so it needs frequent replacement. Even though the bobbin conductive thread placement has many benefits, it is advised not to choose this placement as it has proven inefficient for scaled production, according to [6].

Using conductive threads both for the top and bottom position was studied in [17] and the results were promising, as far as antenna performance is concerned. According to this study, the impedance matching and gain of the dipole antennas were satisfying and the embroidery design was robust. This placement also resulted in more dense embroidery designs, which could offer better conductivity, as will be discussed later in this chapter. Nevertheless, when using conductive threads for both top and bobbin

position, the friction between the two stiff threads gets very high and leads to extensive knotting and fraying. Thus, the breakage of the threads may occur multiple times while embroidering. These stitching errors will greatly increase the manufacturing duration, as the embroidery machine must be stopped, re-threaded and resumed to the point of the design where the threads broke [6]. It is evident that such a choice of conductive thread placement lacks practicality. Also, using conductive threads for the top and bottom position simultaneously would greatly increase the conductive thread usage and consequently the manufacturing costs, compared to embroidering using both conductive and non-conductive threads.

Placing the conductive yarn on the top position is common in conductive embroidery design. Using a conventional thread at the bobbin and a conductive thread on top is more convenient than other thread placements. When utilizing a computerized embroidery machine, the parameters of the embroidery design refer to the top thread. Also, the large industrial cone that the conductive thread comes in from the manufacturer can be directly placed on the top position of the embroidery machine, contrary to the bobbin which can only hold a limited amount of thread.

It was mentioned earlier that the mechanical demands for the top thread are much higher than for the bobbin thread. The stiffness of the conductive threads will pose limitations on the fabrication of e-textile embroideries, especially when used as the top thread. Lubricating the conductive threads will significantly aid the embroidery process. Some conductive threads come pre-lubricated, but the use of an additional lubricant may aid the smooth embroidery process. Still, operating the embroidery machine at low speed is usually essential for embroidery using conductive threads, even if they have been lubricated.

While all of the conductive thread placements have their traits, the trade-off between the performance of the given RF component and the large-scale production costs must be considered when making the final choice. For instance, the performance of dipole antennas with various combinations of different embroidery parameters was studied in [17]. While placing the conductive thread only on the top position was recommended in [6], in this case it proved to be the least effective placement of all. Finally, it is important to keep in mind that the use of different embroidery equipment and materials could also affect the embroidery process and performance, and consequently lead to diverse conclusions.

### 3.3.3 Stitch Pattern and Direction

The stitch pattern and direction of the stitches are probably the most significant characteristics of a conductive embroidery design. Many studies suggest that in conductive embroidery, the current prefers to follow the direction of the stitches instead of jumping between adjacent threads. The resistance that the current meets while trying to jump between adjacent threads further increases when the space between adjacent stitches (i.e., stitch spacing) is larger, as adjacent fibers sparsely touch each other or inductive coupling very weak [18].

The fact that the current mainly flows in direction of the stitches has been reported by many studies. The effect of the stitch pattern and orientation on the DC resistance and RF performance of embroidered microstrip transmission was examined lines in [4]. The transmission lines with stitches parallel to the direction of the current (parallel fill stitch pattern) had lower DC resistance, compared to the lines with perpendicular stitches (perpendicular satin stitch pattern). Consequently, the electrical equivalent models of transmission lines with parallel and perpendicular stitches were also presented based on the assumption that the current path between consequent stitches exhibited lower resistance than the path between adjacent stitches. Moreover, the parallel stitch direction optimized the RF performance of the transmission lines. Microstrips that were embroidered using satin stitch, which was perpendicular to the current direction, had relatively low losses. However, microstrips that consisted of parallel stitches had a better performance in terms of losses.

Apart from microstrip lines, embroidered rectangular microstrip patch antennas were also studied in [4], as far as the optimal stitch pattern and orientation is concerned. Assuming that the current prefers the path of the stitches, a patch antenna was modeled as a continuous zig-zag conductor. This conductor represented the stitches along the stitch direction, separated by lower conductivity sections that played the role of the contact between adjacent stitches. The simulation results correlated the measurements of the patch and verified that the current preferably follows the path of the stitches.

Seager et al. investigated the effect of stitch direction on embroidered patch antennas which operated at low GHz frequencies, in [19]. The results indicated that when the direction of the stitches was parallel to the major current, the antennas had better efficiencies [19]. Moradi et al. studied the effect of the stitch pattern on embroidered dipole-type RFID tag antennas (Figure 3-14) and deduced the same conclusion [20]. Dipole antennas were embroidered with different stitch patterns and their performance was compared in [21]. The dipole antennas which were embroidered with the fill stitch pattern along the current direction, exhibited better measured return loss. This improved the quality factor of the fill stitch antenna compared to the satin stitch antenna, where the stitches were perpendicular to the current flow direction.

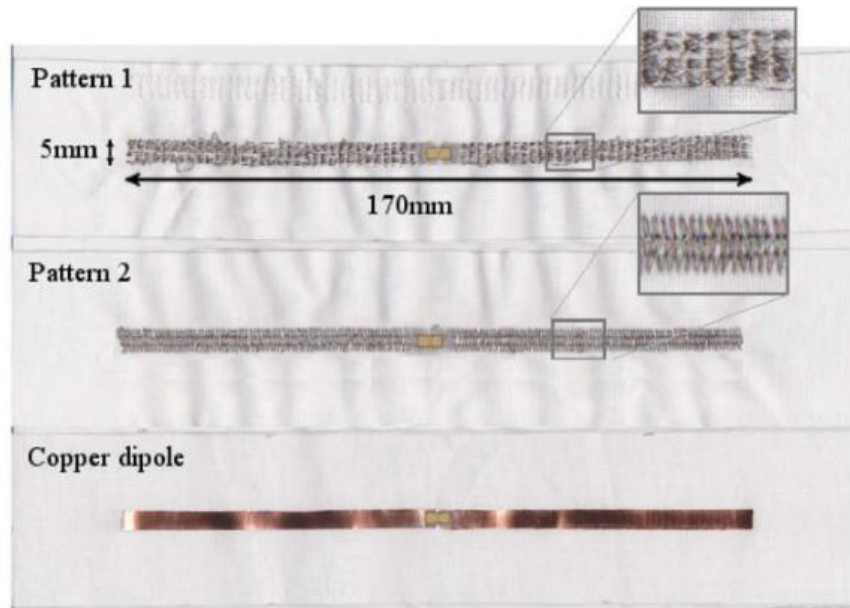


Figure 3-14. Embroidered dipole type RFID tag antennas with different embroidery patterns, along with copper reference antenna on base fabric [20].

Roy et al. carried out an investigation on the performance of a higher order mode circular patch antenna that was embroidered using different stitch patterns in [18]. When operating at a higher mode, the embroidered antenna exhibited a very complicated current distribution. Since the current was assumed to follow the stitch direction, a complex embroidery design that imitated the route followed by the current of the investigated mode was created digitally. The embroidered circular patch with the complex stitch pattern was then measured and compared to embroidered patches of the same dimensions, but with simpler stitch patterns. Perpendicular and parallel fill stitch patterns were embroidered with two different stitch densities and compared with the complicated embroidery pattern, in terms of the antenna's measured performance. The radiation pattern of the patch with the complicated pattern more accurately resembled the radiation pattern of the etched copper antenna, compared to the parallel and perpendicular fill stitch antennas with high stitch density. However, the vertical stitch pattern with very high density had better results in terms of gain and antenna efficiency. Even though the vertical and horizontal stitched antennas lacked in polarization purity and required more thread consumption, the study suggested that they were adequate substitutes for the complicated stitch pattern embroidered antenna [18]. Even though for the examined case the complex stitch pattern proved impractical, in cases with simpler current distribution this approach could possibly lead to high performance antennas. The measured results of this study also verified the fact that the current tends to flow along the direction of the stitches.

The effect of the stitch pattern and direction on the resonant frequency of embroidered antennas has also been investigated. The embroidered microstrip patch antennas that were fabricated in [4]

resonated in lower frequencies when the stitches were horizontal and diagonal, compared to the antenna with the vertical stitch pattern. It was suggested that the lowered resonant frequencies could be a consequence of increased capacitance and inductance caused by the elongated current paths, as well as the anisotropic surface of the base fabric. Gil et al. also observed that there was a frequency shift towards lower frequencies, which was more significant for embroidered dipole antennas with fill stitch pattern, compared to the ones with satin stitch. While the quality factor of the fill stitch pattern antenna was better, the satin stitch created a more accurate embroidery design in terms of dimensions and thus the resonance frequency was more accurate [21].

The effect of the stitch direction on the polarization of a rectangular patch antenna was investigated in [4]. Three embroidered rectangular patch antennas, which differed only in the direction of the stitches, were fabricated; one with perpendicular, one with parallel and one with diagonal stitches relative to the major current direction (Figure 3-15), i.e., along the length of the patch. The polarization purity of the patch with the parallel stitches was lower than the etched patch antenna with the same dimensions, though it had the highest polarization purity among the embroidered antennas. The patch with the perpendicular stitches had weaker polarization purity, while the polarization purity of the patch with the diagonal stitches was significantly worse. Both the perpendicular and diagonal stitches distorted the flow direction of the major current; however, the diagonal threads of the latter caused the current to flow in both vertical and horizontal directions almost equally. This caused the horizontal and vertical components of the polarization to have similar magnitudes, hence the polarization purity was diminished [4].

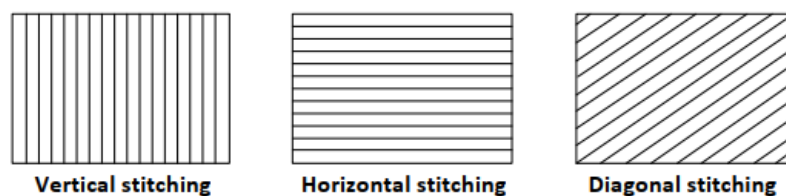


Figure 3-15. Vertical, horizontal, and diagonal stitch directions for embroidered rectangular patch antennas [4].

### 3.3.4 Stitch Density

High stitch density in e-textile embroidery designs is generally favorable since the embroidery becomes more solid and better resembles a sheet metal structure. However, the high price of conductive threads has led to investigations on how to achieve acceptable performance of embroidered RF components, while reducing the consumption of threads. The results of several studies concerning the way the stitch density affects the performance and characteristics of embroidered RF components will be presented in this section. Alternative low density stitch patterns will also be discussed.

The effect of stitch density on the embroidered rectangular patch antennas was thoroughly inspected in [4]. When the stitches became sparser the frequency of the embroidered patch antennas shifted down compared to a conventional copper patch of the same dimensions. The dimensions of higher density embroidery designs are generally closer to the initial model. Sparser stitches in a design may fail to produce the intended dimensions due to inaccuracies caused by the embroidery machine and different tensions produced by the stitches that may deform the base fabric. Higher gain and efficiency antennas were also produced when high stitch densities were deployed. Moreover, antennas with higher stitch densities exhibited improved repeatability of gain and efficiency, which is essential for large scale production. It becomes apparent that as far as antenna performance is concerned, the higher the stitch density, the closer the results to the solid patch antenna. However, denser designs require more thread usage [4]. The high prices of the conductive threads inevitably lead to a trade-off between increasing antenna efficiency and lowering production cost.

The performance of embroidered dipole-type RFID tag antennas with different stitch densities was examined in [20]. According to this study, the differences between conventional copper and

embroidered tag antennas come down to conductivity. The equivalent conductivity of the antenna is determined by the conductivity of the fibers, the stitch pattern and direction, the density of the stitches etc. The results indicated that increasing the stitch density did not always increase the equivalent conductivity of the embroidered antennas. If the stitch pattern is not chosen to comply with the current paths, increasing stitch density may not improve the performance of the antenna or even have a negative effect on the overall conductivity of the embroidery, due to unexpected losses between tightly stitched threads.

The same behavior was also observed in [5], where six tag antennas were embroidered using satin stitch but with different stitch densities, ranging from 2550 stitches, down to 225 stitches per antenna (Figure 3-16). The antennas' read ranges were measured and compared, while a copper dipole of the same dimensions was used as reference. The results are displayed in Figure 3-17. The read ranges of the tag antennas did not change significantly even when the density became 10 times smaller than the maximum density. Indeed, since the stitches are perpendicular to the current route direction, increasing the stitch density did not improve the performance of the tag antennas. The performance of sparser embroidery patterns proved to not be much worse than high density patterns, while thread usage was significantly lower. Last but not least, the measured read ranges are all acceptable even though the stitch pattern was not optimal.

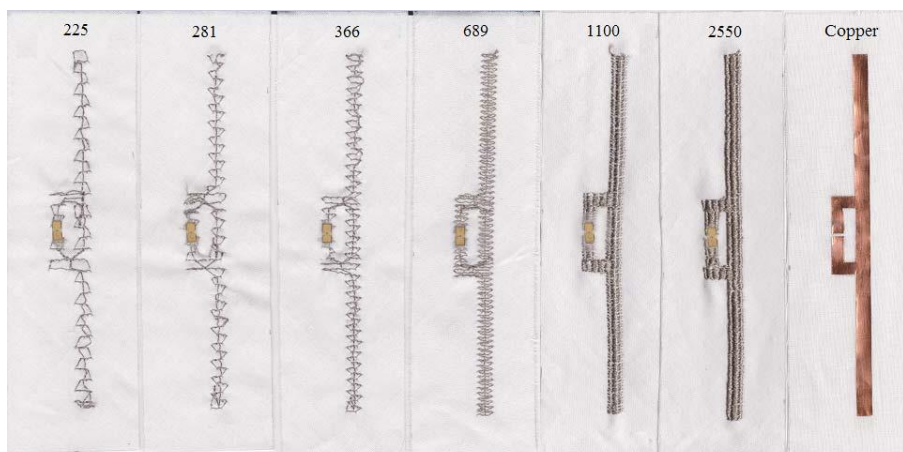


Figure 3-16. Embroidered tag antennas with different densities 9 [5].

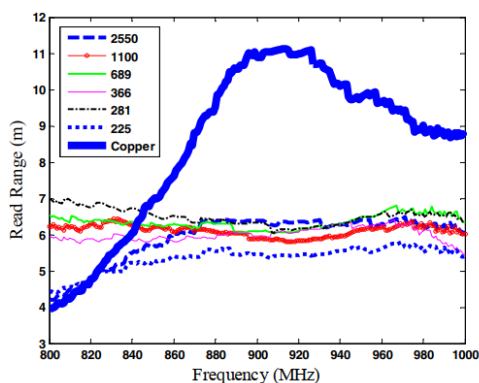


Figure 3-17. Read range of embroidered tag antennas with different stitch densities 9 [5].

Embroidered tag antennas were also studied in [22]. This study presented a way to achieve good antenna performance, while limiting the material usage and production cost. This was achieved by increasing the density of the stitches only in the regions of the antenna where the current density is high (Figure 3-18). The other parts of the antenna may be embroidered sparsely in order to save on conductive thread consumption. A more extreme approach was to only embroider the outline (contour) of the tag antenna (Figure 3-18 E). The results for both these models were promising, as the measured read ranges were very satisfying compared to the copper tag antenna. Although the peak of the frequency range was observed lower in the frequency spectrum for the contour antenna, its performance is satisfying. While the contour embroidered tag antenna minimized the consumption of thread and the duration of the embroidery process, the tag antennas with high and low stitch density regions offered a very attractive solution for high performance embroidered tag antennas with reduced fabrication cost.

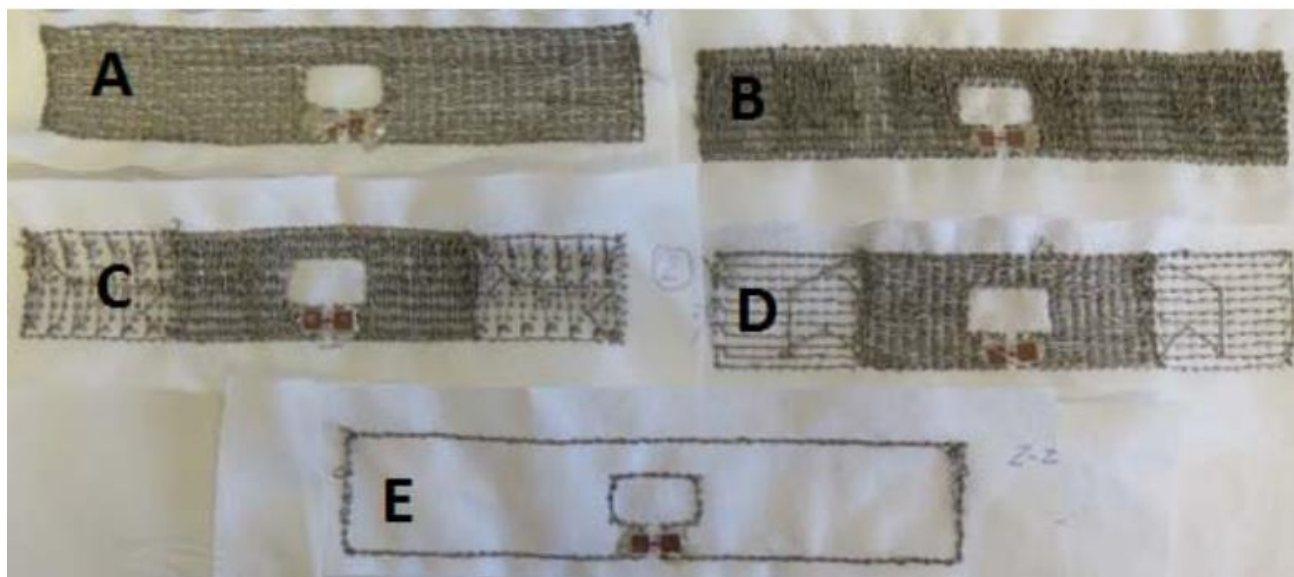


Figure 3-18. Embroidered antennas with: A – full horizontal stitching, B – full vertical stitching, C – partial vertical stitching, C – partial horizontal stitching, E – contour stitching [22].

With the intention of reducing thread, fabrication cost and duration of embroidered microstrip patch antennas, Zhang proposed non-uniform meshed structures in [4]. The idea behind the non-uniform patch is based on the assumption that the vertical conductor paths of a meshed patch antenna are more significant for the  $TM_{01}$  mode operation. Instead of a meshed patch antenna with the same number of vertical and horizontal lines, the number of horizontal lines is greatly reduced in the case of the non-uniform rectangular patch antenna. For the first mode operation, the current mainly flows in the vertical direction of the patch, removing some of the horizontal lines of the meshed patch reduces the metal area coverage, as well as the cost of the antenna without reducing the gain significantly. While the frequency shifts down because of the meshes in the uniform meshed patch, this effect is reduced with the removal of horizontal lines while keeping the same mesh space for the vertical lines. An example of the non-uniform patch design that includes only three horizontal lines is displayed in Figure 3-19. Except for the top and bottom horizontal lines, the third line that crosses the feeding point of the antenna was also kept to provide a current path from the feed point towards all the vertical lines.

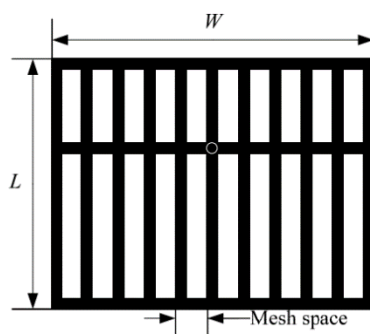


Figure 3-19. Non-uniform mesh patch antenna design [4].

Simulations and measurements of etched copper meshed patches revealed that reducing the lines that are orthogonal to the major current direction did not affect the performance of the antennas. An embroidered non-uniform mesh patch was then fabricated and measured. The embroidered patch only had two horizontal lines, which outlined its shape (Figure 3-20) [4]. The base fabric (denim) with the embroidery was attached on felt and copper tape was used for the ground plane. While the cost of the materials was reduced by approximately 80%, the measured efficiency reached a satisfactory 60%. This sparsely embroidered patch also has a very simple design that reduces fabrication time and is more flexible than densely stitched patches [4].



Figure 3-20. Embroidered non-uniform, meshed microstrip patch antenna [4].

Embroidered mesh antennas were also studied in [1]. In this study, the stitch density of a fully textile planar inverted-F antenna (PIFA) was investigated. A uniform mesh patch was embroidered on fleece. The stitch spacing (mesh size) was equal to approximately  $\frac{\lambda}{50}$ . However, the outline of the patch was densely stitched since the current density is maximized at the edges of the patch. The same stitch pattern was used for embroidering the ground plane (Figure 3-21). This antenna was measured both in free space and in the presence of a human body phantom. The measured input impedance was similar to the input impedance of the metallic meshed patch with the solid ground plane that had the same resonant frequency. Based on the measured results, for frequencies around 2.4 GHz, the meshed ground plane provided sufficient isolation even when the phantom was added. The radiation characteristics of the fully textile PIFA were comparable to the metallic prototype.

The aforementioned study also suggested that the reduction in frequency met in embroidered antennas is mainly due to the lockstitch structure that increases the electrical length of the antenna. It was confirmed that when the actual length of the thread was almost 10 % longer than the visible thread of the embroidery, the size of the patch had to be reduced by the same percentage, compared to the solid metal patch, in order to operate in the desired frequency.

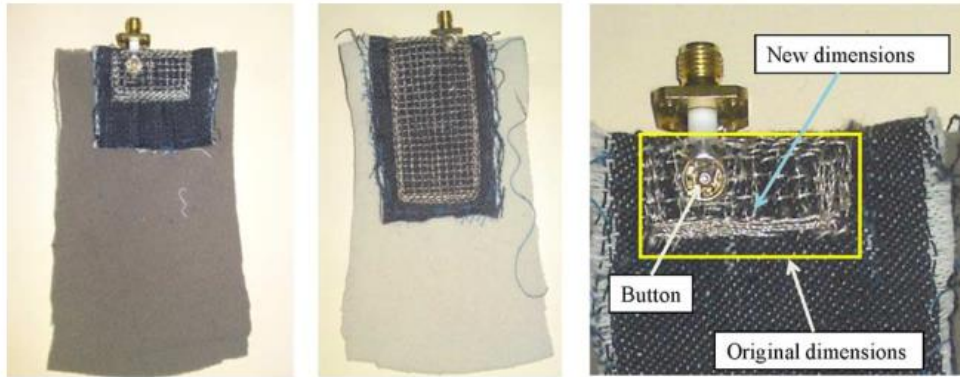


Figure 3-21. Embroidered mesh patch antenna on denim [1].

While the reduction of the thread density has been an overriding concern for embroidered antennas, when embroidering an antenna with a very complex current distribution, choosing a simple stitch pattern with very high density is advised in [18], as mentioned in the previous section. In order to achieve the desired radiation, the density must be high enough for the adjacent threads to be connected. The closely stitched conductive threads provide the complex paths for the current to flow in, even if some paths are more electrically resistant. It is interesting to notice that according to this study, the connection between adjacent stitches is critical for the performance of the antenna.

### 3.3.5 Under Sewing

Under sewing is an essential part of machine embroidery. However, its role in conductive thread embroidery designs has not yet been investigated. It has become clear that e-textile embroidery is challenging because of the stiffness and reduced elasticity of the conductive fibers. Apart from frequent stitching errors, accurate embroidery design dimensions are not easy to accomplish, due to the high tensions produced by the metallic threads. Adding under sewing in a conductive embroidery design could possibly prevent some stitching errors, while ensuring correct pattern dimensions.

However, as mentioned at the beginning of this chapter, under sewing stitches are usually perpendicular to the stitches of the embroidery design. Since it is considered optimal for the stitch direction to follow the direction of the major current, adding underlay stitches perpendicular to said direction could have a negative effect to the DC and RF performance of the structure [4]. For example, embroidered microstrip lines exhibited higher DC resistances and higher insertion loss in [4], when their stitches were perpendicular to the direction of the current, compared to when they were embroidered using parallel stitches. In the same project, embroidered microstrip patch antennas with stitches parallel to the major current direction had higher efficiencies than the microstrip patches that were embroidered with perpendicular stitches. At the same time, adding perpendicular stitches to the design would increase the conductive thread consumption. Last but not least, including conductive under sewing to the primary design would decrease the flexibility of the embroidery, but at the same time it would make the design more robust.

Later in this thesis, in an attempt to reduce the amount of conductive thread while ensuring high design definition and accurate dimensions, an under sewing pattern will be manually designed and embroidered using conventional threads.

### 3.3.6 Base Fabric

The base fabric is another important parameter of e-textile embroidery. This fabric should ideally have dielectric properties that are as close as possible to air.

Cotton and denim fabrics are most commonly used for embroidery, as they provide a sturdy but also soft base for the embroidery designs. Eike et al. recommend medium-weight cotton twill fabric for fabricating embroidered dipole antennas [6]. Gil et al. compared the performance of dipole antennas with satin and fill stitch patterns on two different base fabrics; a cotton woven fabric and a polyester felt fabric [21]. Their properties are presented in the table below. While their dielectric constants are similar, the loss tangent and height differ significantly. Dipole antennas designed using both satin and fill stitch patterns had better efficiencies when embroidered on felt. Indeed, the very low loss tangent of felt makes it a very attractive choice for conductive embroidery. However, felt substrates are generally thicker than other fabrics. Thus, when embroidering on felt, the electrical length will be greatly increased, along with the thread consumption and fabrication cost. According to [11] organza is another great choice of base fabric. Its dielectric characteristics are close to those of air, while it is a lightweight and flexible fabric.

	$\epsilon_r$	$\tan\delta$	$h$ (mm)
Cotton	1.3	0.058	0.4
Felt	1.2	0.0013	1

Table 3-1

## References

- [1] B. Ivsic, D. Bonfacic, and J. Bartolic, "Considerations on Embroidered Textile Antennas for Wearable Applications," *IEEE Antennas and Wireless Propagation Letters*, vol. 12, pp. 1708-1711, 2013.
- [2] What are Underlay Stitches for Embroidery & Digitizing? Available: <https://www.digitizingmadeeasy.com/understanding-underlay-stitches-for-machine-embroidery-digitizing/>
- [3] Shieldex® 117/17 x2 Datasheet. Available: <https://www.shieldex.de/en/products/shieldex-117-17-x2/>
- [4] S. Zhang, "Design advances of embroidered fabric antennas," PhD, Loughborough University, 2014.
- [5] E. Moradi, "Characterization of embroidered dipole-type RFID tag antennas," Tampere University of Technology, 2012.
- [6] R. J. Eike, "Technical considerations and specifications for conductive machine embroidery," *Trends in Textile Engineering and Fashion Technology*, vol. 6, 2020.
- [7] Straight stitch. Available: [https://en.wikipedia.org/wiki/Straight\\_stitch](https://en.wikipedia.org/wiki/Straight_stitch)
- [8] How to choose the right underlay for your machine embroidery designs? Available: <https://blog.hatchembroidery.com/how-to-choose-the-right-underlay-for-your-machine-embroidery-designs/>
- [9] Lockstitch. Available: <https://en.wikipedia.org/wiki/Lockstitch>
- [10] L. Torsten, "Analysis of Failure Mechanisms of Machine Embroidered Electrical Contacts and Solutions for Improved Reliability," PhD, Ghent University 2011.
- [11] A. Kiourti and J. Volakis, *Wearable Antennas and Electronics*, 2022.
- [12] A. Chauraya, S. Zhang, W. Whittow, T. Acti, R. Seager, T. Dias, et al., "Addressing the challenges of fabricating microwave antennas using conductive threads," pp. 1365-1367, 2012.
- [13] Electrical resistivity and conductivity. Available: [https://en.wikipedia.org/wiki/Electrical\\_resistivity\\_and\\_conductivity](https://en.wikipedia.org/wiki/Electrical_resistivity_and_conductivity)
- [14] Units of textile measurement. Available: [https://en.wikipedia.org/wiki/Units\\_of\\_textile\\_measurement](https://en.wikipedia.org/wiki/Units_of_textile_measurement)
- [15] C. Loss, "Study of the Electromagnetic Properties of Textiles: Development of Textile Antennas for Energy Harvesting," PhD, 2017.
- [16] Nylon 66. Available: [https://en.wikipedia.org/wiki/Nylon\\_66](https://en.wikipedia.org/wiki/Nylon_66)
- [17] D. Agu, R. J. Eike, A. Cliett, D. Michaelson, R. Cloud, and Y. Li, "Investigation of e-textile dipole antenna performance based on embroidery parameters," *Textile Research Journal*, p. 004051752110134, 2021.
- [18] R. B. V. B. Simorangkir, Y. Yang, and K. P. Esselle, "Performance of embroidered higher-order mode antennas with different stitching patterns," pp. 177-180, 2017.
- [19] R. Seager, S. Zhang, A. Chauraya, W. Whittow, Y. Vardaxoglou, T. Acti, et al., "Effect of the fabrication parameters on the performance of embroidered antennas," *IET Microwaves, Antennas & Propagation*, vol. 7, pp. 1174-1181, 2013.
- [20] E. Moradi, T. Bjorninen, L. Ukkonen, and Y. Rahmat-Samii, "Effects of Sewing Pattern on the Performance of Embroidered Dipole-Type RFID Tag Antennas," *IEEE Antennas and Wireless Propagation Letters*, vol. 11, pp. 1482-1485, 2012.
- [21] I. Gil, R. Fernández-García, and J. A. Tornero, "Embroidery manufacturing techniques for textile dipole antenna applied to wireless body area network," *Textile Research Journal*, vol. 89, pp. 1573-1581, 2018.
- [22] J. Virkki, X. Chen, T. Bjorninen, and L. Ukkonen, "Embroidered antennas and antenna-electronics interfaces for wearable RFID tags," pp. 1-3, 2017.
- [23] Wonderfil. Available: <https://www.wonderfil.ca/blog/comparing-hand-embroidery-thread-weights-12wt-8-5-3/8/28/2019-28esw-j7dwt-mfk88>

## Chapter 4 Embroidered Microstrip Transmission Lines

### Abstract

In this chapter, embroidered microstrip transmission lines were designed, fabricated, and measured, in order to evaluate different embroidery patterns in terms of transmission losses and thread consumption. The conclusions from this study will then be used for the development of the feedline of the textile antennas, but also for creating the embroidery designs of the antenna itself.

Fill stitch pattern with stitches parallel to the direction of the current was used for all the embroidered lines. Three different stitch densities (1.3, 2.5 and 4 *lines/mm*) will be examined for the embroidery designs of the microstrip lines. For each density, three microstrip lines were embroidered, each with a different under sewing alternative (non-conductive, conductive, and no under sewing). In order to reduce the number of variables, a standard rigid microwave substrate (FR4) was used for the embroidered microstrips, and no soldering was applied for the connection of the SMA connectors to the ends of the embroidered microstrip. A copper sheet transmission line was also created using the same base fabric and substrate, to serve as reference.

### 4.1 Design, Fabrication and Measurement of Copper Microstrip Line

A conventional microstrip line on rigid substrate was designed and simulated at first, to be used as reference. The characteristic impedance of a microstrip line is dependent on the width of the microstrip ( $W$ ), as well as the height ( $h$ ) and the effective permittivity ( $\epsilon_{eff}$ ) of the dielectric substrate. More specifically, the characteristic impedance ( $Z_0$ ) can be calculated from the following equation:

$$Z_0 = \begin{cases} \frac{1}{\sqrt{\epsilon_{eff}}} 60 \ln \left( \frac{8h}{W} + \frac{W}{4h} \right), & \text{for } \frac{W}{h} \geq 1 \\ \frac{1}{\sqrt{\epsilon_{eff}}} \frac{120\pi}{\frac{W}{h} + 1.393 + 0.677 \ln \left( \frac{W}{h} + 1.444 \right)}, & \text{for } \frac{W}{h} \leq 1 \end{cases} \quad (18)$$

Where  $\epsilon_{eff}$  is the effective permittivity, which expresses the equivalent permittivity of a homogeneous medium, which could replace the air above the microstrip and the dielectric substrate [1]. It can be calculated using the following formula:

$$\epsilon_{eff} = \frac{\epsilon_r + 1}{2} + \frac{\epsilon_r - 1}{2} \frac{1}{\sqrt{1 + 12h/W}} \quad (19)$$

Where,

$\epsilon_r$ : permittivity of the substrate.

In order to design a microstrip line with characteristic impedance equal to  $50 \Omega$ , the width of the microstrip can be calculated from the characteristics of the substrate, based on the next equation.

$$\frac{W}{h} = \begin{cases} \frac{8e^A}{e^{2A} - 2}, & \text{for } \frac{W}{h} < 2 \\ \frac{2}{\pi} \left( B - 1 - \ln(2B - 1) + \frac{\epsilon_r - 1}{2\epsilon_r} \left( \ln(B - 1) + 0.39 - \frac{0.61}{\epsilon_r} \right) \right), & \text{for } \frac{W}{h} > 2 \end{cases} \quad (20)$$

Where:

$$A = \frac{Z_0}{60} \sqrt{\frac{\epsilon_r + 1}{2}} + \frac{\epsilon_r - 1}{\epsilon_r + 1} \left( 0.23 + \frac{0.11}{\epsilon_r} \right) \quad (21)$$

$$B = \frac{377\pi}{2Z_0\sqrt{\epsilon_r}} \quad (22)$$

Based on the characteristics of the FR4 substrate that would be used for fabrication, a substrate of dielectric constant equal to  $\epsilon_r = 4.4$  and loss tangent equal to  $\tan\delta = 0.02$  was designed using ANSYS HFSS. The width and length of the substrate were set to 3 cm and 10 cm respectively. The thickness of the substrate's copper ground plane was 35  $\mu\text{m}$ . Since the height of the substrate was 1.6 mm, the width of the copper line was set to 3 mm, according to the above equations. The length of the line was designed to be equal to the length of the substrate, so that two SMA connectors can be connected on the two open ends of the line. A 70  $\mu\text{m}$ -thick copper tape was used for fabricating the line. The SMA connectors used for feeding the line were also included on the HFSS design, as seen in Figure 4-1.

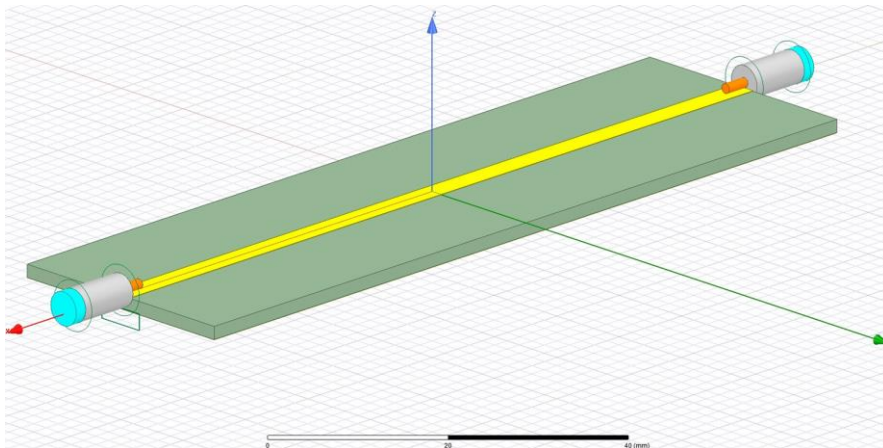


Figure 4-1. HFSS model of copper microstrip line on FR4 substrate.



Figure 4-2. Prototype of reference copper microstrip line.

Figure 4-3 shows the measurement set-up, with the fabricated reference copper microstrip line. The two ports of a Vector Network Analyzer (VNA) were connected on the SMA connectors, which were soldered on the open ends of the transmission line. The VNA was also connected to a computer, where the measurement results were illustrated. The results for the  $S_{21}(dB)$  parameter over the 2 – 3 GHz frequency range can be seen on Figure 4-4.



Figure 4-3. Microstrip line measurement set-up.

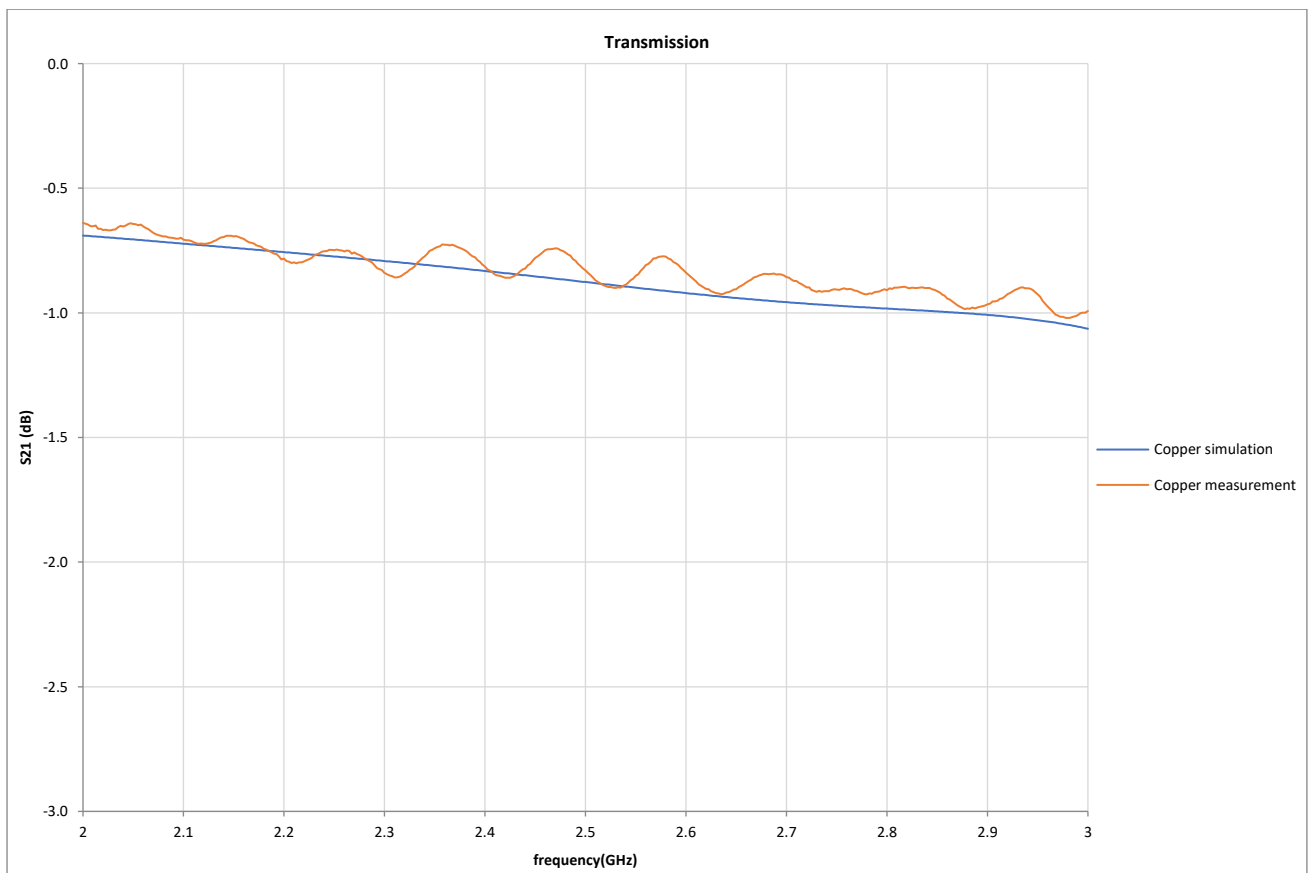


Figure 4-4. Simulated and measured  $S_{21}(dB)$  parameter of reference copper transmission line.

The objective of this chapter is to evaluate different stitch patterns and densities, based on the transmission losses of the embroidered microstrip lines. The denim base fabric that the transmission lines will be embroidered on will contribute on the total measured transmission losses. Thus, in order to take into account the influence of the denim on the insertion loss of the embroidered microstrip lines, a strip of denim was sandwiched between the copper line and the FR4 substrate. As seen in Figure 4-5, the copper tape line was attached on the denim strip, which was then affixed to the substrate using paper tape. Two small pieces of copper were used at the open ends to ensure good connection with the SMA connectors, without need for soldering.

Figure 4-6 shows the insertion loss of the copper microstrip line with and without the denim fabric. At 2.5 GHz, the transmission loss of the copper line on denim exceeded the transmission loss of the copper microstrip that was placed directly on the FR4 by approximately 0.7 dB (Figure 4-6).

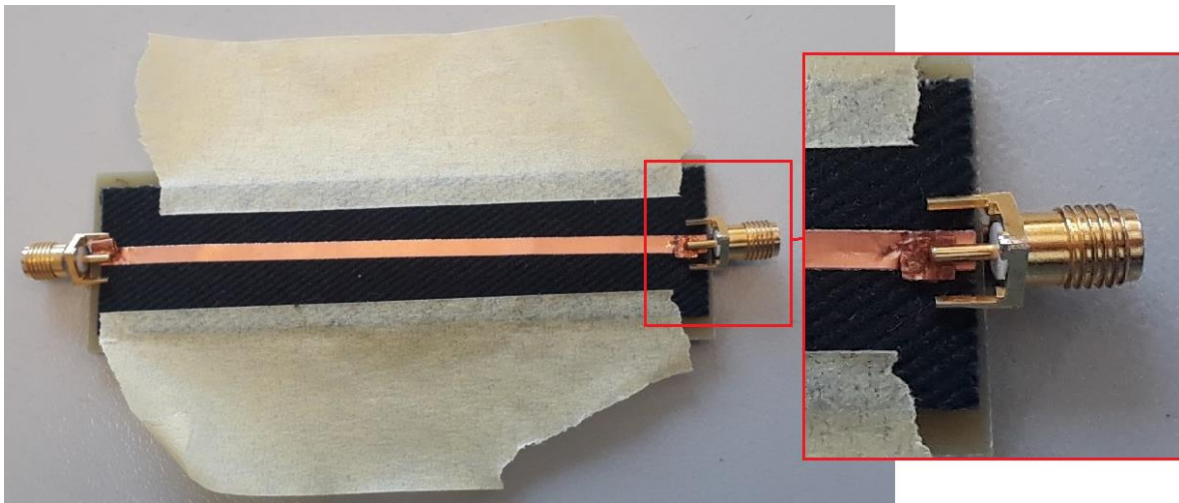


Figure 4-5. Copper tape over denim reference microstrip line prototype.

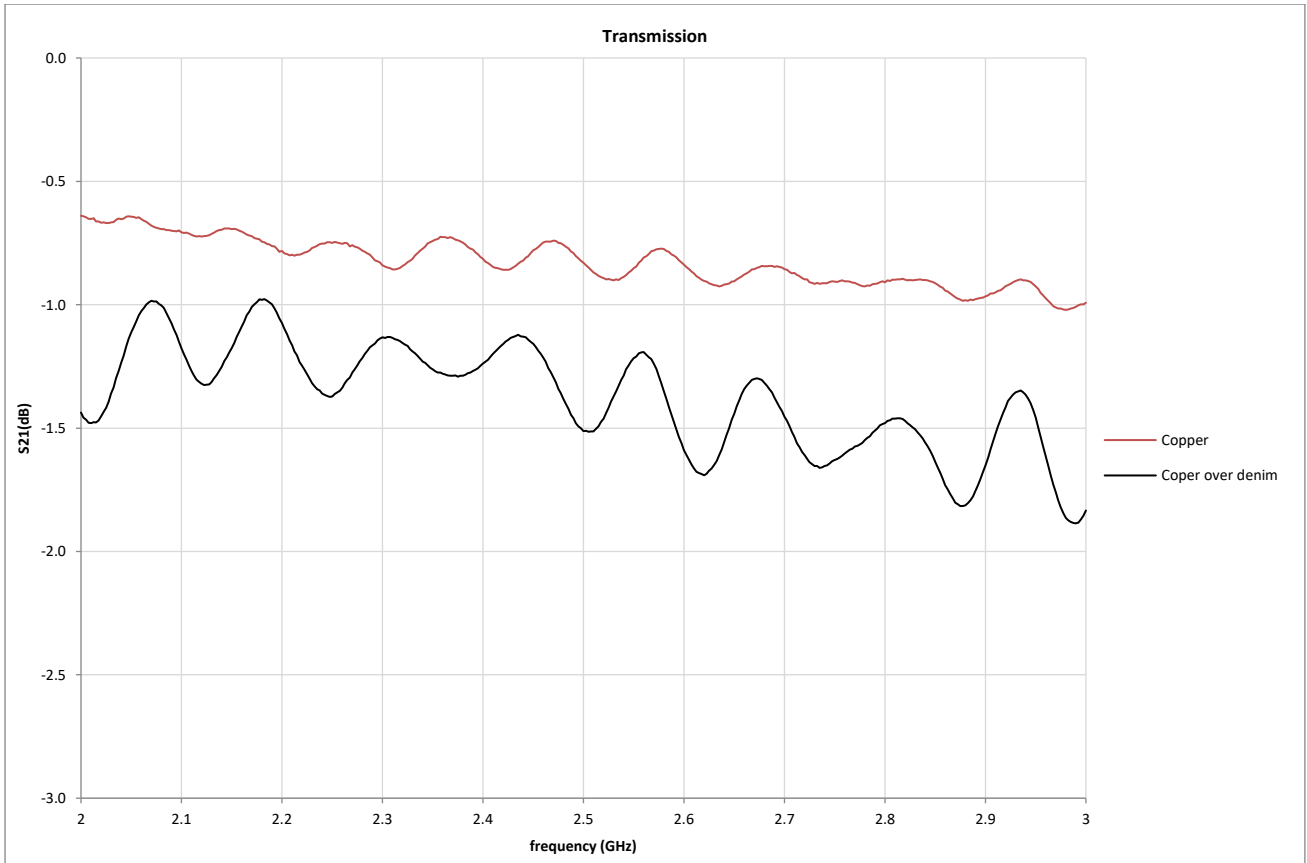


Figure 4-6. Measured insertion loss of reference microstrip lines; with and without denim.

## 4.2 Embroidered Microstrip Transmission Lines

### 4.2.1 Embroidery Designs

The embroidered lines were designed directly on PE-DESIGN PLUS 2, Brother's Personal Embroidery Design Software package. The stitch direction of all the embroidery designs was chosen to be parallel to the electric current flow, i.e., along the length of the line. This is the optimal stitch direction, according to many studies, as it minimizes surface resistance, as well as insertion loss [2]. "Fill stitch" pattern was used for all the embroidered lines, as it better suited transmission line shape, when parallel stitches were used. The stitch length for filling the area of each line was automatically set to 4 mm by the software and could not be altered. A running stitch outline was also included in the embroidery designs of the transmission lines, with the intention of creating a neater design with more accurate dimensions (Figure 4-7). The stitch length of the outline was set to 2 mm.

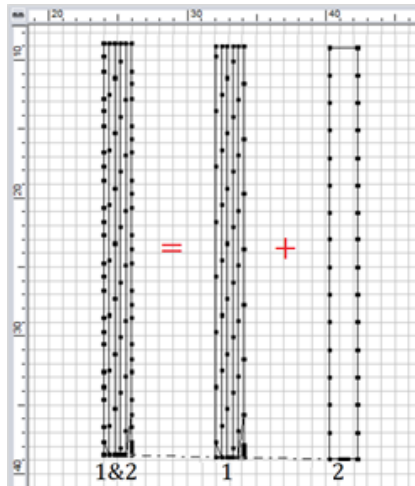


Figure 4-7. Outline example on a section of a 2 mm-wide transmission line

Since the thickness of the yarn is not considered when creating an embroidery design, some adjustments had to be made on the dimensions of the designs, compared to the reference copper line (width = 3 mm, length = 10 cm). Supposing that the dimension along the direction of the stitches will increase by approximately 1 mm due to the thickness of the yarn (i.e., 0.5 mm increase in each side), the width of the lines was set to 2 mm on the embroidery design software. Moreover, on account of the excessive pulling caused by the stiff conductive yarns, shrinking of the fabric and the embroidery design was expected. Thus, the length of the designed lines also had to be increased, to make up for the pulling together of the base fabric. The length of the transmission lines was set to 12 cm.

Three sets of embroidered transmission lines were examined. Each set consisted of three lines with the same stitch density; 1.3, 2.5 and 4 lines/mm. One line was designed to be embroidered using a simple fill stitch pattern, with stitches parallel to the line. The second line was the same as the first, except in this design the under sewing option on the embroidery software was selected. When the "Under sewing" attribute is selected, the software automatically creates underlay stitching. Specifically, it creates a ladder-like pattern that is parallel to the line (Figure 4-8). The underlay stitches get embedded to the main embroidery pattern and they constitute the very first stitches of the design. This way, a strong base of underlay stitches is created for the main pattern to get embroidered on top of it. By default, the automatically created underlay stitches as well as the embroidery pattern use the same yarn. Therefore, the second transmission line of each set consists of both vertical (embroidery design) and horizontal (underlay) conductive thread stitches. On the other hand, the remaining line of each set is composed of a conductive and a non-conductive embroidery pattern. At first, a manually designed under sewing pattern that is identical to the one that gets automatically created, was set to be embroidered using red, 100% polyester thread (marked with red colored stitches on Figure 4-8). The second part is identical to the pattern of the first line and was designed to be embroidered on top of the non-conductive under sewing pattern, using the conductive yarn. The idea behind creating the underlay using a conventional yarn is to create a strong base of horizontal lines underneath the conductive transmission line.

The direction of the conductive stitches one of the most important parameters when creating embroidered transmission lines. Parallel stitch direction was chosen as it is considered to provide optimal current flow. Introducing underlay to the embroidery design could potentially improve the RF performance of the microstrip line, by ensuring accuracy of the dimensions of the line. Underlay stitches could minimize pulling from the stiff conductive threads and therefore diminish stitching errors, such as thread breakage. Stitching errors may result in conductive frayed ends and knots, which could introduce losses. All in all, using under sewing is expected to improve stitch consistency, reduce stitching errors and ensure correct dimensions of the finished embroidery.

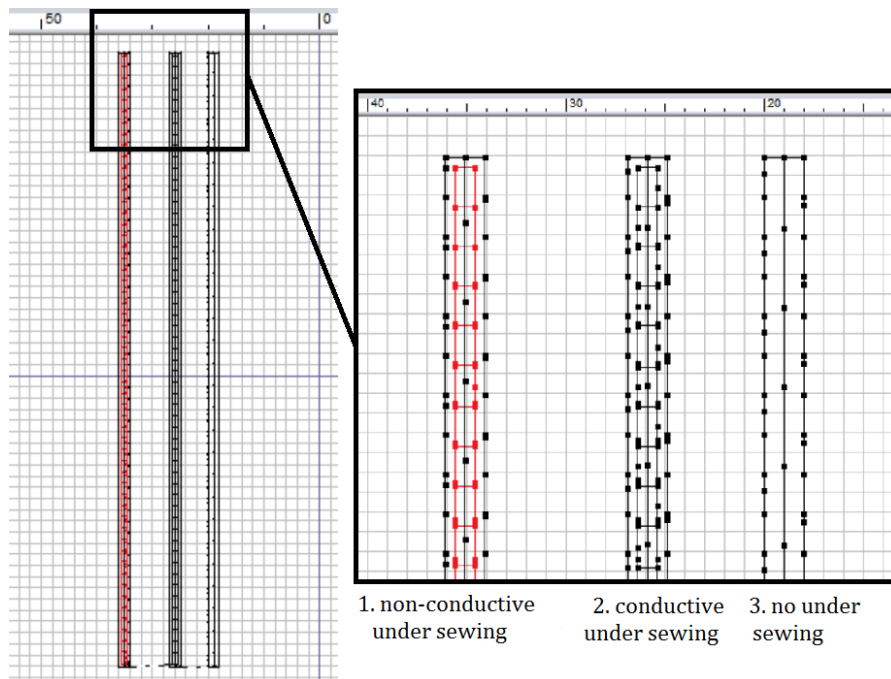


Figure 4-8. Same density lines with three different under sewing options.

However, the same thread that is used for the embroidery design is used to create the underlay stitches by default. Underlay stitches consist of horizontal stitches along the length of the line, which are connected through two parallel lines. However, introducing horizontal conductive stitches could increase losses. On the other hand, the two parallel lines will probably reduce losses since the conductive pattern will appear denser. Conductive under sewing will also significantly increase the thread usage and cost of the embroidery. Lastly, sewing the embroidery pattern over the conductive underlay stitches could lead to increased stitching errors due to the friction between the conductive threads. Using conventional thread to create the underlay stitches before embroidering the pattern of the line with conductive thread could help overcome these limitations, while improving embroidery pattern consistency. One downside of using conventional threads to create the under sewing pattern are the possible dielectric losses due to the additional layer that is inserted between the conductive stitches and the base fabric. Last but not least, the embroidery duration is increased since the machine must stop, cut the conventional thread and change to the conductive thread position after embroidering the underlay stitches.

#### 4.2.2 Embroidery Process and Microstrip Line Assembly

The conductive yarn used for the embroidered transmission lines is Shieldex 117/17 2-ply. The base fabric used for the embroidery is a black denim fabric. Its thickness was measured at approximately  $0.66 - 0.67 \text{ mm}$ . This denim fabric was dielectrically characterized using a split post dielectric resonator at Loughborough University. The dielectric constant and loss tangent were measured at  $2.4 \text{ GHz}$  and their values are 2.1 and  $8.3 \cdot 10^{-2}$  respectively.

The conductive thread was placed only at the top position of the embroidery machine, while a conventional polyester white thread was placed in the bobbin position. While the embroidery machine has 6 top thread positions available, only the second and the sixth positions were used. The conductive thread was placed at the sixth position, while the second position was threaded with a red, 100% polyester thread (Figure 4-9). This thread arrangement was kept unchanged throughout the project of this thesis.

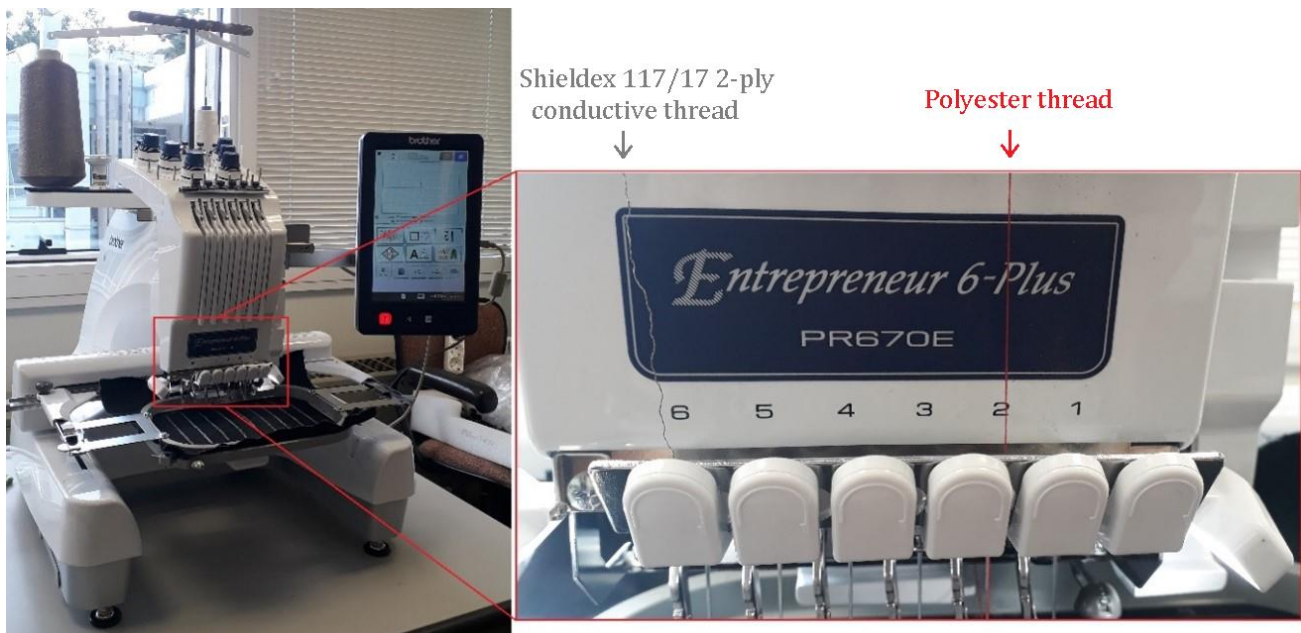


Figure 4-9. Conductive and conventional thread positions on embroidery machine.

The "large" embroidery frame (height = 130 mm, width = 180 mm), which was provided with the embroidery machine, was used for embroidering the transmission lines. When placing the lines parallel to the frame's height, all the transmission lines (9 lines in total) could fit and be embroidered, including the safety margins between each line. This way the consumption of fabric was minimum. Also, the embroidery process duration was reduced, since the number of times that the base fabric at the frame had to be replaced was kept at a minimum. This is a very time-consuming procedure, since it includes cutting a new piece of base fabric and placing it in the frame, flattening the fabric by pulling out its edges and firmly tightening the frame's screw. However, the fabric can get loose after embroidering a few lines and creases will be created. These creases can affect the shape of the adjacent lines and cause errors in the embroidery process. It is advised to manually stop the embroidery machine after embroidering 3 lines, or if creases appear, and flatten out the fabric. The screw of the frame should also get tightened before resuming the embroidery process. The effect of puckering can be then minimized, thus better accuracy of size and shape of the embroidered lines can be ensured.

After hooping the fabric and securing the frame on the embroidery machine, the embroidery patterns were imported from the computer to the embroidery machine. Some parameters had to be adjusted at this point, such as the exact position of the embroidery on the selected frame and the embroidery speed. In order to minimize thread breakage, the speed of the embroidery machine was set to the lowest setting (400 *stitches/minute*). Last but not least, the "automatic lock stitch" option was selected for the beginning of each pattern. With this key selected, the machine creates a knot at the beginning of each pattern or after automatically trimming the thread. The confined elasticity of the conductive thread leads to frequent errors, such as the thread coiling and slipping out of the base fabric at the beginning of the embroidery or after thread trimming. Errors of this kind may increase the embroidery duration significantly since the embroidery machine must be stopped (automatically or manually) and restarted. Rethreading the machine may also be required before restarting the process. Consequently, creating a knot at the beginning of the embroidery pattern contributed in minimizing the embroidery errors and duration. Since the knot was only visible from the bottom side of the embroidery (where the non-conductive, bobbin thread is visible), part of the conductive thread was also pulled to the non-conductive side. To minimize this effect, these strands were manually trimmed after the embroidery process.

The line with the non-conductive under-sewing was set to be embroidered at the beginning of each same-density set. Since the under-sewing gets embroidered at the beginning of the embroidery pattern, a minimum number of thread changes was achieved. After completing the non-conductive part of the embroidery, the machine would automatically trim the red thread. It would then proceed to embroider the rest of the pattern with the conductive thread, i.e. the thread in the sixth position. Special treatment had to be given when the machine was sewing using the conductive thread, because of its distinctive nature.

Figure 4-10 shows the embroidered lines after the embroidery process was completed. The duration of embroidering each line varied between 1 – 2 min, depending on the stitch density and type of under sewing. This procedure was repeated, and a duplicate of each line was created, resulting in a total of 18 embroidered lines.



Figure 4-10. Embroidered lines on frame after the completion of the embroidery process.

After completing the embroidery, the frame was extracted from the embroidery machine, and the fabric was removed. Figure 4-11 shows the fabric with 3 sets of embroidered lines, with densities equal to 1.3, 2.5 and 4 lines/mm respectively.

When designing the embroidery patterns for the lines, extra length was added to compensate for shrinking of the base fabric and stitching errors, such as the bobbin thread getting pulled on the top, which could further reduce the length of the final embroidery. The embroidered lines came indeed in varying lengths. The shrinking effect was more visible on the last lines of each set, which lacked under lay stitches; hence pulling of the base fabric from the conductive threads was stronger.

The same FR4 substrate was used for measuring all the embroidered lines. The substrate was identical to the reference, but with the top left blank. One SMA connector was also placed on each side, with soldering applied only on the ground plane. Since the length of the substrate was 10 cm, the varying-length lines had to be cut to fit the substrate. Each line was cut down to approximately 9.8 cm, in order to properly fit on the substrate, without creasing. Figure 4-11 depicts the base fabric with the embroidered lines, with white marks for cutting.

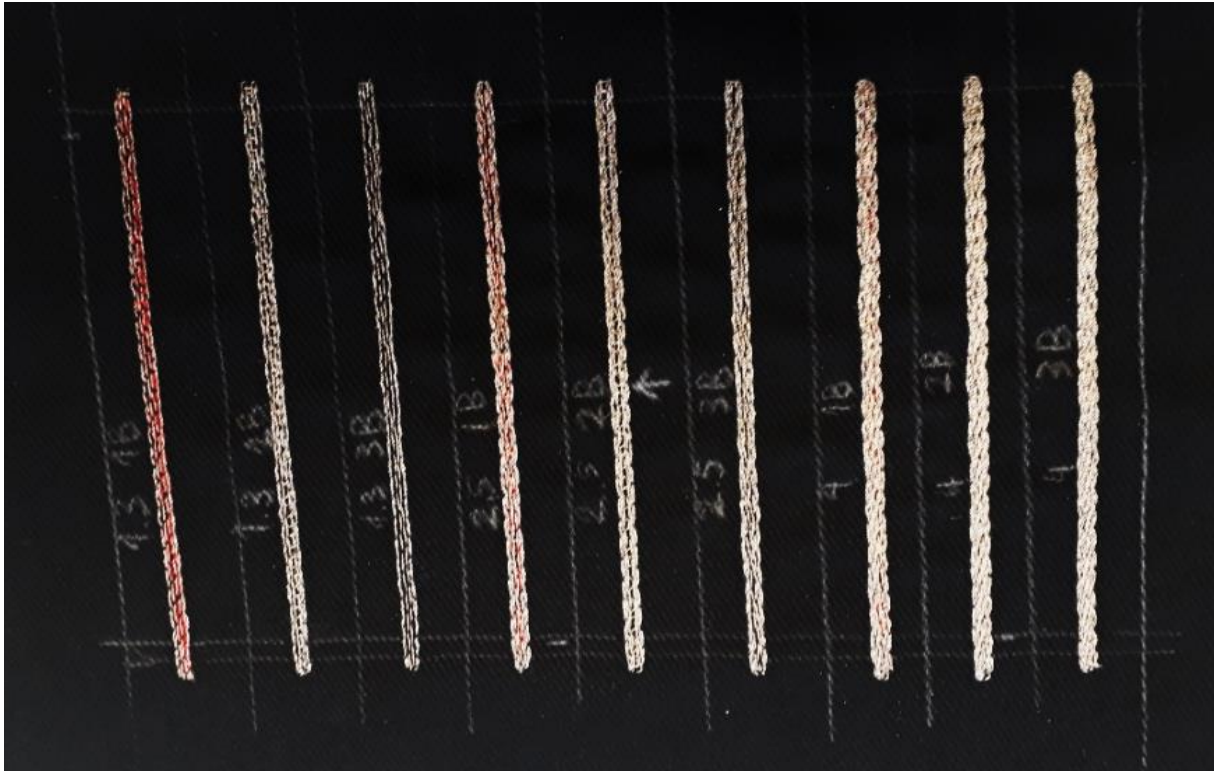


Figure 4-11. Embroidered lines on base fabric with markings for cutting.

Two small rectangular pieces of copper tape were attached on the open ends of each line after cutting. Copper tape provides better connection between the flat conductive stitches and the pin of the SMA connectors (Figure 4-12). Additionally, sticking the copper tape pieces at the open ends of the lines keeps the cut stitches into place. In order to use the same substrate for measuring all the samples, no soldering was applied to connect the SMA pins to the open ends the transmission lines. Instead, after placing the embroidered line on the substrate for measuring, an additional piece of copper was sandwiched between the pin of the SMA connector and the copper tape at each of its open ends, to ensure

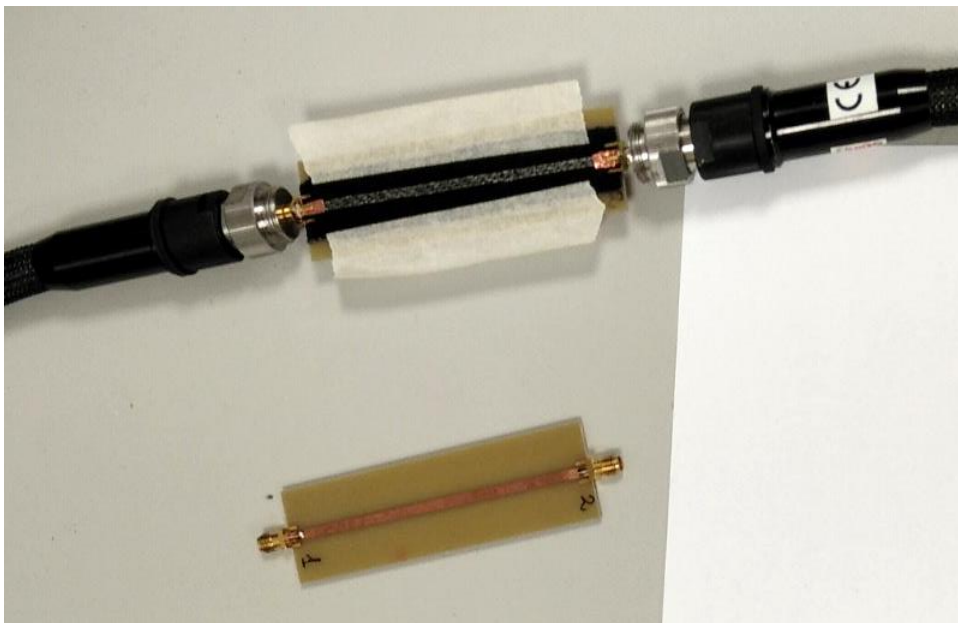


Figure 4-12. Measurement arrangement for embroidered microstrip lines.

good connection. Lastly, the base fabric of the embroidered line would get attached to the substrate, using paper tape. After measuring the transmission line, the additional copper pieces would be extracted and the embroidered line would be carefully removed, with the paper taped still attached to the base fabric. A new line could then be placed on the substrate and measured, following the same steps.

### 4.3 Results/Discussion

Due to manufacturing tolerances, we can notice non-negligible variations in the dimensions of embroideries with the same embroidery design when created for multiple times. In order to reduce this uncertainty in our measurement results, a duplicate of each transmission line prototype was created and measured. In this chapter, all the measurements of the embroidered microstrips which will be presented correspond to the average of the measurements of each of the two duplicates <sup>1</sup>. It should be also noted that extensive repeatability measurements are needed to more accurately evaluate the performance of embroidered microstrip lines.

The measured insertion loss of all the embroidered transmission lines as well as the reference copper line with the denim base fabric can be seen in Figure 4-13. At 2.5 GHz, all the lines exhibited losses higher than 3 dB. However, part of these losses (approximately 0.5 – 1 dB) can be attributed to the presence of the lossy base fabric.

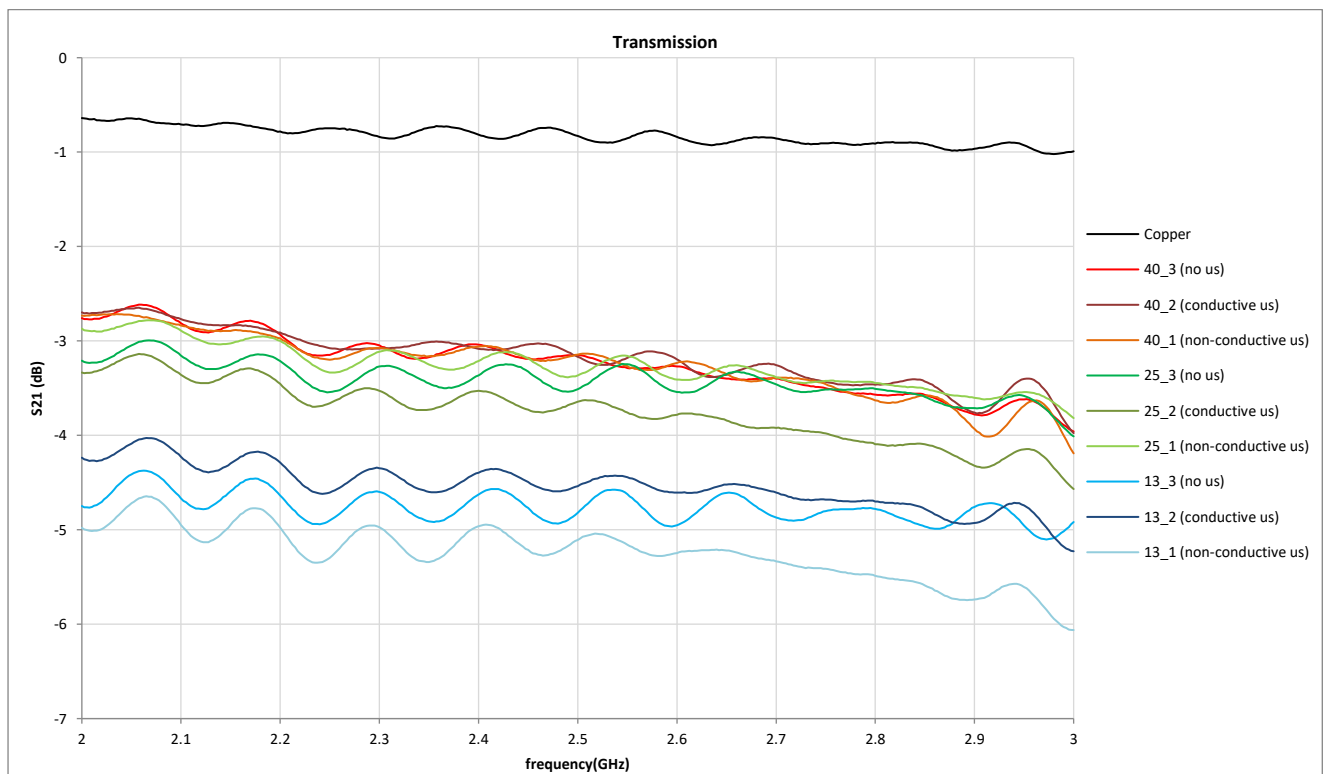


Figure 4-13. Measured insertion loss of all the embroidered transmission lines, reference copper line and copper line over denim base fabric.

In the entire examined frequency range, the embroidered lines with the highest density (i.e., 4 lines/mm, denoted as 40\_i, where i= 1, 2, 3) have the best performance. However, in the 2.5-3 GHz frequency range, the performance of the 2.5 lines/mm-density microstrips with non-conductive under sewing (non-conductive us) and no under sewing (no us) (i.e., 2.5 lines/mm, denoted as 25\_i, where i= 1, 3) exhibit approximately the same losses as the highest density microstrips. The microstrip line which has conductive under sewing from the same set (i.e., 25\_2) displays higher losses from the other

lines of the 4 and 2.5 *lines/mm*-density sets, especially at the 2.5-3 GHz frequency range, where the difference in the insertion loss is around 0.5 *dB*. At 3 GHz, the losses of the 25\_2 microstrip line exceed 4.5 *dB*.

All the lines from the lowest density group (i.e., 1.3 *lines/mm*, denoted as 13\_i, where i= 1, 2, 3) have losses higher than 4 *dB*, even at 2 GHz. In the higher end of the examined frequency range, the microstrip line with the worst performance is the line with non-conductive under sewing (i.e., 13\_1), with losses as high as 6 *dB*. This indicates that almost 75% of the power that inserts the microstrip line gets lost while propagating through it.

The values of the  $S_{21}$  (*dB*) parameter at 2.5 GHz for all the microstrips are displayed in Table 4-1, sorted from lower to higher transmission losses. The number of the stitches made using conductive thread (i.e., the number of stitches made with polyester thread for the non-conductive under sewing is not considered), are also presented. It should be noted that same density microstrips with no under sewing and non-conductive under sewing have the same conductive stitch pattern, thus the same number of conductive stitches. Microstrip lines with a relatively small stitch count have comparable losses to microstrips with higher thread usage. It becomes apparent that a larger number of stitches, therefore larger conductive thread usage, do not always equal reduced losses.

A more detailed look into the performance of the embroidered lines will be presented in the following sections.

Type	$S_{21}_{2.5\text{ GHz}}(\text{dB})$	Conductive stitches
<b>copper</b>	-0.830	-
<b>copper denim</b>	-1.513	-
<b>40_3 (no us)</b>	-3.152	475
<b>40_2 (conductive us)</b>	-3.170	805
<b>25_1 (non-conductive us)</b>	-3.366	361
<b>40_1 (non-conductive us)</b>	-3.444	475
<b>25_3 (no us)</b>	-3.512	361
<b>25_2 (conductive us)</b>	-3.643	691
<b>13_2 (conductive us)</b>	-4.538	575
<b>13_3 (no us)</b>	-4.819	245
<b>13_1 (non-conductive us)</b>	-5.107	245

Table 4-1

### 4.3.1 Effect of Stitch Density on the Performance of Embroidered Microstrip Lines

Figure 4-14 to Figure 4-17 display the insertion loss of the embroidered microstrip lines with no under sewing, conductive under sewing and non-conductive under sewing respectively. The insertion loss of the copper microstrip line over denim is also displayed in all graphs, to serve as reference.

As seen in Figure 4-14, the microstrip lines with densities equal to 4 and 2.5 *lines/mm* (i.e., 40\_3, 25\_3) have very similar performance, especially in higher frequencies. Close to 2 GHz, the difference between the losses of the two lines does not exceed 0.5 *dB*.

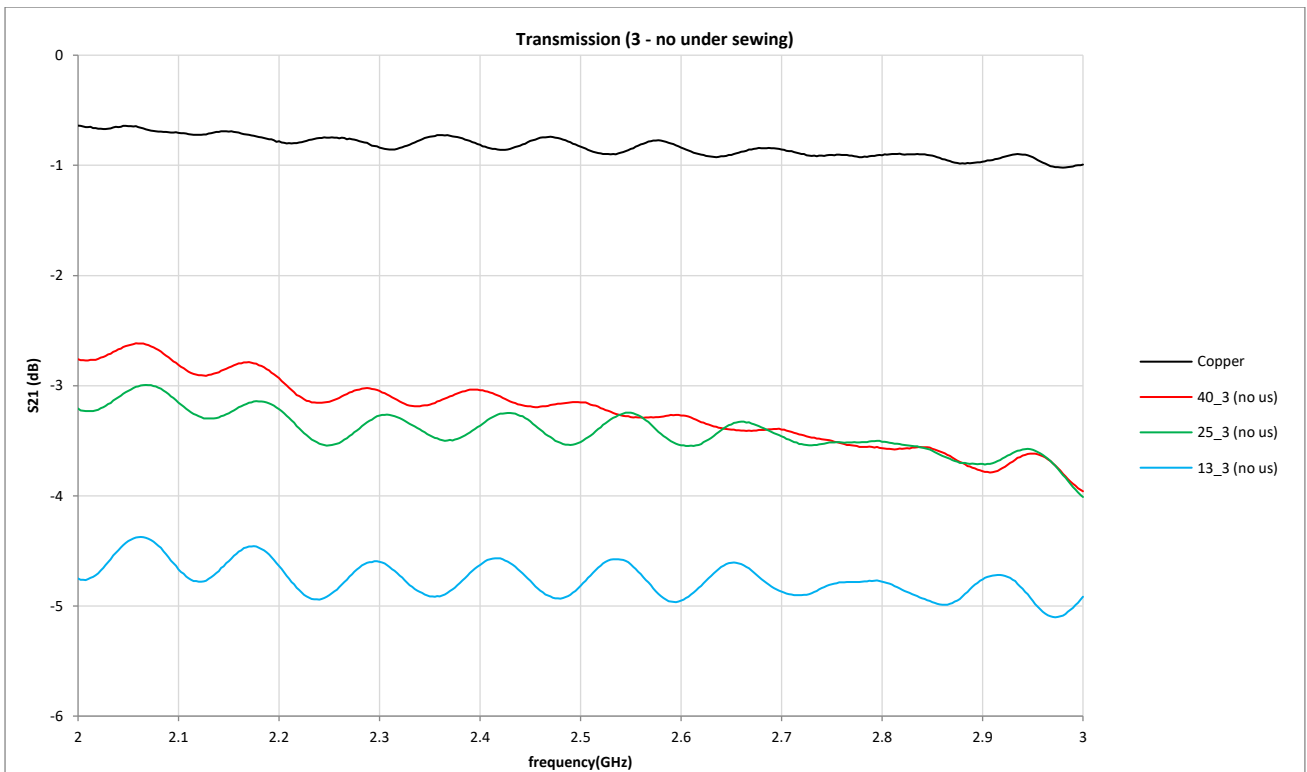


Figure 4-14. No under sewing: Insertion loss of different density embroidered microstrip lines.

On the other hand, the performance of the 1.3 *lines/mm*-density microstrip line with no under sewing is degraded. At 2.5 GHz, the  $S_{21}$  (dB) parameter of the 13\_3 microstrip is almost 1.5 dB lower than the more densely stitched lines of this category.

In the conductive under sewing category (Figure 4-15), the 25\_2 microstrip line exhibited approximately 0.5 dB higher losses than the 40\_2 microstrip, at 2.5 GHz. At the same frequency, the microstrip with the sparser stitches (i.e., 13\_2) had almost 0.9 dB higher losses than the 25\_2 microstrip.

With almost 30% less conductive thread, the lowest density microstrip line had almost 1.4 dB higher losses, compared to the highest density microstrip.

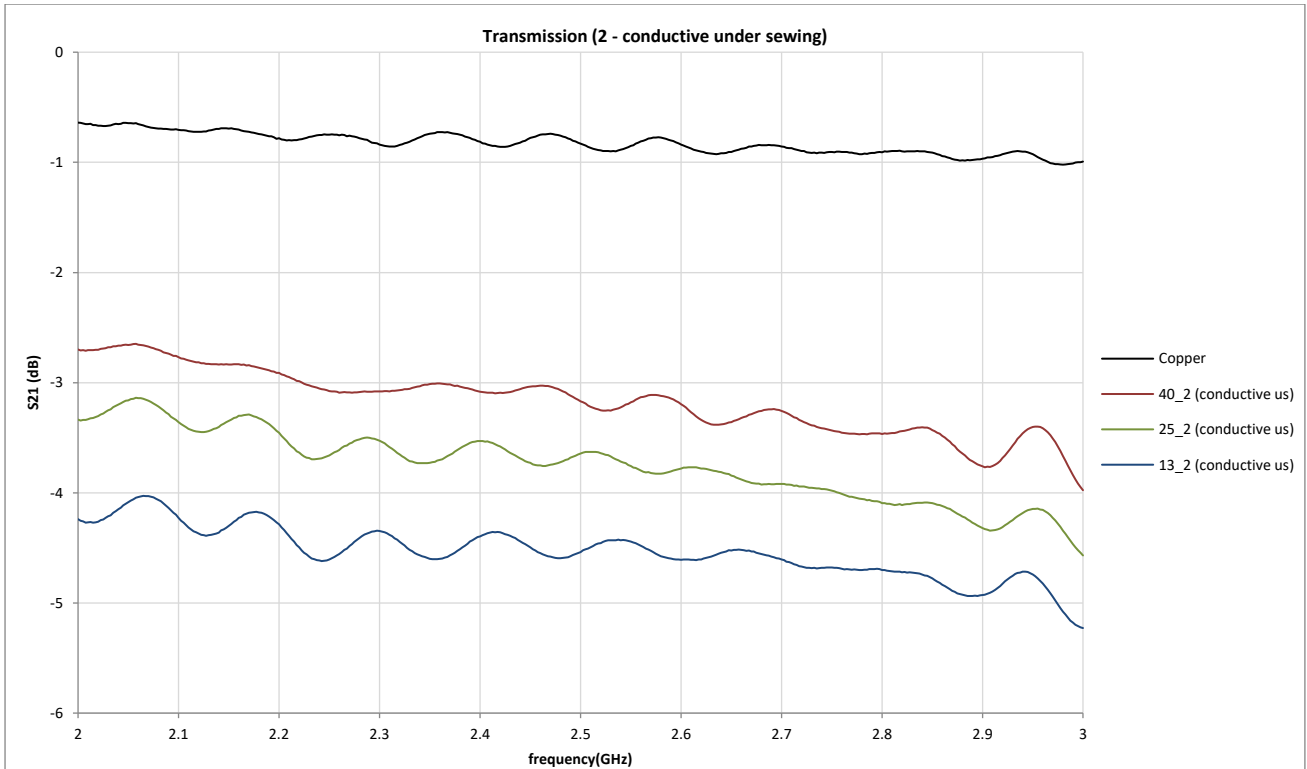


Figure 4-15. Conductive under sewing: Insertion loss of different density embroidered microstrip lines.

The embroidered microstrips of the group with non-conductive under sewing (Figure 4-16) had similar behavior to the microstrips of the group with no under sewing. More specifically, the microstrips with the two highest densities (i.e., 40\_1, 25\_1) display almost identical losses over the studied frequency spectrum. Moreover, these microstrip designs had approximately the same losses as the 40\_3 and 25\_3 microstrips, which can also be observed in Figure 4-13. However, the 2.5 *lines/mm*-density microstrip lines have almost half the number of stitches than the 4 *lines/mm* microstrips. The microstrip line with the lowest density exhibited approximately 1.7 *dB* higher losses than the denser lines of the non-conductive under sewing group.

The close resemblance of the two graphs can be attributed to the fact that the two groups (i.e., the no under sewing group and non-conductive under sewing group) have the same conductive stitch pattern, while only the last group has non-conductive under sewing with 100% polyester thread.

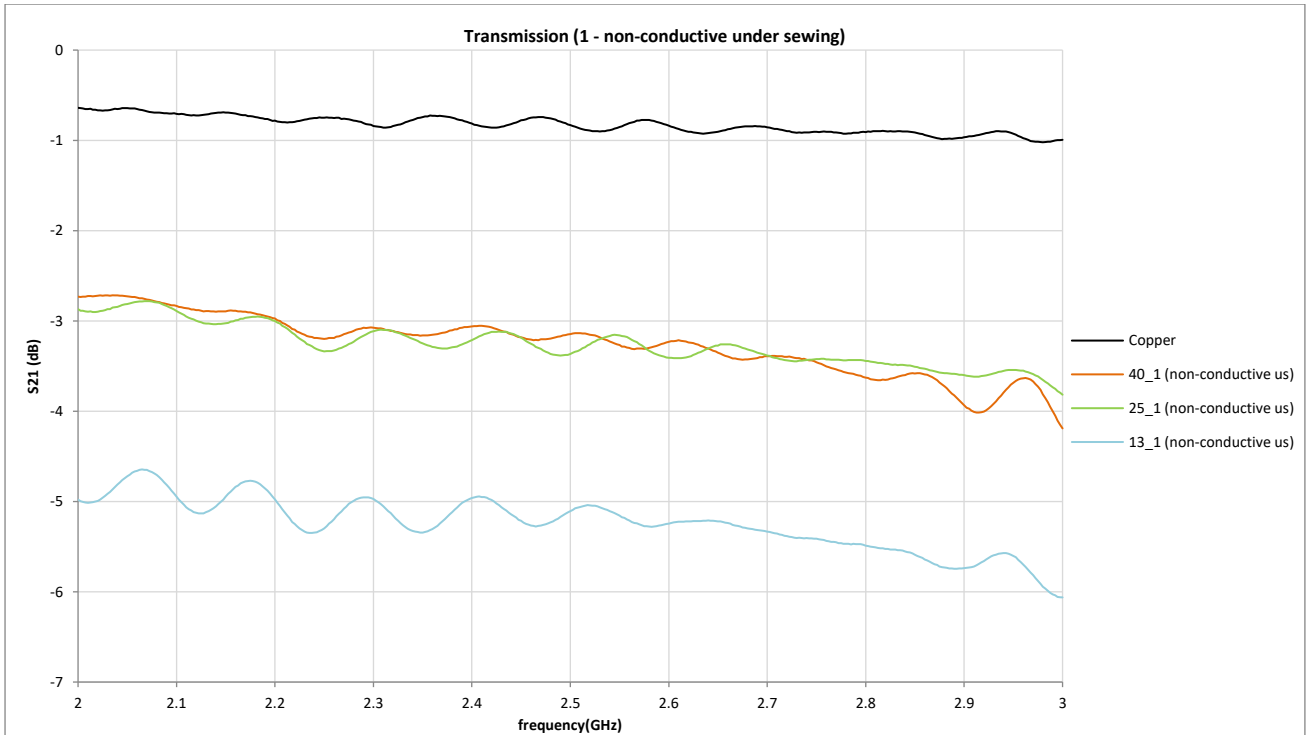


Figure 4-17. Non-conductive under sewing: Insertion loss of different density embroidered microstrip lines

### 4.3.2 Effect of Under Sewing on the Performance of Embroidered Microstrip Lines

As seen in Figure 4-18, all the microstrips from the 4 *lines/mm*-density group had essentially the same performance. Close to 2 GHz, the insertion loss is lower than 3 dB, while at higher frequencies it does not exceed 4 dB. At 2.5 GHz, all the microstrips of this group had 3.25 dB losses on average.

It can be assumed that when the stitch density is high, the use of under sewing has no effect on the insertion loss of the microstrips. In order to save on conductive thread as well as duration of fabrication, under sewing can be neglected.

Figure 4-19 shows the insertion loss of the 2.5 *lines/mm*-density group. The performance of the microstrips was satisfying, considering that the thread consumption was diminished by approximately 14% for the conductive under sewing microstrip (i.e., 25\_2) and 24% for the non-conductive and no under sewing microstrips (i.e., 25\_1 and 25\_3).

The last microstrips had relatively low losses, especially at higher frequencies. On the other hand, the losses of microstrip with the conductive under sewing were similar to the other two microstrips of the same group at lower frequencies, while at 3 GHz it exhibited more than 0.5 dB higher losses. It should be noted that the microstrip of the 2.5 *lines/mm*-density group with the worst performance used approximately 52% more conductive thread, compared to the other two microstrips of the same group.

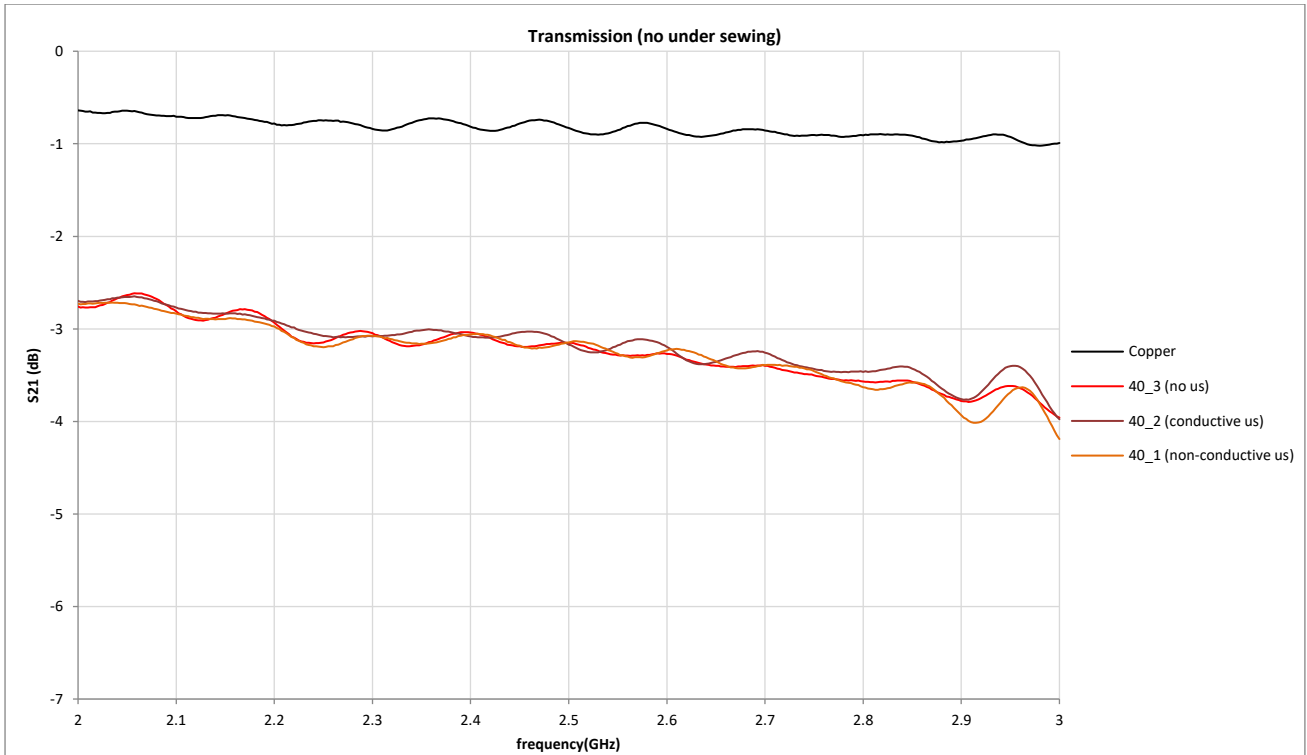


Figure 4-18. Insertion loss of 4 *lines/mm*-density embroidered microstrip lines.

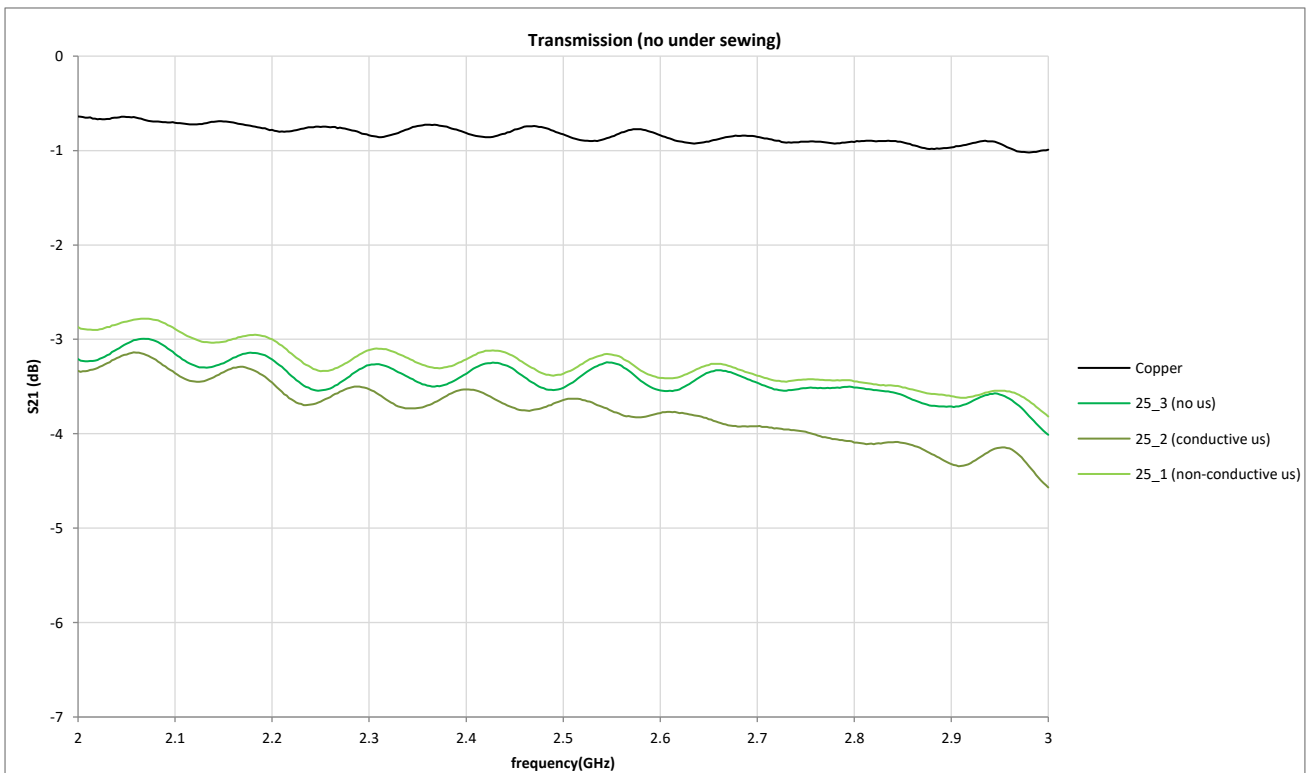


Figure 4-19. Insertion loss of 2.5 *lines/mm*-density embroidered microstrip lines.

Figure 4-20 displays the  $S_{21}$  (dB) parameter over the 2 – 3 GHz frequency range of the group with the embroidered microstrip lines which had the lowest density. Contrary to the previous group, in this group the microstrip line with the best performance was the one with the conductive under sewing. However, at higher frequencies the microstrip line with no under sewing had comparable losses. The losses of the microstrip line with non-conductive under sewing were close to 5 dB at 2 GHz, while near 3 GHz they increased up to 6 dB.

At 2.5 GHz, even the microstrip with the best performance in the group (i.e., 13\_2) had almost 0.9 dB more losses compared to the lossier microstrip of the previous group (i.e., 25\_2). As far as thread consumption is concerned, the 25\_2 microstrip used approximately 20% more conductive thread compared to the 13\_2 microstrip.

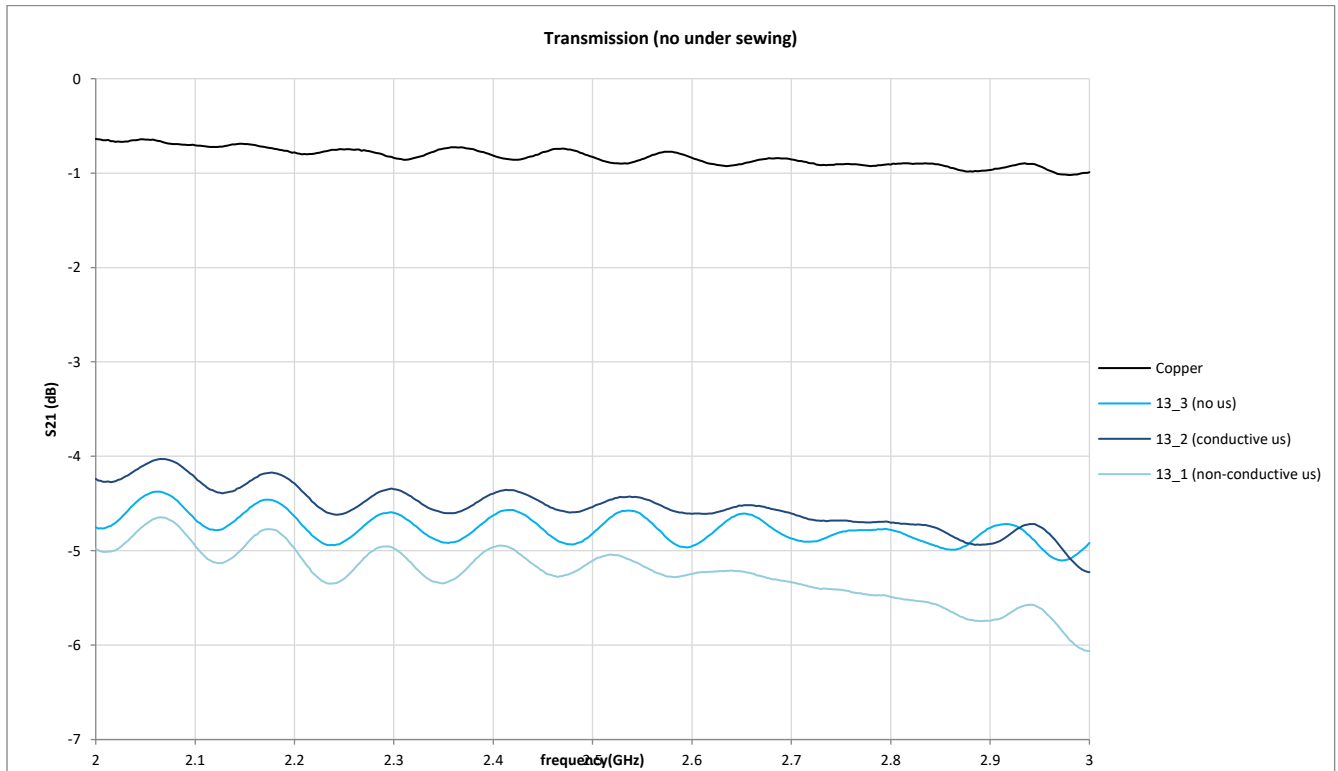


Figure 4-20. Insertion loss of 1.3 lines/mm-density embroidered microstrip lines.

## 4.4 Conclusions

The RF performance of embroidered microstrip transmission lines with different stitch densities and under sewing options was studied in this chapter. The microstrip lines were evaluated based on the insertion loss.

While the microstrips with the highest stitch density (i.e., 4 lines/mm) had the best performance, the insertion loss of microstrips with stitch density equal to 2.5 lines/mm was not much higher. At the same time, the microstrip lines of the second group had reduced stitch count and correspondingly reduced fabrication cost as well as duration. The microstrip lines with the sparsest stitches exhibited losses are on average 1 – 1.5 dB larger than the 2.5 lines/mm category.

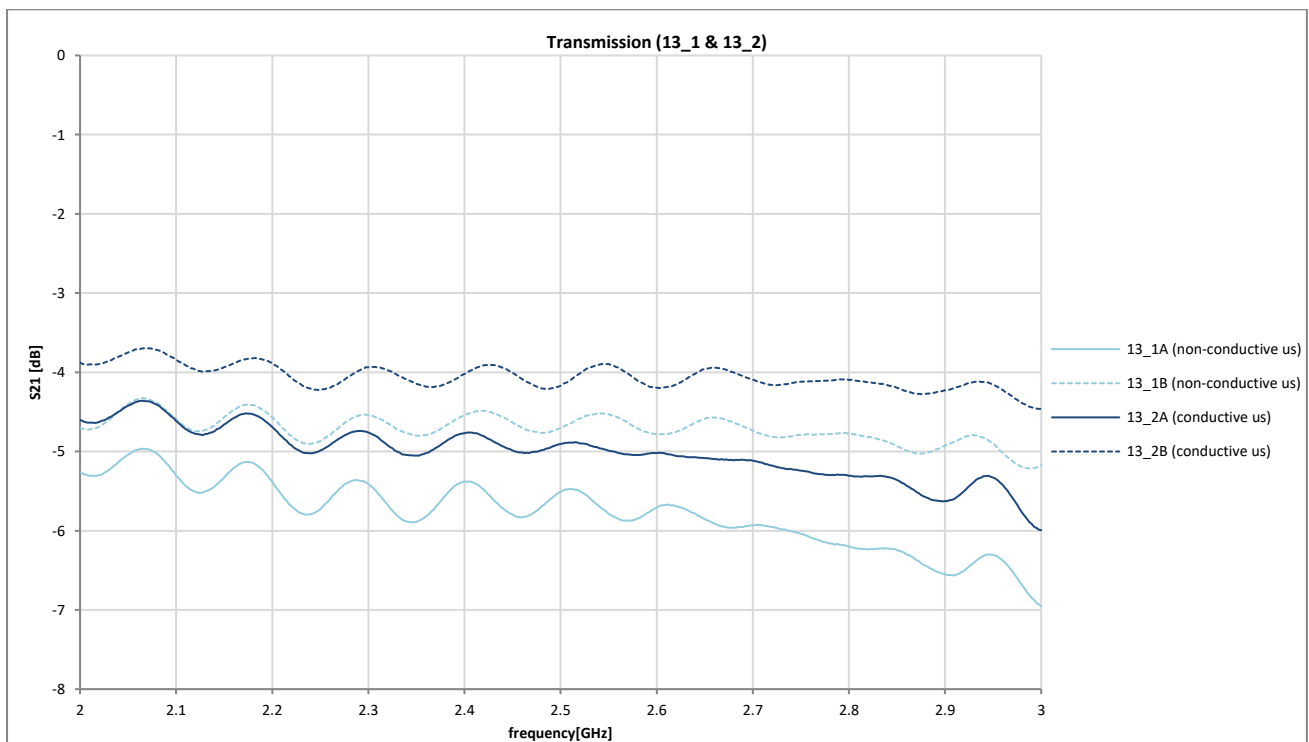
The use of under sewing did not seem to have a significant effect on the performance of the embroidered microstrip lines, especially when high stitch density was used for embroidering the microstrip lines. Moreover, under sewing did not improve the accuracy in the dimensions of the embroidery designs noticeably. As far as conductive under sewing is concerned, the extra conductive stitches contributed in increasing the tensions between the conductive threads, which in some cases led to excessive creasing. Additionally, conductive under sewing can significantly increase the fabrication cost of the microstrip lines.

## References

- [1] Pozar, David M. *Microwave Engineering*. Hoboken, NJ :Wiley, 2012.
- [2] S. Zhang, "Design advances of embroidered fabric antennas," PhD, Loughborough University, 2014.

<sup>i</sup> The difference in the measured  $S_{21}(dB)$  of each microstrip and its duplicate (marked as A and B accordingly) did not exceed  $0.5\text{ dB}$  for all the microstrips apart from 13\_1 and 13\_2 (i.e.,  $\text{density} = 1.3\text{ lines/mm}$ , with non-conductive under sewing and conductive under sewing accordingly). As seen in the following Figure, there is a significant difference in the losses of each duplicate. The difference in the losses of the duplicates with conductive under sewing (i.e., 13\_2A and 13\_2B) was more than  $0.7\text{ dB}$  in lower frequencies, while near  $3\text{ GHz}$  the deviation exceeded  $1.5\text{ dB}$ . The deviation observed in the measurement of the microstrips with the non-conductive under sewing of the same density ranged from approximately  $0.57\text{ dB}$  and up to almost  $1.8\text{ dB}$ .

As seen in the next figure, both microstrips from the second embroidery group (i.e., 13\_2B and 13\_1B) have better performance than their duplicates from set A (i.e., 13\_2B and 13\_1B).



Insertion loss of  $1.3\text{ lines/mm}$ -density embroidered microstrip lines.

# Chapter 5 Embroidered Microstrip Patch Antennas

## Abstract

The purpose of this chapter is to present the design and fabrication of a fully textile rectangular microstrip patch antenna using embroidery techniques.

A reference copper patch antenna on felt substrate was fabricated first. The effect of the base fabric on the RF performance of the antenna was also examined. Based on the conclusions of Chapter 4, two different density embroidered patch antenna designs were created. A microstrip line with a quarter wavelength transformer was also included in the antenna embroidery designs. Since the embroidered microstrips with 2.5 and 4 *lines/mm* densities had similar performance in terms of transmission losses, these densities were also examined. The embroidered antennas of both densities resonated lower than the copper reference antenna, as a result of the complex current routes created by the conductive stitches. Increase of input reflection coefficient were also observed (impedance mismatch), especially for the 2.5 *lines/mm* density antenna.

A new embroidered patch antenna was then created, based on the observations of the previous models. The density of the embroidery design was set to 4 *lines/mm*. The physical length of the patch was reduced compared to the previous models, in order to compensate for the reduction of the resonant frequency (increase of electrical length of the antenna) due to the complex nature of the stitches. Lastly, the dimensions (width) of the embroidered microstrip feed line were adjusted to provide impedance matching.

## 5.1 Copper Microstrip Patch Antenna

According to the following equations for optimal antenna efficiency, the width of a microstrip patch antenna can be calculated as follows [1]:

$$W = \frac{c}{f_r} \sqrt{\frac{2}{\epsilon_r + 1}} \quad (23)$$

Where:

$c$ : light velocity in free space

$f_r$ : resonant frequency of the antenna, and

$\epsilon_r$ : substrate permittivity.

The frequency of resonance for the dominant mode ( $TM_{010}$ ) of the rectangular patch antenna can be obtained from the following equation [1]:

$$(f_{rc})_{010} = \frac{1}{2(L_{eff}\sqrt{\epsilon_{r,eff}}\sqrt{\epsilon_0\mu_0})} \quad (24)$$

Where  $L_{eff}$  is the effective length of the patch, due to the fringing effects. More specifically, the electrical length of the patch is longer than its physical length ( $L = \frac{\lambda}{2}$ ) by a factor  $2 \cdot \Delta L$  (Figure 5-1), which is a function of the height of the substrate ( $h$ ), the effective relative permittivity ( $\epsilon_{r,eff}$ ) and the width of the patch ( $W$ ). The elongation of the patch ( $\Delta L$ ) (as seen in Figure 5-1) can be calculated from the following equation [1]:

$$\Delta L = 0.412h \frac{(\epsilon_{r,eff} + 0.3) \left(\frac{W}{h} + 0.264\right)}{(\epsilon_{r,eff} - 0.258) \left(\frac{W}{h} + 0.8\right)} \quad (25)$$

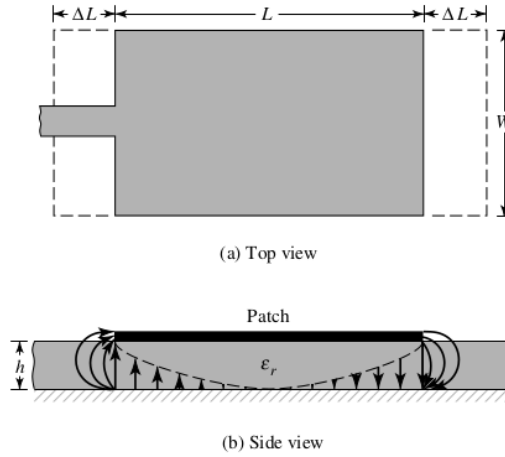


Figure 5-1. Physical and electrical length of a rectangular microstrip patch [1].

The length of the patch can be calculated from the following equation in order to resonate in the desired frequency [1]:

$$L = \frac{1}{2f_r \sqrt{\epsilon_{r,eff}} \sqrt{\epsilon_0 \mu_0}} - 2\Delta L \quad (26)$$

A microstrip line with a quarter-wavelength  $\left(\frac{\lambda_{eff}}{4}\right)$  transformer was designed for feeding the patch. In order to provide impedance matching between the edge of the patch and the input feedline, the characteristic impedance ( $Z_0$ ) of the quarter-wavelength microstrip segment should be equal to:

$$Z_0 = \sqrt{Z_L Z_{in}} \quad (27)$$

Where:

$Z_L$ : the real part of the impedance at the edge of the patch, and

$Z_{in}$ : the characteristic impedance of the input transmission line (Figure 5-2) [1].



Figure 5-2. Quarter wavelength transformer schematic [2].

The width of the  $50 \Omega$  input transmission line as well as the width of the quarter wavelength transformer were calculated according to the equations ( 18)-( 22) in Paragraph 4.1.

### 5.1.1 Antenna Modeling

When fabricating the reference antenna, the felt fabric whose dielectric properties were measured in Chapter 2 would be used as the substrate. Shieldex's metallized nylon fabric Nora Dell would be used as a textile ground plane for the copper patch antenna. However, copper would be used for the patch and feedline the antenna would be used as reference. According to the mechanical and electrical properties of these materials, a microstrip patch antenna model was created in HFSS.

The dimensions of the microstrip patch antenna and the feed line were calculated according to the equations above, and a microstrip patch antenna model was created in HFSS. The dimensions of the structure were then optimized for the microstrip patch antenna to resonate at approximately 2.4 GHz (Figure 5-4). The final dimensions of the antenna can be seen in Table 5-1, and the model of the antenna is displayed in Figure 5-3. The length ( $L$ ) and width ( $W$ ) of the felt substrate were 88 mm and 70 mm accordingly.

Dimensions (mm)				
Length (L)	Width (W)	$\lambda/4$ transformer length (fl1)	$\lambda/4$ transformer width (fw1)	Input feedline width (fw2)
52	59	22	5	15

Table 5-1

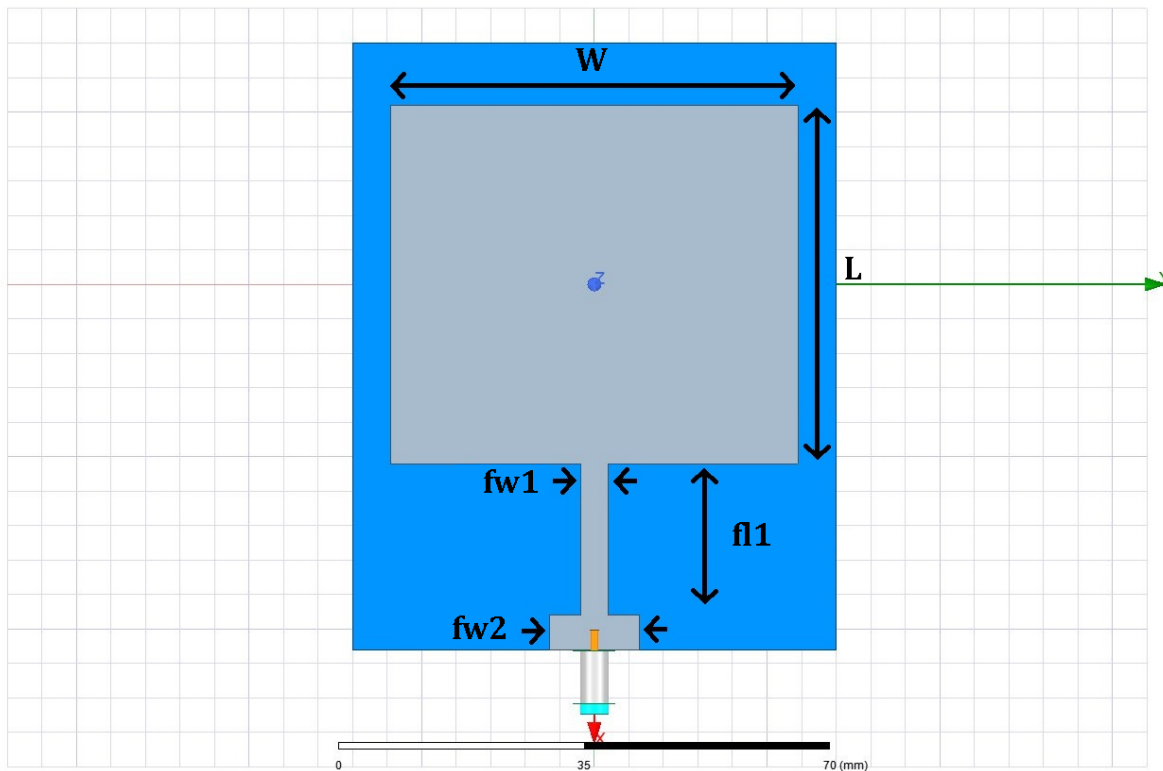


Figure 5-3. HFSS model of copper microstrip patch antenna on textile (felt) substrate.

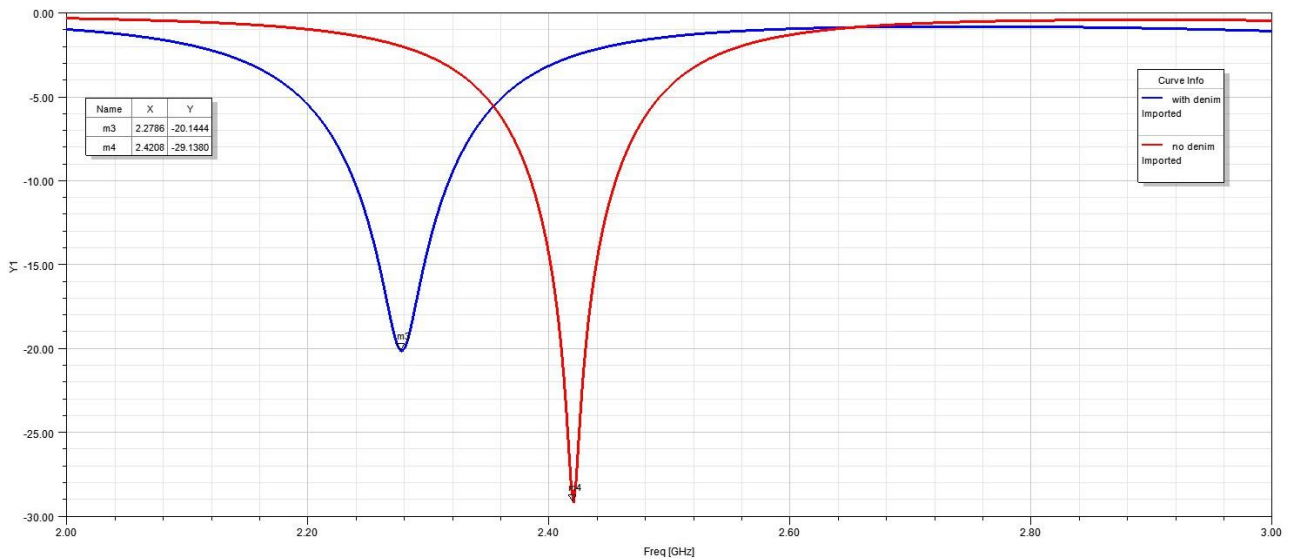


Figure 5-4. Simulated  $S_{11}(dB)$  graph of copper microstrip patch antenna on felt substrate with (blue trace) and without (red trace) denim base fabric.

As mentioned in Paragraph 4.1, the base fabric that the microstrips were embroidered on contributed on the total insertion loss of the microstrip lines. Since the same base fabric would be used for embroidering the antennas, a second model was created on HFSS. The base fabric was included in this model, sandwiched between the felt substrate and the copper patch. While the dimensions of the rest of the structure remained the same, the resonance appeared at a much lower frequency, around 2.28 GHz (Figure 5-4). Moreover, due to the additional losses as well as the mismatched conditions caused by introducing the denim base fabric, the impedance match ( $S_{11}$ ) was also diminished at resonance.

Consequently, the dimensions of the patch were altered, in order to increase the resonant frequency up to approximately 2.4 GHz, while the dimensions of the feed line and quarter wavelength transformer were also adjusted to the two-layered substrate. The dimensions of the model with the denim base fabric are displayed in Table 5-2, and the HFSS model can be seen in Figure 5-5.

Dimensions (mm)				
L	W	fl1	fw1	fw2
48.5	59.2	19.9	5	15.5

Table 5-2

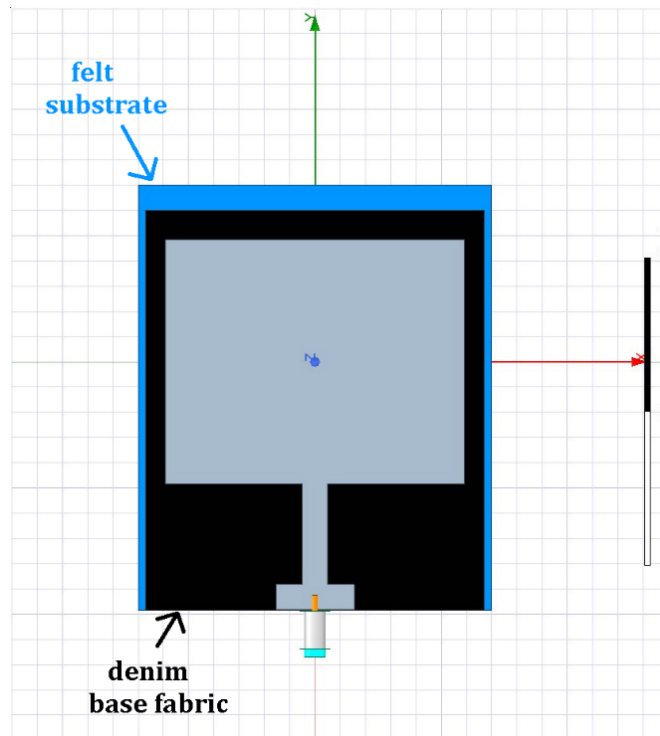


Figure 5-5. Copper microstrip patch antenna with denim base fabric over felt substrate.

### 5.1.2 Fabrication and Measurement

Figure 5-6 shows the fabricated reference copper patch antenna. The base fabric was attached to the (blue) felt substrate using hot melt adhesive web that is commonly used for textiles. The same method was used for gluing the rest of the antenna parts together (i.e., denim (black) and Nora Dell (silver) ground plane on top and bottom of felt correspondingly).

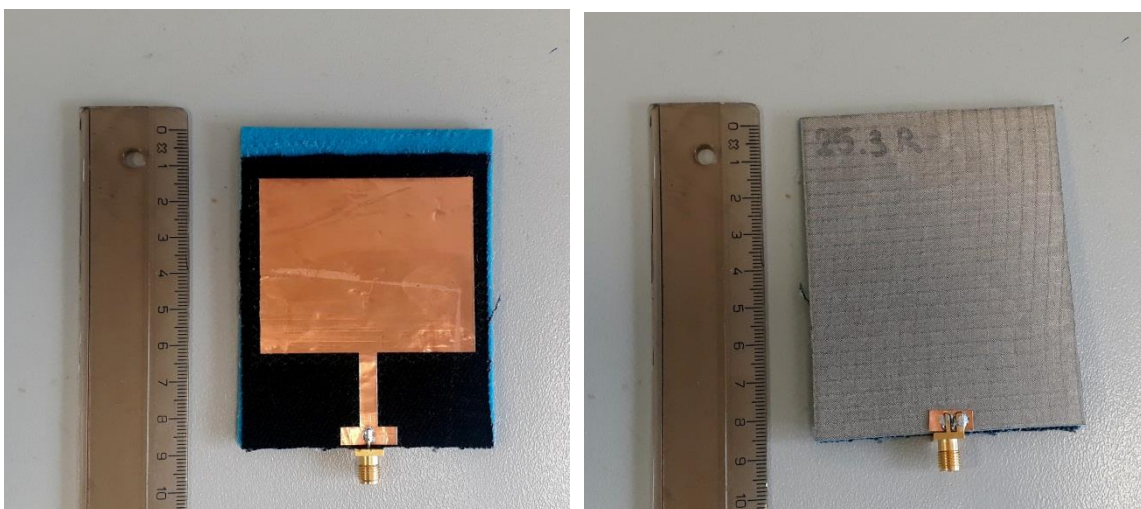


Figure 5-6. Fabricated reference copper patch antenna on textile substrate (Right: top, Left: back).

The antenna was measured using a VNA and the results are displayed in Figure 5-7, along with the simulation results. The fabricated reference copper patch resonated at approximately 2.45 GHz, where the value of the  $|S_{11}(dB)|$  parameter reached  $-25\text{ dB}$ . An LPKF PCB-plotter was used to cut the copper patch, in accordance with the HFSS model. However, due to the limited accuracy of the plotter, a small difference was observed in the dimensions of the HFSS model and the fabricated antenna prototype (exact dimensions can be seen in Table 5-4). More specifically, the length of the copper patch was 0.7mm shorter than the model, which may be the reason behind the +28 MHz difference in the resonances of the modeled and fabricated antennas accordingly. Moreover, the fabricated antenna exhibited higher reflections, which could be a result of the hot melt adhesive layers between the different parts of the antenna, which were not considered in the HFSS design. The bandwidth ( $BW_{-10dB}$ ) of the fabricated reference antenna was measured at approximately 99 MHz, which is close to the simulated 97 MHz bandwidth.

The gain radiation pattern of the reference copper antenna was then measured in the anechoic chamber (antenna Far-Field measurements test site). The E-plane and H-plane gain measured radiation patterns are displayed in Figure 5-8 and Figure 5-9 accordingly. The simulated radiation patterns are also included for comparison reasons.

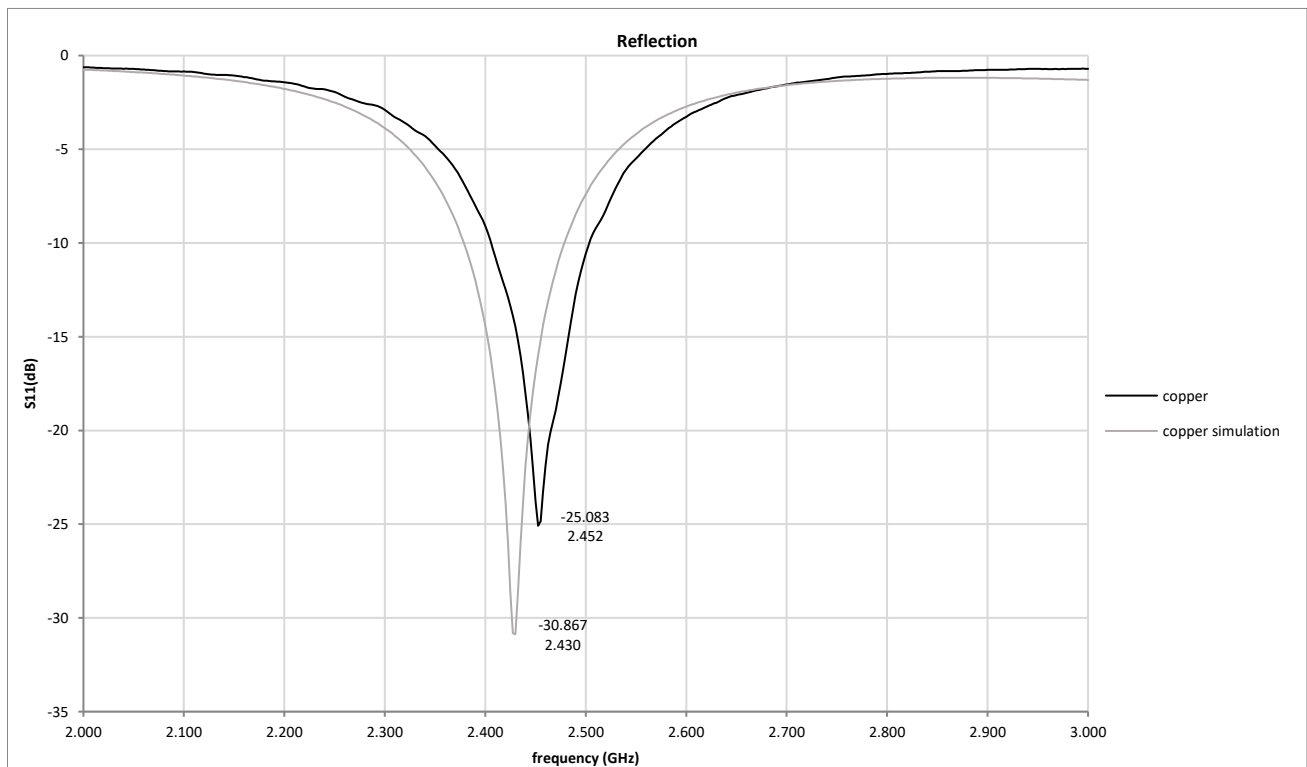


Figure 5-7. Measured and simulated  $S_{11}(dB)$  of reference copper patch antenna on textile substrate.

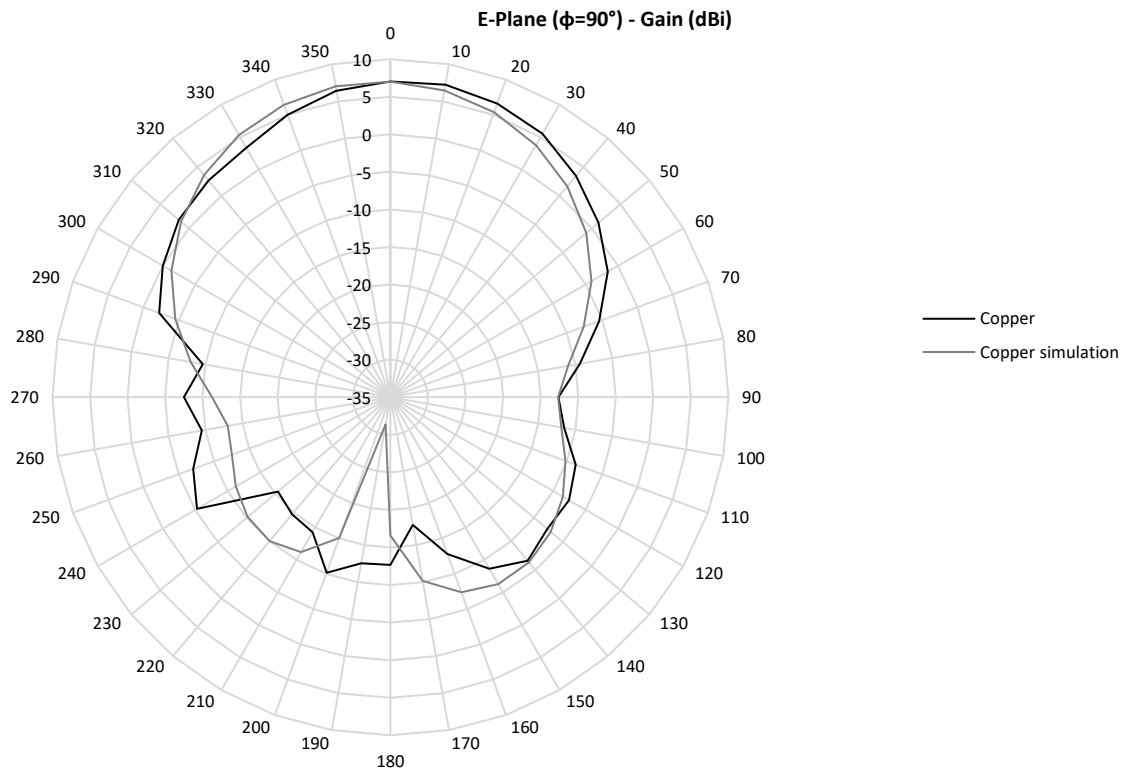


Figure 5-8. E-plane ( $\phi = 90^\circ$ ): Simulated and measured gain radiation patterns of copper patch antenna.

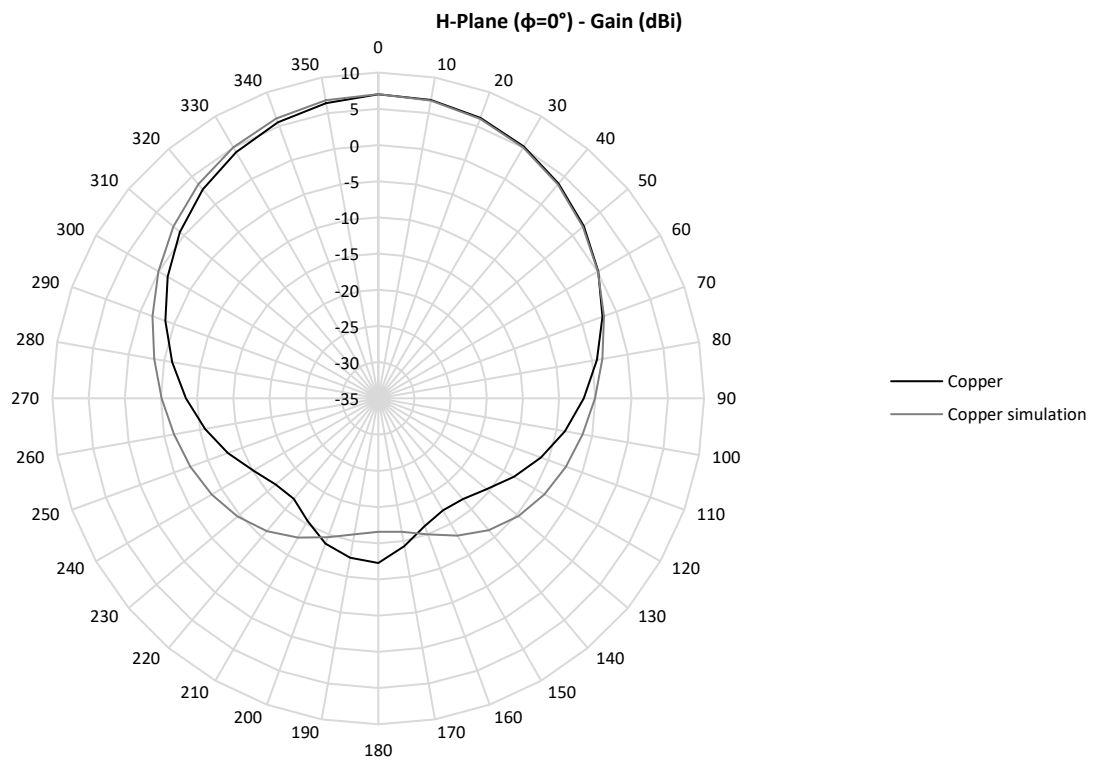


Figure 5-9. H-plane ( $\phi=0^\circ$ ): Simulated and measured gain radiation patterns of copper patch antenna.

## 5.2 Embroidered Microstrip Patch Antennas

After fabricating and measuring the reference copper microstrip patch antenna, embroidery designs were created based on its dimensions. Two different densities were examined, while all the embroidery parameters were selected according to the observations made in Chapter 4.

### 5.2.1 Embroidery Designs

The embroidery designs for the patch antennas were directly created on PE-DESIGN, according to the dimensions of the reference antenna since the shape was relatively simple. Fill stitch pattern with stitch direction parallel to the major current of the antenna's dominant mode (i.e., parallel to the length of the patch [3]) was chosen for all the embroidery designs (Figure 5-10). No under sewing was included in the embroidered antenna designs, since according to the conclusions of Chapter 4, it wouldn't significantly improve the performance of the antenna.

Two different density designs were examined at first ( 2.5 and 4 *lines/mm*), and two duplicates of each embroidery design were created. All the other embroidery parameters (stitch length, pull compensation, base fabric etc.) were the same as the ones mentioned for the embroidered transmission lines in Paragraph 4-5.

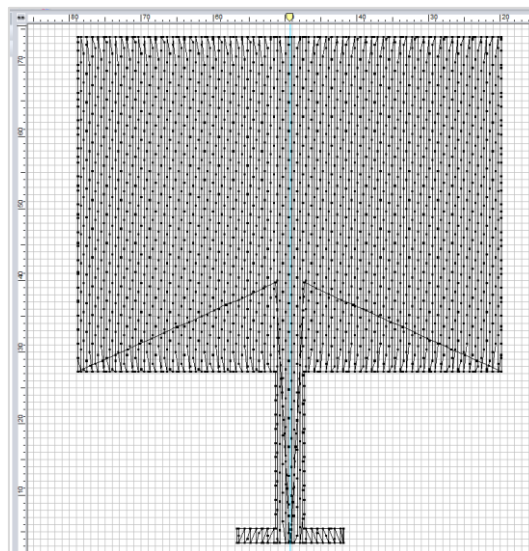


Figure 5-10. 2.5 *lines/mm*-density patch antenna design on PE design.

### 5.2.2 Embroidery Process and Patch Antenna Assembly

The embroidery process of the textile patch antennas was the same as described in Paragraph 4.2.2. However, a small piece of Nora Dell was attached to the denim base fabric at the point where the wider part of the feeding microstrip line (50  $\Omega$  input feed line) would be embroidered. Only the upper half of the 50  $\Omega$  microstrip was embroidered, as seen in the following figures. Since applying soldering directly on the conductive threads would severely damage them, soldering cannot be used on top of the embroidery. Thus, soldering was applied on the non-embroidered, bottom half of the 50  $\Omega$  microstrip, in order to attach the SMA connector to the antenna. The SMA connector was the only non-textile component of the antenna and was included in the structure solely for the purpose of conducting the measurements.

After embroidering the microstrips, the base fabric was cut, and the embroideries were glued to the felt substrate using melt adhesive. Nora Dell was also attached on the bottom side of the felt substrate, to serve as ground plane. Lastly, an SMA connector was soldered on the feeding point of each microstrip patch antenna. The SMA connectors and soldering were the only non-textile parts of the antennas. The finished embroidered microstrip patch antennas can be seen in Figure 5-11 and Figure 5-12.

As already mentioned, a duplicate of each microstrip patch antenna was also created, resulting in a total of four antennas. The dimensions of each embroidered antenna can be seen in Table 5-3. Apart from the precision of the embroidery machine, other parameters such as stretching of the base fabric, or tensions between the conductive threads resulted in a significant deviation of the antenna and feed line dimensions. For example, if the base fabric was overly stretched when placed on the embroidery frame, the resulting embroidery would be shrunk when taken out of the frame.

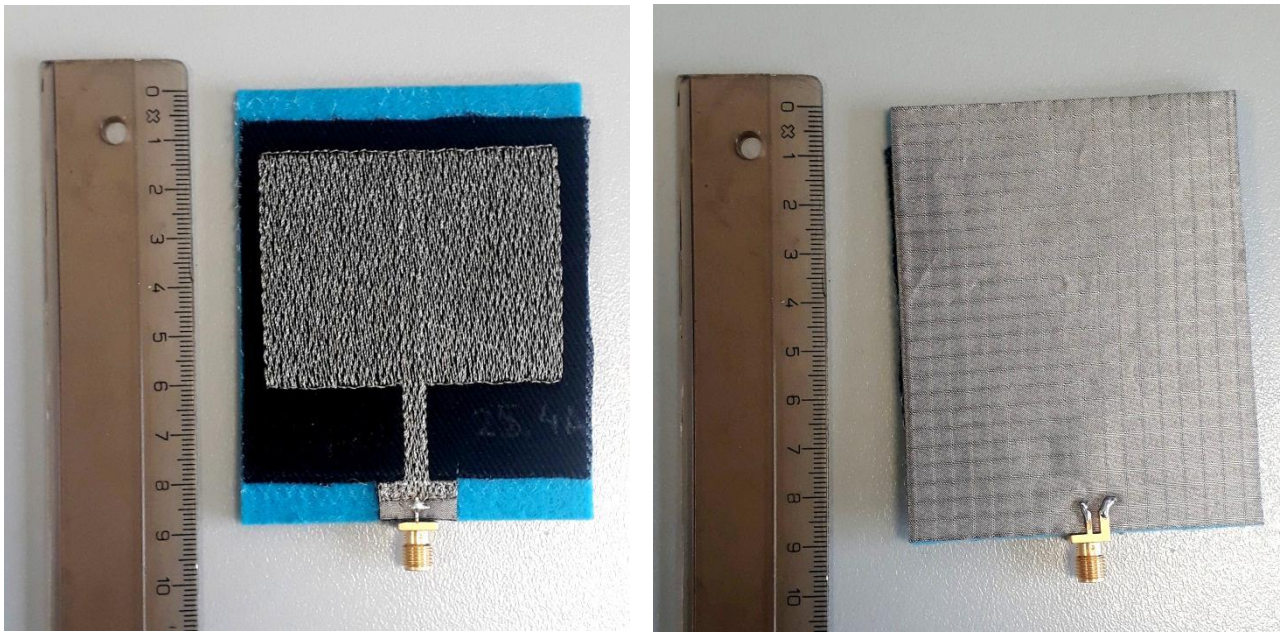


Figure 5-11. 2.5 lines/mm-density embroidered microstrip patch antenna front and back.

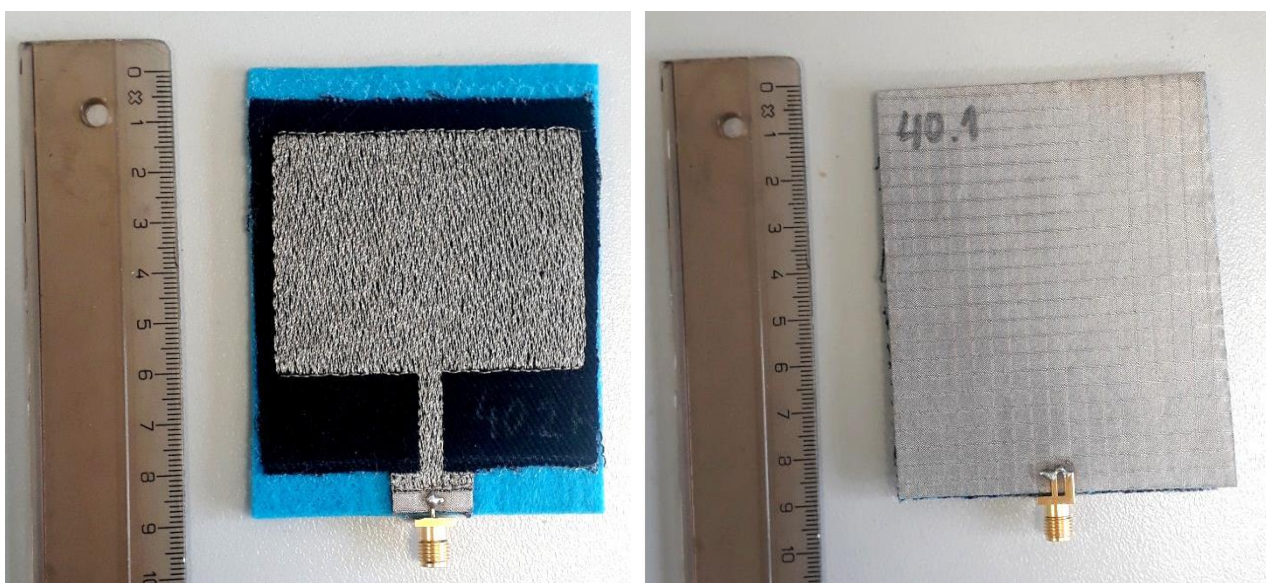


Figure 5-12. 4 lines/mm-density embroidered microstrip patch antenna front and back.

### 5.2.3 Measurement and Results

Table 5-3 displays the dimensions of each of the embroidered microstrip patch antennas, along with their resonant frequencies. The dimensions of all the antennas were based on the HFSS design of the reference copper patch antenna over denim, which was described in Paragraph 5.1. When designing the embroideries on PE design, the dimensions were adjusted to compensate for pulling of the fabric as well as for the increase in the dimensions due to the thickness of the threads. While all the embroidered antennas were designed to have the same dimensions, there was a non-negligible deviation on the dimensions of the finished embroideries. Since the resonant frequency of microstrip patch antennas changes significantly with the length of the patch, the deviation in the length of the embroidered antennas resulted in deviation on the frequency of resonance.

40A and 40B refer to the embroidered antennas whose stitch density was set to 4 *lines/mm*, whereas the antennas with 2.5 *lines/mm*-density are denoted as 25A and 25B.

Embroidery parameter		40A	40B	25A	25B	
Density ( <i>lines/mm</i> )		4	4	2.5	2.5	
Pull comp. ( <i>mm</i> )		1	1	1	1	
Dimensions ( <i>mm</i> )	HFSS	L	48.5	48.5	48.5	48.5
		W	59.2	59.2	59.2	59.2
		f1	19.9	19.9	19.9	19.9
		fw1	5	5	5	5
		fw2	15.5	15.5	15.5	15.5
	PE design	L	48	48	48	48
		W	59	59	59	59
		f1	22	22	22	22
		fw1	4	4	4	4
		fw2	14.9	14.9	14.9	14.9
	Physical	L	48.8	47.9	47.7	47.9
		W	59.7	61	60.82	60.5
		f1	19.53	18.1	18.79	18.1
		fw1	4.97	4.87	4.89	4.84
		fw2	15.9	16.12	16.4	16.22
f (GHz)		2.36	2.39	2.4	2.41	

Table 5-3

Figure 5-13 displays the measured  $S_{11}(dB)$  parameter of all the embroidered antennas (dotted traces) as well as the average values of the same density antennas (solid traces). The measured  $S_{11}(dB)$  of the reference copper patch antenna is also displayed for comparison.

Both embroidered antennas resonated in lower frequencies compared to the copper reference antenna, while the physical length of the embroidered patches was smaller than the length of the copper patch. Thus, the measurement results indicate that the electrical length of the embroidered patches is actually longer than the electrical length of the physically longer copper reference antenna.

Moreover, a change in the frequency of resonance was also observed among the embroidered antennas. More specifically, the resonant frequency of the 2.5 *lines/mm*-density antennas was approximately 2.4 GHz, which is 27 MHz higher than the resonance of the 4 *lines/mm*-density antennas. Since both 2.5 *lines/mm*-density patches turned out smaller in length compared to the denser ones, this difference in resonance is natural. More specifically, the resonant frequency of a solid copper patch antenna with dimensions equal to the average dimensions of the 2.5 *lines/mm*-antennas would operate

approximately 28 MHz higher than a solid copper antenna with dimensions equal to the 4 lines/mm-density embroideries, if the same substrate was used.

As far as the input reflections are concerned, the embroidered antennas with higher density had better performance, even though the  $|S_{11}(dB)|$  parameter still higher than  $-15$  dB. The excessive reflections which were observed in all the embroidered microstrip patch antennas may be attributed to the low equivalent conductivity of the embroideries. According to [3] the discontinuous, non-uniform conductive surface of the embroideries results in low equivalent conductivity of the embroidery. This effect is reinforced by poor connection between adjacent stitches, according to the same study. Indeed, in this thesis, even in the embroidered patch antennas with the highest density (i.e., 4 lines/mm), the base fabric was visible through embroidered parts of the patch antenna. In other words, adjacent stitches were scarcely connected in the 4 lines/mm patch antenna, while only a small fragment of the total adjacent stitches made contact with each other in the 2.5 lines/mm antenna.

The bandwidth of the 4 lines/mm-density patch antenna was larger, compared to the reference copper antenna. More precisely, the bandwidth of the reference antenna at  $-10$  dB was approximately 99 MHz, whereas it reached 140 MHz for the densely stitched antenna. Increased bandwidth may imply that the embroidered antenna has higher losses, which is to be expected due to the non-uniform conductive pattern of the embroidery. As far as the 2.5 lines/mm-density embroidered antenna is concerned, the resonance barely exceeded  $-10$  dB, so its bandwidth was only 20.5 MHz.

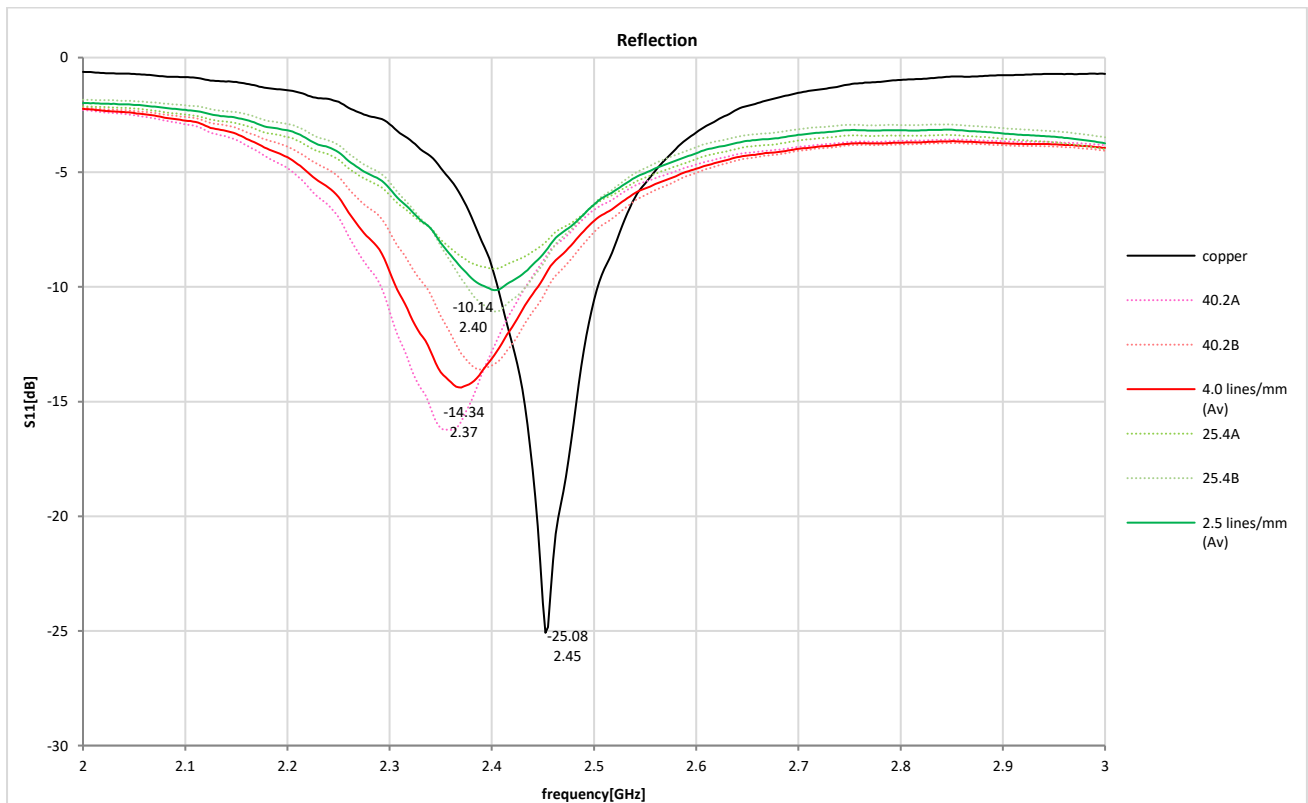


Figure 5-13.  $S_{11}(dB)$  of embroidered microstrip patch antennas with two different stitch densities.

### 5.3 Optimized Embroidered Microstrip Patch Antenna

An attempt to create a microstrip patch antenna model on HFSS, whose performance is similar to the 4 lines/mm-density embroidered antenna was made at first.

It was assumed that due to the complex current routes created by the conductive threads, the embroidered antenna became electrically longer, thus it resonated in a lower frequency compared to the

solid conductive sheet patch model. On the other hand, since both the reference copper antenna and the embroidered antennas were placed on the same substrate and base fabric, it was assumed that the reduced equivalent conductivity of the embroidered antennas was the main factor that resulted in a high level of reflections. According to these assumptions, the dimensions and conductivity of the modeled patch were altered.

After creating an equivalent model of the 4 lines/mm-density embroidered antenna, adjustments on the patch and feedline dimensions were made, in order to improve its performance. According to the new antenna model, an embroidered antenna was fabricated and measured.

### 5.3.1 Simulation Model Modification

With the intention of reducing the resonant frequency of the simulated model, so it would match the measured resonant frequency, the length of the patch had to be increased by 1.9 mm. It is thus indicated that the electrical length of the embroidered patch antenna is longer than its physical length.

Without changing any of the other variables of the model, the conductivity of the modeled patch was decreased. When the conductivity of the patch was reduced to  $\sigma = 0.011 \cdot 10^6 \frac{S}{m}$ , the  $S_{11}(dB)$  parameter reached approximately  $-14.5 dB$ , which is close to the measured  $S_{11}(dB)$  value of the 4 lines/mm embroidered patch antenna at resonance. A slight shift in the resonant frequency was also observed, compared to the high conductivity model ( $\sigma_{copper} = 58 \cdot 10^6 \frac{S}{m}$ ).

Figure 5-14 displays the simulated  $S_{11}(dB)$  of the low conductivity model with modified dimensions, along with the measured embroidered microstrip patch with 4 lines/mm density.

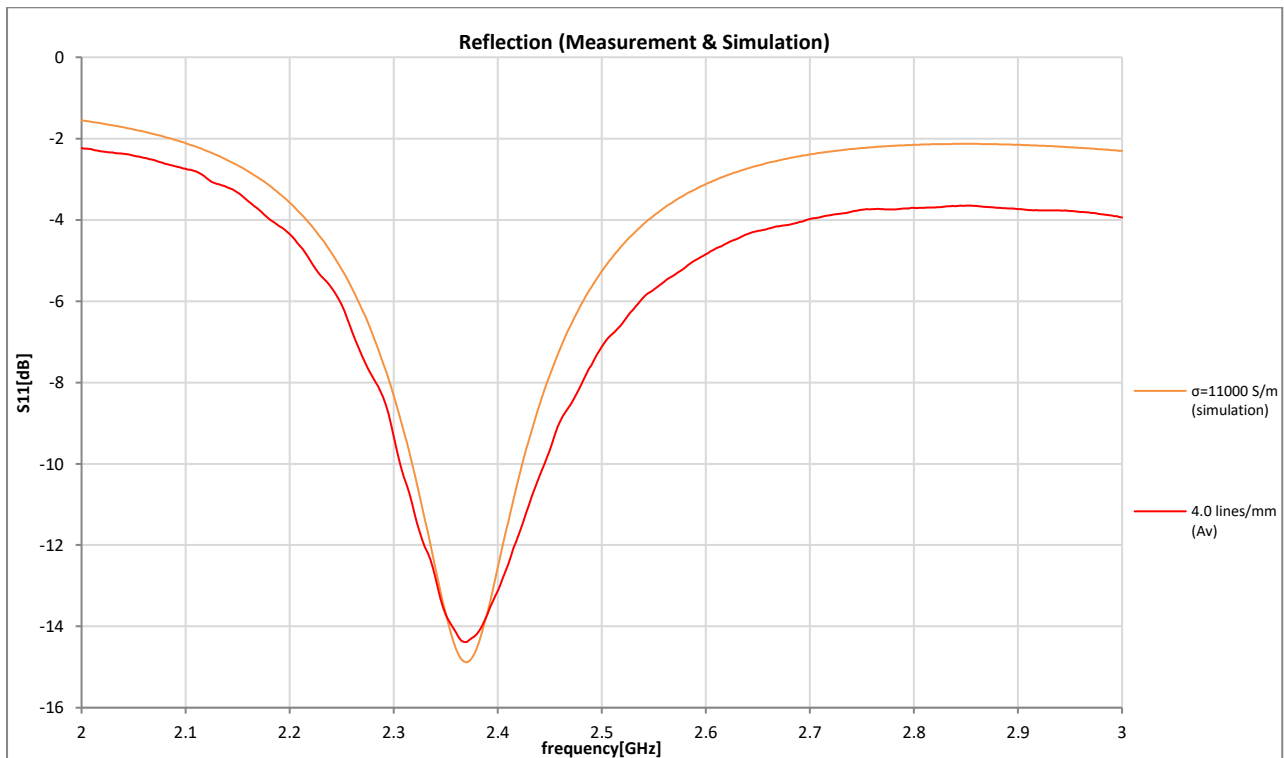


Figure 5-14. Simulated  $S_{11}(dB)$  parameter of the modified HFSS patch antenna model and measured  $S_{11}(dB)$  of the 4 lines/mm-density embroidered patch antenna.

### 5.3.2 Antenna Design Model Adjustment

The initial goal was to create using embroidery techniques a fully textile patch antenna which operates near  $2.4\text{ GHz}$ . However, a shift in lower frequencies was observed in the embroidered antenna prototypes, compared to the reference copper patch antenna. This change in the resonant frequency was attributed to the complex structure of the embroidery, which elongated the electrical length of the patch. According to this assumption, the physical length of the patch had to be reduced, in order to achieve a  $2.4\text{ GHz}$  resonance.

As already mentioned, according to simulations, the electrical length of the patch was approximately  $1.9\text{ mm}$  longer than its physical length. Thus, reducing the physical length of the embroidered antenna by an equal length would bring the resonance up to the desired frequency. Consequently, a  $49.9\text{ mm}$ -long embroidered microstrip patch antenna was fabricated, following the steps mentioned in Paragraph 5.2. The rest of the parameters and dimensions of the embroidered antenna were not altered.

Figure 5-15 shows the measured  $S_{11}(\text{dB})$  graph of the embroidered antenna with the modified dimensions, along with the initial embroidered antenna and the reference copper antenna. By increasing the length of the antenna, the resonant frequency reached approximately  $2.44\text{ GHz}$ , which is close to the resonant frequency of the reference copper antenna. However, the value of the  $S_{11}(\text{dB})$  parameter was approximately  $-12\text{ dB}$  at the resonating frequency, which indicates that a large portion of the input power gets reflected.

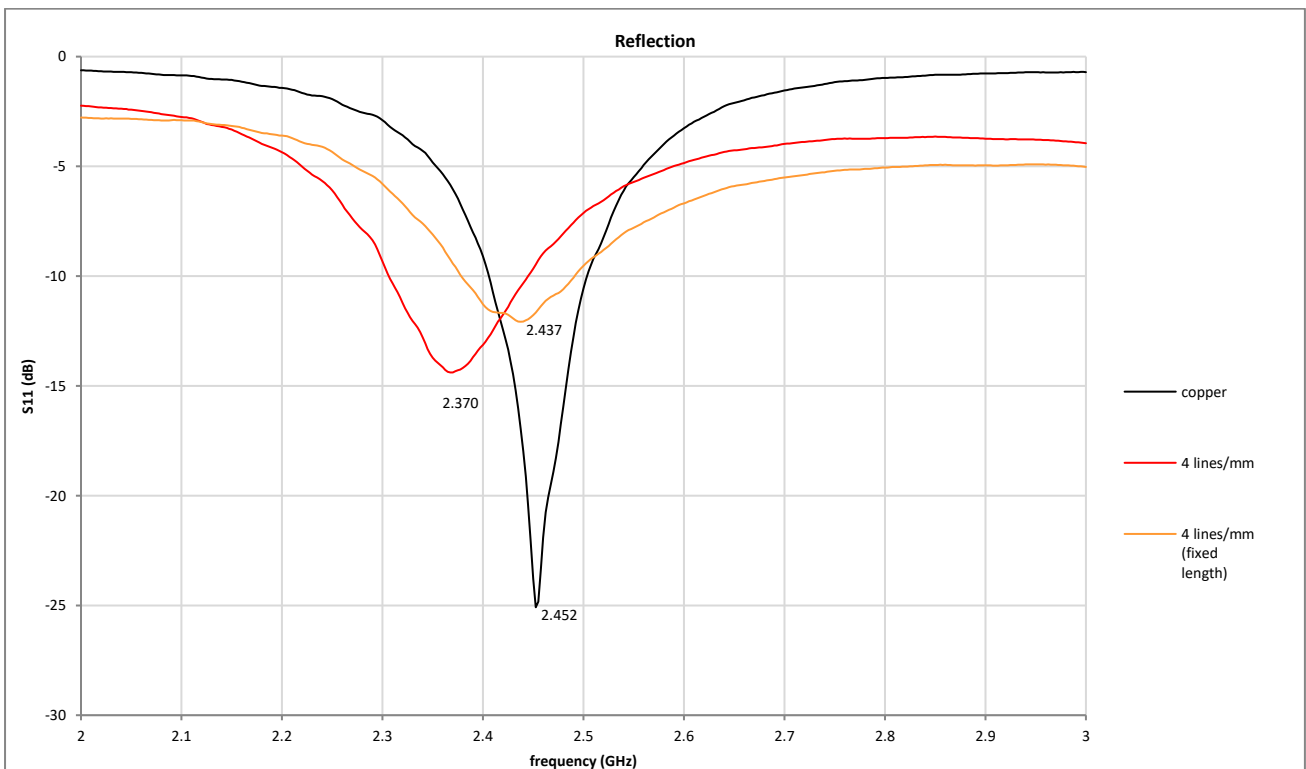


Figure 5-15. Measured  $S_{11}(\text{dB})$  parameter of embroidered microstrip patch antenna with modified dimensions (orange trace), initial embroidered patch antenna (red trace) and reference copper patch antenna (black trace).

It has already been suggested that the excessive input reflections of the embroidered patch antenna were ascribed to the low equivalent conductivity of the embroidered parts of the antenna. Assuming that the reduced conductivity of the patch would result in a drop of its input impedance at the resonant frequency, the characteristic impedance of the quarter wavelength transformer had to be

readjusted. Consequently, the width of the quarter wavelength microstrip line was altered, in order to provide impedance match and thus minimize the input reflections.

More specifically, compared to the quarter wavelength transformer, which was designed for the copper patch antenna model, its characteristic impedance ( $Z_0'$ ) had to be reduced, to match the reduced input impedance ( $Z_L'$ ) of the embroidered patch at the resonant frequency, as seen in the following equation:

$$Z_0' = \sqrt{Z_{in}Z_L'} \quad (28)$$

Consequently, the width of the quarter wavelength microstrip was increased to 7 mm, to provide impedance matching at 2.4 GHz.

The embroidered microstrip patch antenna that was fabricated according to the new microstrip dimensions (adjusted length and quarter wavelength microstrip width) is displayed in Figure 5-16.

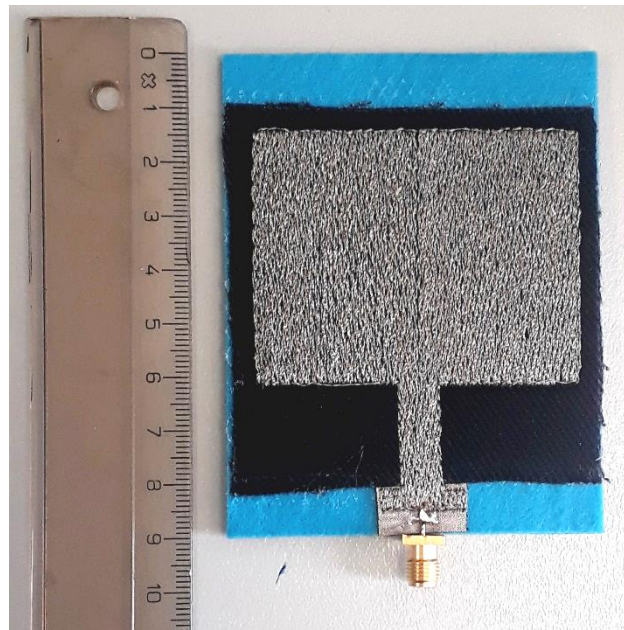


Figure 5-16. Final embroidered patch antenna prototype with 4 lines/mm density and modified patch and microstrip dimensions.

### 5.3.3 Measurement

The  $S_{11}(dB)$  parameter of two identical optimized embroidered microstrip patch antennas are displayed in Figure 5-17. The characteristics, dimensions, and resonant frequencies of all the measured antennas can be seen in Table 5-4. The embroidered antenna with modified patch length is denoted as "40.3", while the identical antennas whose feedlines have been adjusted are denoted as "40.4A" and "40.4B".

As seen in Figure 5-17, changing the width of the quarter wavelength microstrip contributed to decrease the  $S_{11}(dB)$  value, as it reached approximately  $-18.5 dB$  at resonance. The resonant frequency did not change significantly since the antennas had approximately the same dimensions. However, all the antennas resonated in a lower frequency compared to the reference copper patch antenna. This indicates that the length of the embroidered patch should have been further reduced, in order to resonate in the same frequency as the reference antenna.

Embroidery parameter		copper	40.3	40.4A	40.4B	
Density (lines/mm)		-	4	4	4	
Pull comp. (mm)		-	1	1	1	
Dimensions (mm)	HFSS	L	49	47.6	47.6	47.6
		W	59	59	59	59
		fl1	22	22	22	22
		fw1	5	5	7.6	7.6
		fw2	15	15	15	15
	PE design	L	-	47	47	47
		W	-	59	59	59
		fl1	-	22	22	22
		fw1	-	4	7	7
		fw2	-	14.9	14.9	14.9
	Physical	L	48.3	47.1	47.2	46.8
		W	59.4	60.6	60.55	60.53
		fl1	19.9	18.59	18	18.52
		fw1	5	4.9	8.12	7.75
		fw2	15.5	16.7	16.7	16.52
f (GHz)		2.450	2.438	2.438	2.443	

Table 5-4

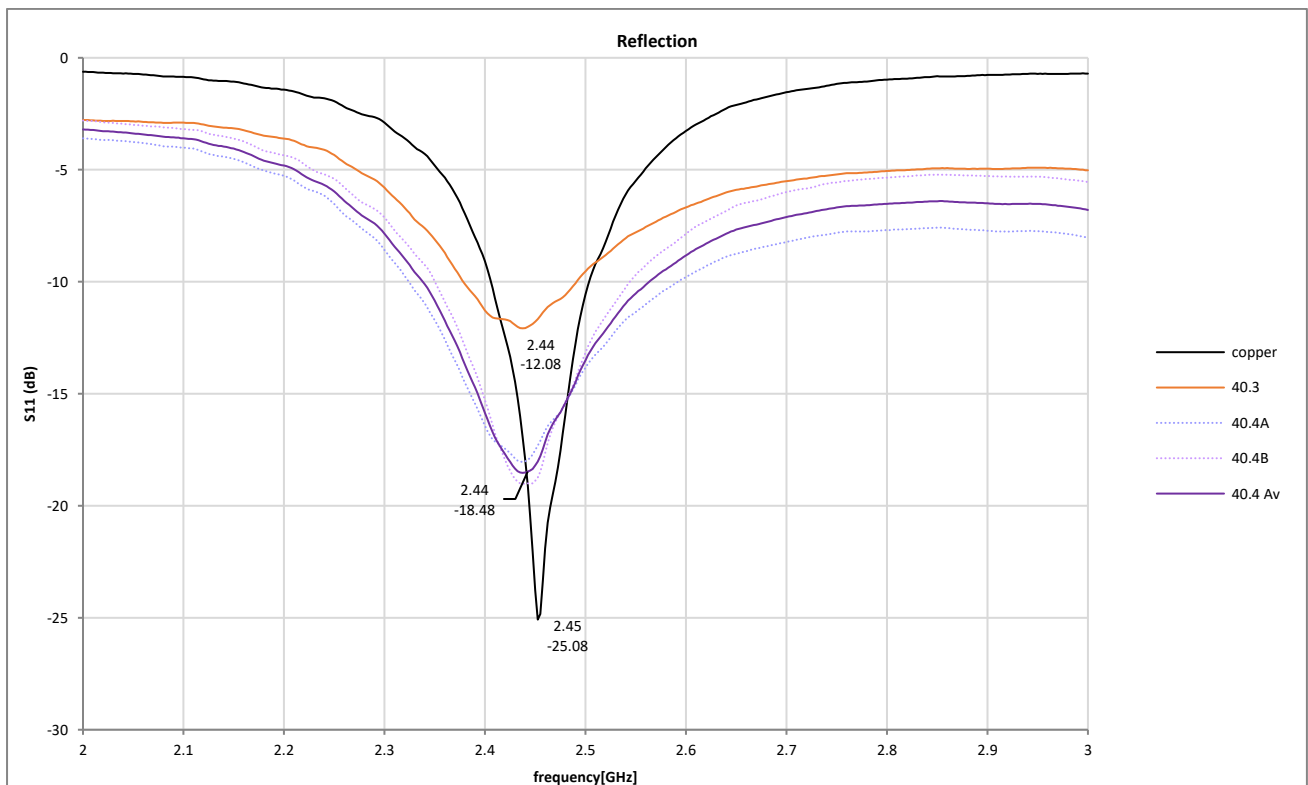


Figure 5-17.  $S_{11}(dB)$  parameter of embroidered microstrip patch antennas with modified dimensions (orange trace), and also corrected microstrip dimensions (light purple dashed traces). The purple trace is the average of the two dashed purple traces.

The far-field performance of the optimized antennas and reference copper patch antenna was also measured in the anechoic chamber (Figure 5-18). Each antenna was appropriately placed on the positioner, which is displayed in the following picture. A horn antenna was used to measure the  $S_{21}(dB)$  parameter of the antennas under test, as seen in Figure 5-18. The measurement was conducted at the resonant frequency of the reference copper antenna (i.e.,  $2.45\text{ GHz}$ ), by appropriately rotating the positioner in order to measure the E-plane and H-plane of the antennas.

The total gain of the antennas was then plotted for the E-plane and H-plane, according to the results of the measurement (Figure 5-19, Figure 5-20). The gain of the embroidered antennas was lower ( $> 5\text{ dB}$  in the bore side direction) compared to the copper patch antenna. This indicates that the embroidered antennas have higher losses, as expected, which may be attributed to the increased conduction losses of the embroidery patterns as well as additional dielectric losses introduced by the hot melt adhesive, the polyester bobbin threads at the back of the embroideries and the non-uniform structure of the embroidered base fabric. The prominent back lobe that was observed on all the antennas' radiation patterns can be ascribed to the measurement tower inside the chamber.

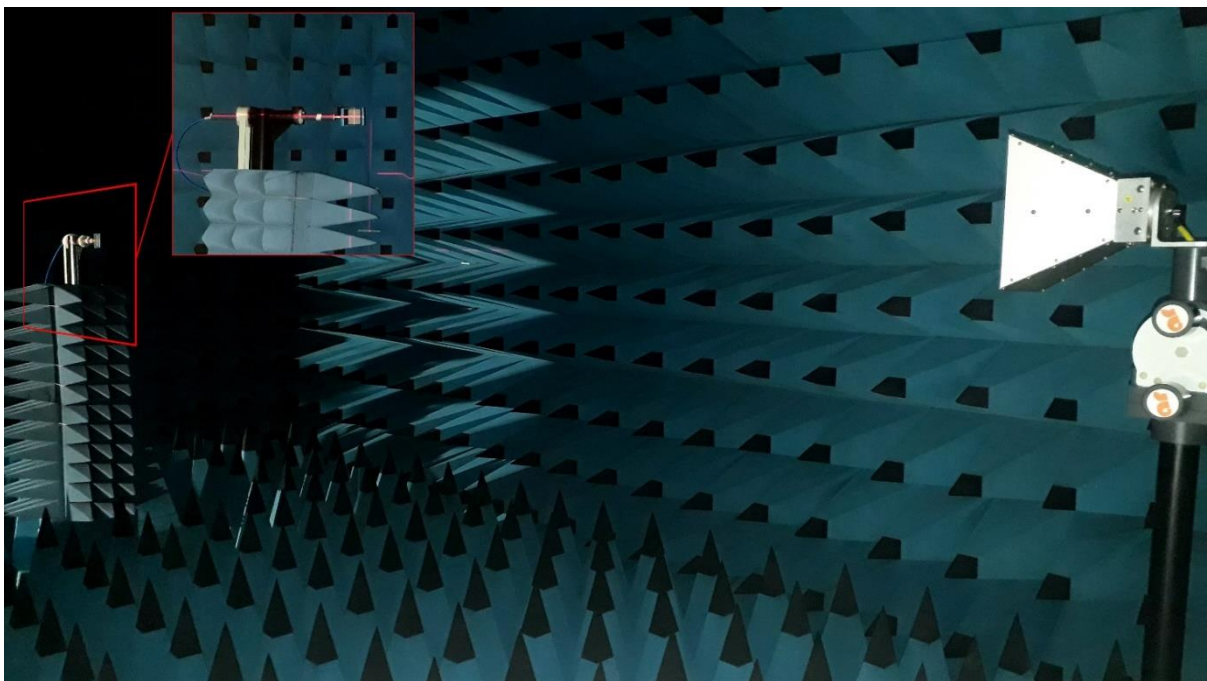


Figure 5-18. Measurement set-up inside the anechoic chamber.

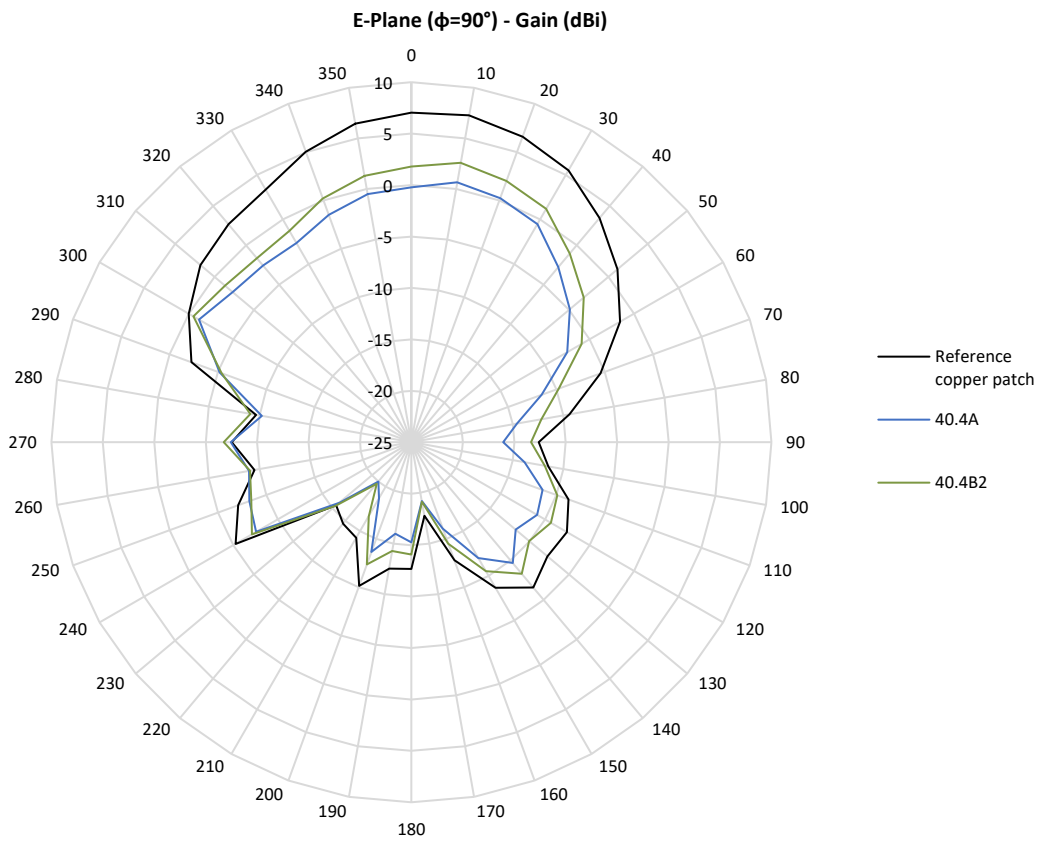


Figure 5-19. E-plane ( $\phi = 90^\circ$ ): gain radiation patterns of copper and embroidered patch antennas.

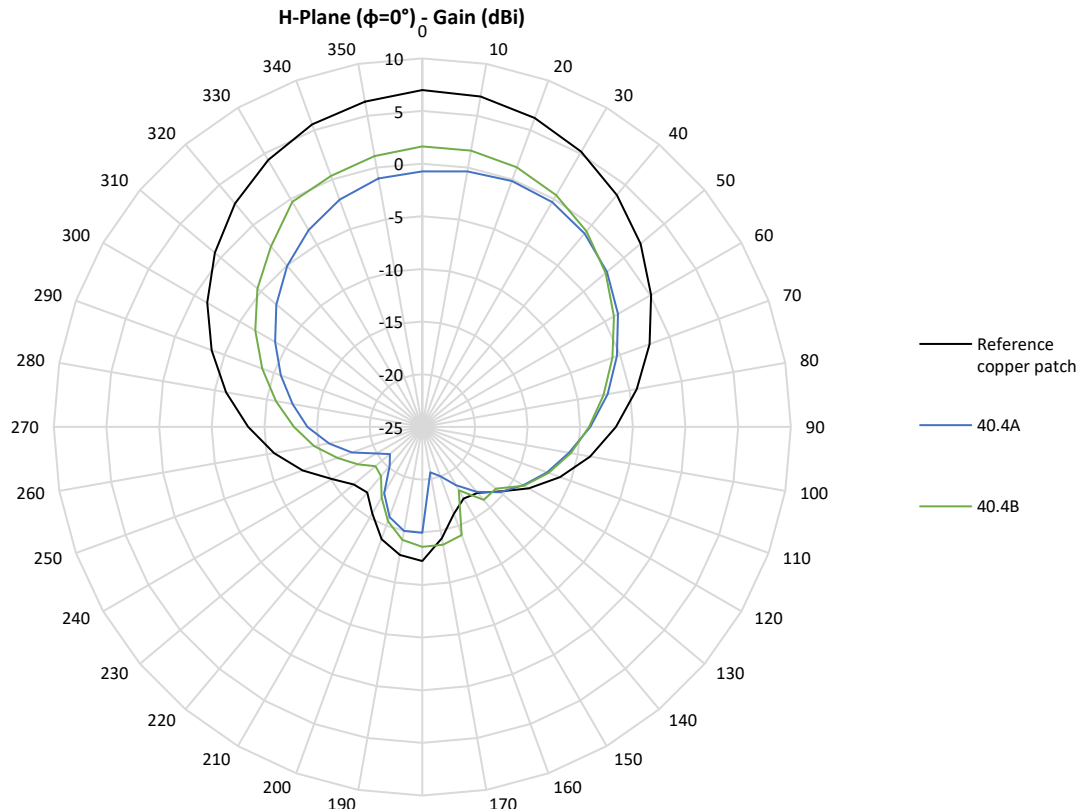


Figure 5-20. H-plane ( $\phi = 0^\circ$ ): gain radiation patterns of copper and embroidered patch antennas.

## 5.4 Conclusions

The RF performance of embroidered, textile microstrip patch antennas was studied in this chapter. A copper patch antenna was fabricated to serve as reference. Two different stitch densities were examined at first;  $4 \text{ lines/mm}$  and  $2.5 \text{ lines/mm}$ . While the same densities were also used for embroidering microstrip transmission lines in the previous chapter with satisfying results, this was not the case for the embroidered microstrip patch antennas. Both density antennas exhibited high input reflections, however the performance of the  $2.5 \text{ lines/mm}$ -density antennas was notably worse. Moreover, both antennas resonated in lower frequencies compared to the reference copper patch, even though their dimensions were a bit smaller. It was suggested that due to the complex current routes created by the conductive threads, the electrical length of the patches was increased resulting in a lower resonance frequency. Last but not least, the shrinking effect was more prominent for the two duplicate antennas whose stitch density was  $2.5 \text{ lines/mm}$ . Although the dimensions of the embroidery designs had already been increased in order to compensate for shrinking, further attention is needed in properly adjusting the embroidery design dimensions, especially for lower stitch densities.

In an attempt to create an improved embroidered antenna model, the dimensions of the embroidered patch were altered. Consequently, a  $4 \text{ lines/mm}$ -density antenna with reduced patch length was fabricated. While the frequency of operation increased, the input reflections remained high. It was suggested that the diminished conductivity of the embroidery was responsible for the low value of the  $S_{11}(dB)$  parameter of the embroidered microstrip patch antenna. After creating a low equivalent conductivity antenna model on HFSS, the width of the quarter wavelength feedline was adjusted. By increasing the width of the microstrip feedline, impedance matching was achieved for the low

conductivity patch antenna. A textile, embroidered patch antenna was created, based on the optimized model.

By adjusting the patch and feedline dimensions, the performance of the embroidered patch antenna significantly improved. At 2.45 GHz, the  $|S_{11}(dB)|$  parameter exceeded 17 dB. The radiation pattern of the embroidered antennas with adjusted dimensions was also plotted, for the E-plane and H-plane of the antennas. Even though the embroidered antennas exhibited lower gain ( $\approx 1.5$  dB) compared to the reference copper antenna ( $\approx 7$  dB), the radiation patterns were satisfying.

## References

- [1] C. Balanis, *Antenna Theory: Analysis and Design*, 3rd ed., 2005.
- [2] *Quarter wave transformer impedance calculator*. Available: <https://www.everythingrf.com/rf-calculators/quarter-wave-transformer-impedance-calculator>
- [3] S. Zhang, "Design advances of embroidered fabric antennas," PhD, Loughborough University, 2014.

## Chapter 6 Summary and Future Work

### Summary

The effect of the e-textile embroidery parameters on the RF performance of embroidered microstrip patch antennas has been experimentally investigated in this thesis. Textile patch antennas were fabricated using embroidery with conductive threads, conductive and conventional fabrics. The different components of the antenna were glued together using hot melt adhesive that is commonly used for fabrics, resulting in a low-profile, lightweight, and discreet antenna, which could be easily integrated into clothing for wearable applications.

The most common methods of fabricating e-textiles were outlined in Chapter 1. E-textile embroidery stands out for its high resolution and fabrication advantages that make it an attractive option for mass manufacturing wearable antennas and RF components. The process of creating a textile antenna with a computerized embroidery machine was also briefly described.

Felt is a conventional fabric that is usually used as a dielectric substrate for wearable, textile antennas. Accurately measuring the dielectric properties of felt substrates is essential for designing wearable antennas. Typical methods of electrically characterizing planar materials like fabrics were introduced in Chapter 2. Consequently, a felt substrate sample was electrically characterized using two different methods; the T-resonator method and Split-Post Dielectric Resonator method.

With the aim of creating antenna embroidery designs, the basic parameters of embroidery using a computerized embroidery machine were explained in Chapter 3. Thorough details on the embroidery process using conductive threads were introduced. Moreover, an extensive study on how several e-textile embroidery parameters affect the RF performance of electronics was carried out.

Based on the conclusions of the previous chapters, microstrip transmission line embroidery designs were created in Chapter 4. In order to evaluate the effect of different stitch densities and "under sewing" options, the performance of the embroidered microstrips on a rigid, FR4 substrate was examined. While increasing the stitch density generally decreased the transmission losses of the microstrip lines, including under sewing in the design did not have a significant effect on their performance.

Two different stitch densities (4 and 2.5 *lines/mm*) were examined in the context of textile, embroidered, microstrip patch antennas at the beginning of the next chapter. A copper patch antenna on a textile substrate was used as reference. Even though shrinking of the base fabric was taken into account when designing the embroideries, the fabricated antennas had notably smaller dimensions than expected. However, since all the antennas resonated in higher frequencies compared to the reference antenna, it was assumed that the complicated structure of the conductive threads in the embroideries increased the electrical length of the patches.

Consequently, a new embroidered patch antenna was created, based on the observations of the previous models. The highest examined stitch density was selected (i.e., 4 *lines/mm*), while the dimensions of the antenna were adjusted, in order to resonate higher in the frequency spectrum. Slightly decreasing the length of the patch successfully increased the resonant frequency.

Finally, assuming that the low equivalent conductivity of the embroidered patch was responsible for the high input reflections of all the embroidered antennas, a low conductivity model was created in HFSS. It was observed that increasing the width of the feedline provided impedance matching when the conductivity of the antenna was diminished. Indeed, the fabricated embroidered antenna with modified feedline width exhibited lower input reflection coefficient at resonance. The radiation pattern of the adjusted textile, embroidered microstrip patch antenna was measured in the anechoic chamber of the Institute of Informatics and Telecommunications, at NCSR 'Demokritos'.

## Future Work

SMA connectors were soldered on the conductive fabric at the input feedline of the textile antennas which were fabricated for this thesis. Even though the conductive fabric was not visibly damaged, the high temperatures required for applying soldering may affect its performance. A small change in the input impedance of the antennas was indeed observed before and after applying soldering. On the other hand, when soldering was not applied yet, the  $S_{11}(dB)$  curve was not stable, due to the improper contact between the SMA connector and the input of the antenna. It is thus essential to study and develop new methods of connecting the textile antennas and other RF components with the measuring equipment, without using techniques that could possibly harm the e-textiles or significantly affect the measurement results. Moreover, the development and integration of textile connectors into wearable antennas is an open research challenge.

Another aspect of the textile antenna structure that may have contributed in the observed variations between the simulation and measurement results, was the hot melt adhesive. The adhesive was used for attaching all the layers of the antenna together (i.e., embroidered base fabric, felt substrate and Nora Dell ground plane). However, the effect of the adhesive was not taken into account when creating the antenna designs on HFSS, due to the lack of information on its dielectric properties. Thus, in future works, it is crucial to determine the effect of the adhesive on the equivalent permittivity of the antenna substrate.

Non-negligible variations were observed on the dimensions of embroideries that were created from the same embroidery design. Also, due to the non-uniform surface of the base fabric, there was also variation on the exact position of each needle punch and consequently on the stitch length and direction. These deviations resulted in variations on the performance between microstrip transmission lines that were theoretically identical. The same phenomenon was also prominent when embroidering microstrip patch antennas. Therefore, it is necessary to conduct extensive repeatability measurements in the future, in order to properly evaluate the performance of textile RF components.

A divergence between the physical and electrical dimensions of the embroidered microstrip patch antennas was also observed throughout the course of this thesis. More specifically, the embroidered antennas resonated in lower frequencies compared to the copper patch reference antenna. Repeatability measurements are also required to numerically investigate the increase of the electrical dimensions of the embroideries, according to their stitch density, stitch length, pattern, and direction.

Another factor that contributed in the variation between the simulated and measured results was the estimated equivalent conductivity of the embroideries. Further investigation on the effect of the embroidery parameters on the equivalent conductivity of the embroideries is required, in order to properly design textile, embroidered antennas for wearable applications.

Last but not least, the effect of the conductive threads on the performance of embroidered antennas should also be studied in the future. While the linear resistance of the Shieldex 117/17 2-ply thread that was used in this thesis was as high as  $1500 \Omega/m$  [1], a variety of conductive threads with lower linear resistance are commercially available. A highly conductive thread by Elitex, whose linear resistance is approximately  $20 \Omega/m$  [2], will be used to create the same microstrip patch antennas that were fabricated in the last section of Chapter 6. The high conductivity of these threads is expected to play a key role on the performance of the embroidered antennas. However, extensive stitching errors (breakage of filaments, fraying etc.) are also expected due to the pronounced stiffness of the high conductivity thread. Therefore a corresponding trade-off analysis should be conducted.

## References

- [1] Shieldex® 117/17 x2 Datasheet. Available:  
<https://www.shieldex.de/en/products/shieldex-117-17-x2/>
- [2] Available: <https://www.imbut.de/en/special-threads#conductive-threads-elitex>